Forschungszentrum Karlsruhe
in der Helmholtz-Gemeinschaft

Wissenschaftliche Berichte
FZKA 6895

Optimised Design and Thermal-Hydraulic Analysis of the IFMIF/HFTM Test Section

**S. Gordeev, V. Heinzel, K.H. Lang,
A. Möslang, K. Schleisiek, V. Slobodtchouk,
E. Stratmanns**

**Institut für Reaktorsicherheit
Institut für Material- und Festkörperforschung**

Oktober 2003

Forschungszentrum Karlsruhe

in der Helmholtz-Gemeinschaft

Wissenschaftliche Berichte

FZKA 6895

Optimised Design and Thermal-Hydraulic Analysis of the IFMIF/HFTM Test Section

S. Gordeev, V. Heinzel, K.H. Lang,
A. Möslang, K. Schleisiek*,
V. Slobodtchouk, E. Stratmanns

Institut für Reaktorsicherheit
Institut für Material- und Festkörperforschung

* Firma Ingenieurbüro Dr. Ing. W. Hering

Forschungszentrum Karlsruhe GmbH, Karlsruhe

2003

Impressum der Print-Ausgabe:

Als Manuskript gedruckt

Forschungszentrum Karlsruhe GmbH
Postfach 3640, 76021 Karlsruhe

Mitglied der Hermann von Helmholtz-Gemeinschaft
Deutscher Forschungszentren (HGF)

ISSN 0947-8620

Optimierter Entwurf und thermohydraulische Analyse des Hochfluss-Testmoduls für die Internationale Fusionsmaterial-Bestrahlungseinrichtung IFMIF

Zusammenfassung

Aufbauend auf den früher entwickelten Konzepten sowie den durchgeführten Analysen und Experimenten, wurde der Hochfluss-Testmodul (HFTM) für die Internationale Fusionsmaterial-Bestrahlungseinrichtung (IFMIF) weiter verbessert. Die Arbeit konzentrierte sich auf den Entwurf und die thermohydraulische Analyse der HFTM-Teststrecke mit dem darin enthaltenen Bestrahlungsmaterial. Hauptziel war die Verbesserung des Konzepts im Hinblick auf die optimale Raumnutzung des Bestrahlungsvolumens und die Temperatur der Materialproben. Dabei wurde besonderer Wert auf die Anwendung von Konstruktionsprinzipien gelegt, die zu stabilen und reproduzierbaren Temperaturen in den Proben führen.

Die erzielten Ergebnisse bestätigen die Eignung und Machbarkeit des optimierten Entwurfs der Teststrecke mit schokoladentafel-förmigen Bestrahlungseinsätzen. Insbesondere zeigte sich, dass die vorgesehenen Bestrahlungstemperaturen bei akzeptablen Temperaturdifferenzen im Probenstapel erreicht werden können. Dazu ist jedoch die elektrische Beheizung der beiden Kapselenden erforderlich. Die Aufteilung der Heizzone in drei Bereiche mit separater Leistungsversorgung und Regelung ist zweckmäßig. Die elektrische Beheizung ist ebenfalls zur Aufrechterhaltung der Temperatur während Strahlunterbrechungen erforderlich. Die erforderlichen mineralisolierten Heizleiter sind kommerziell verfügbar.

Die Eignung der CFD Computerprogramms STAR-CD für die thermohydraulische Analyse komplexer Systeme wie das HFTM wurde bestätigt. Ungeachtet dessen ist eine experimentelle Bestätigung der erzielten Ergebnisse wünschenswert; entsprechende Experimente befinden sich in der Vorbereitung. Zur Bestätigung der angenommenen thermischen Widerstände an Kontaktflächen und in engen Spalten mit speziellen Abstandshaltern werden gezielte Experimente empfohlen. Die vorliegenden Ergebnisse müssen durch eine thermomechanische Analyse des HFTM, insbesondere der Rig-Wand, ergänzt werden. Darüber hinaus wird die Untersuchung des HFTM-Verhaltens bei Leistungsänderungen für notwendig gehalten.

Abstract

On the basis of previous concepts, analyses and experiments, the High Flux Test Module (HFTM) for the International Fusion Materials Irradiation Facility (IFMIF) was further optimised. The work focused on the design and the thermal hydraulic analysis of the HFTM section containing the material specimens to be irradiated, the “test section”, with the main objective to improve the concept with respect to the optimum use of the available irradiation volume and to the temperature of the specimens. Particular emphasis was laid on the application of design principles which assure stable and reproducible thermal conditions.

The present work has confirmed the feasibility and suitability of the optimised design of the HFTM test section with chocolate plate like shaped rigs. In particular it has been shown that the envisaged irradiation temperatures can be reached with acceptable temperature differences inside the specimen stack. The latter can be achieved only by additional electrical heating of the axial ends of the capsules. Division of the heater in three sections with separate power supply and control units is necessary. Maintaining of the temperatures during beam-off periods likewise requires electrical heating. The required electrical heaters – mineral isolated wires – are commercially available.

The potential of the CFD code STAR-CD for the thermal hydraulic analysis of complex systems like the HFTM was confirmed. Nevertheless, experimental confirmation is desirable. Suitable experiments are under preparation. To verify the assumptions made on the thermal conductivity of the contact faces and layers between the two shells of the rig, dedicated experiments are suggested. The present work must be complemented by a thermal mechanical analysis of the module. Most critical component in this respect seems to be the rig wall. Furthermore, it will be necessary to investigate the response of the HFTM to power transients, and to determine the requirements on the electrical heating control system.

Content

1. Introduction

The “International Fusion Materials Irradiation Facility” (IFMIF) is an accelerator-based D-Li neutron source. It has the capability to produce neutrons at sufficient energy and intensity to test specimens of candidate materials up to the full lifetime of nuclear fusion reactors. In the High Flux Test Module (HFTM) which is arranged next to the lithium target a damage rate of more than 20 dpa/fpy (iron) will be achieved in a volume of about 0.5 litre. The HFTM should principally allow irradiation temperatures between about 250 and 1023 ^{0}C [1]. For the near-term design this range is restricted to 250 to 650 ^{0}C. The deviations from the temperature specified for a test unit (rig) should be as small as possible.

After the completion of the Conceptual Design Activity (CDA) of IFMIF in 1996 [1], a second phase of work was carried out in 1997/98 which was called Conceptual Design Evaluation (CDE), [2]. The activities of this phase were mainly concentrated on design improvements, on an evaluation of instrumentation tools, and on detailed neutronics calculations. Special emphasis was put on the validation and improvement of a helium cooled HFTM. As a result the CDA design concept of the HFTM was basically confirmed, but some modifications were carried out in particular with respect to the hydraulics and the design of the rigs. The revised design of the HFTM had 27 vertical rigs arranged in three rows with 9 rigs each. The helium is streaming upward from the bottom to the top of the rigs cooling two sides of the test module. A single-rig test module was designed and fabricated to verify the key parameters of the helium cooled concept. The testing of this module and the subsequent detailed evaluation including extensive numerical analyses was continued until the end of 2000 [3]. It was found that the determination and the control of the temperature in the testing region is much more complicated than anticipated. Effects like small thermal bridges, clearances, thermal expansions, deformations etc. are of importance and have to be taken into account. Significant space is needed to accommodate the necessary thermal insulation and electrical heating. This reduces the volume available for the material to be irradiated. The lessons learned from these investigations, and the intention to increase the usable irradiation volume led us to the decision to further optimise the conceptual design of the HFTM maintaining the acknowledged basic features. The work was restricted to the lower section of the HFTM (subsequently addressed as “test section”) containing the rigs with the material specimens, the

surrounding reflector, and the helium supply line. The optimised concept (rigs shaped like chocolate plates) used as working basis is the result of a series of initial design, manufacturing, and thermal hydraulic studies which are briefly described in Annex 1. The work consisted of three parts: the design, the overall thermal-hydraulic analysis of the test section, and the detailed thermal-hydraulic analysis of the rigs with the specimens. The results of these activities are presented in this report.

2. Objectives and boundary conditions of the design

2.1 General design requirements

The design of the HFTM test section is basically determined by requirements derived from the test objectives and from the features of the test machine. The main requirements can be summarised as follows:

- The available test volume should be used to the maximum possible degree, i.e. the packing density of the specimens in the test section should be as high, or respectively, the volume occupied by structural parts, heaters, isolation, cooling channels, etc., as low as possible.
- The specimens have to be kept at temperatures between 250 and 650 ^{0}C.
- The deviations from the target temperature within a rig should be as low as possible. A range of +/- 10 to 15 K is considered as reasonable.
- The irradiation temperature should be kept constant during beam intensity variations and beam-off periods, i.e. electrical heating is required.
- To avoid uncontrollable temperature variations, all clearances, tolerances, thermal expansions etc. should be accommodated in such a way that the components of the test section are always in a defined and reproducible configuration.

2.2 Irradiation volume

Corresponding to the preceding design studies [1,2, 4], the dimensions of the HFTM irradiation volume were initially chosen as follows:

- in the beam direction (z-axis): 5 cm
- perpendicular to the beam (beam footprint): 20 cm in horizontal direction (x-axis) and 5 cm in vertical direction (y-axis).

As the nuclear calculations showed a significant neutron flux also outside the footprint it was decided to enlarge the vertical extension of the irradiation volume to about 8 cm which allows e.g. to pile-up three tensile test specimens of 27 mm in length. This provides additional irradiation capacity with lower, but nevertheless, interesting damage rate. Furthermore, the HFTM is laterally (x and y-direction) surrounded by a 10 cm thick reflector.

2.3 Power density

Nuclear calculations have been carried out for the geometry described in Sect. 2.2 assuming a void fraction in the irradiation volume of 20 % which corresponds to an average steel density of 6.4 g/cm^3 [5]. The power density distribution calculated for 250 mA accelerator current and with EUROFER reflector is shown in Fig. 1. It is between 3.9 W/g at the central beam impact point (x = y = z = 0) and about 1.17 W/g at the rear corner points (x = 10 cm; y = 2,5 cm; z = 5 cm). With the assumed void fraction of 20 % this corresponds to a volumetric power generation rate between 25 W/cm^3 and 7.5 W/cm^3, respectively. The above values are not significantly affected by replacing the helium in the void by a liquid metal (Na or NaK) [6].

2.4 Cooling of the HFTM

The HFTM is cooled by helium at low pressure (0.3 MPa at the inlet) and low temperature (about 323 K at the inlet), see Sect. 4.2. Helium was selected because it is inert, does not undergo nuclear and chemical reactions, and has – compared to other gases - a high cooling capacity. Low pressure is important to avoid excessive mechanical loads to the structures, although a higher pressure would be desirable to reduce the coolant velocity and hence, the pressure drop. The low inlet temperature is necessary to realise the low irradiation temperatures. The temperature rise of the coolant inside the HFTM should be in the range of 30 K. The flow direction is downward in the helium supply duct, and upward in the test volume.

3. Description of the design

The optimised design of the HFTM test section with chocolate plate rigs is shown in Fig. 2. Based on preliminary hydraulic calculations (see Sect. 4.2) a single rectangular duct with a cross section of 52 x 88 mm has been chosen for the helium flow to the test section. It is positioned asymmetrically at one side of the test section. The uniform feeding of helium to the rigs is improved by two baffles inserted in the 180^0 bend joining the ducts with downward and upward flow. The lateral reflectors are integral parts of the container housing the test rigs. Helium cooling of the reflectors is provided by a bypass to the main flow. The lower axial reflector is a single block with appropriate channels to lead the helium flow to the rigs. The upper axial reflector is split into 12 single parts according to the number of rigs. The outer shape is selected such that cooling channels of the necessary dimensions are generated. Holes in the blocks allow the insertion of thermocouples and heater wires.

Fig. 3 shows a horizontal cross section of the test section (x,z-plane) in the region of the irradiation zone. It consists of a container with an inner cross section of 203 x52 mm and the two lateral reflectors. In the y-z plane the container is divided into four compartments by stiffening plates serving to stabilise the container walls. Each compartment is filled with 3 rigs. The rigs have an outer cross section of 49x16 mm. Cooling channels are provided at all sides of the rigs with a width of 1.0 mm at the large sides and of 0.5 mm at the small sides. The dimensions of the cooling channels are assured by small vertical ribs at the corners and the side walls of the rigs. The attachment of the rigs inside the container is not yet included in the design.

Details of the rig design are shown in Fig. 4. They consist of the outer housing (rig wall) and the inner capsule containing the specimens separated by a thermal insulation with a thickness of 1.35 mm at the large side and 1 mm at the small side. The capsule has an inner cross section of 40x9.3 mm. This allows a rather dense arrangement of most of the envisaged test specimens (see Fig. 2). Electrical heaters are wrapped around the capsule in horizontal windings. This concept will lead to temperatures of the capsule close to the irradiation temperature of the specimens, whereas the rig wall is at about the level of the helium temperature.

The length of the rig without the upper reflector is 144 mm. The capsules have a length of 125 mm and are closed by two cup-shaped caps giving the testing zone a

length of 81.5 mm. This includes 0.5 mm for the accommodation of thermal expansion differences. The capsules are filled with a liquid metal (Na or, if possible NaK) to increase the thermal contact between the specimens and the capsule walls (see Sect. 4.3). The upper cap has two holes connecting the test zone with the NaK expansion volume of about 20 mm length located at the top end of the rig. To facilitate filling of the capsule with NaK to a defined level, two tubes are provided at the top side of the expansion tank. One of these tubes dips into the tank to the envisaged filling level, the other one ends at the top plate. The filling level is established by at first filling the tank completely, and then blowing out the surplus NaK via the dip tube by applying a gas pressure to the other one. Finally, both tubes have to be cut and sealed. The volume of the expansion tank and the filling level have been determined taking into account the NaK volume, the filling temperature and the operating temperature.

The main design problem of the rigs is to realise the specified level and constancy of the irradiation temperatures. The maximum thickness of the capsule (in z-direction) is given by the power density and the thermal conductivity of the specimens/NaK mixture in connection with the allowable maximum temperature difference across the specimens. This consideration leads to a maximum thickness of about 10 mm for the first row of rigs. At the rear side of the HFTM the capsule thickness can be larger according to the decrease in power density, but in order to minimise the design and manufacturing effort it was decided to use identical dimensions for all rigs. Taking into account the dimensions and possible arrangements of the specimens (see Fig. 3), 9.3 mm has been chosen as internal capsule widths.

Of cause, the specified constancy of the specimen temperature must likewise be achieved in the two other directions, i.e. x and y. The latter is of particular importance because of the large variation in the power density, the coolant temperature rise and heat transfer coefficient variation along the flow channel. Different solutions have been studied, e.g. variable thermal insulation, or compensation by electrical heating (see Annex 1). The latter way was finally adopted mainly for the following two reasons:

a) This solution allows the use of a uniform thermal insulation with the advantage of easier manufacturing.
b) Electrical heating is necessary in any case to maintain the temperature during beam-off periods.

In detailed analyses (see Sect. 4.3) it was found that three sections with different but constant heating power are necessary and sufficient to reach the desired temperature constancy. The upper and lower heaters are continuously in operation, whereas the middle section may be operating during beam-off periods only. In order to allow the compensation of uncertainties in the temperature prediction, individual power supply and control of each section is required.

Mineral insulated wires of 1 mm diameter are envisaged as heating elements. To assure sufficient thermal contact, they have to be attached to the capsules by brazing them into grooves. The sectioning of the heating necessitates horizontal winding (in the x,z-plane) of the heaters. A high density of the heaters is necessary to reach the required temperature without exceeding the specified power limits of the heaters. On the other hand the ribs between the heaters must be sufficiently large to facilitate manufacturing. Based on manufacturing trials, a distance of 1.6 mm between the heater windings has been adopted.

The thermal insulation between the rig wall and the capsules must be designed such that the irradiation temperature specified for each rig is reached in a reliable and reproducible way. It was estimated that a helium layer between about 0.1 and 1 mm thickness would fullfil the thermal requirement. However, the side walls of the rigs and the capsules with a thickness of 0.5 and 1 mm, respectively, are rather flexible and could be deflected by pressure or temperature differences. This could cause significant uncertainties in the irradiation temperature. To solve the problem two design concepts were elaborated. In the first concept, steady and constant distance and contact conditions between the rig wall and the capsule are reached by a staggered pressure decreasing from the cooling channels to the interior of the capsules. The intermediate pressure in the insulating gap between the rig wall and the capsule can be achieved by joining the gap to the helium coolant at the outlet of the rig. The low pressure inside the capsule can be established during the NaK filling procedure. As the stiffness of the rig wall is less than that of the capsule wall, the first one will be pressed via the insulation layer against the latter one. The effect may be enhanced by the support which is provided by the specimens to the inner surface of the capsule. This solution implies that the thermal insulation is able to carry the related pressure load. To achieve this, it is suggested to provide the outer surface of the capsule with a large number of equally distributed small spacers. These spacers

can be manufactured by machining off most of the ribs between the grooves needed for embedding of the heaters. E.g., a net of spacers with a spacer cross section of 0.5x0.5 mm and a distance of about 5 mm requires machining off 93% of the ribs. The effective thermal conductivity of such an insulating layer taking into account a typical contact resistance between the spacers and the rig wall is only about a factor of 1.65 higher than that of helium layer of the same thickness. The thermal conductivity can be easily modified by changing the size and/or the density of spacers.

The disadvantage of this concept is that the different thermal expansion of the outer rig and the inner capsule could lead – in connection with the contact pressure – to frictional effects and subsequent deformations of the spacers, in particular if numerous temperature cycles have to be anticipated. Therefore, this concept is mainly suggested for the lower range of the irradiation temperatures where the differential expansions are small. For the upper temperature range another concept is suggested: a plane helium gap between the rig wall and the capsule with a pressure which is higher than in the cooling channel. This can easily be realised by joining the gap and the helium coolant at the rig inlet. At these pressure conditions the rig wall is deflected toward the cooling channel. First estimates have shown that this deflection amounts to about 0.1 mm which is in the range of 10 % of the thickness of the insulation layer. This could affect the specimen temperature. The effect can be significantly reduced by increasing the thickness of the rig wall, or by providing a vertical rib in the middle of the cooling channel (already included in the design, see Fig.3).

As explained before, electrical heating is provided with three heating zones. The heaters are embedded in grooves and joined to the surface of the capsule by brazing. The grooves have a width of 1.1 mm and a distance of 1.6 mm. The six cold ends of the heaters are led to the top end of the rigs along the small sides of the capsules via vertical grooves located below the peripheral grooves. The thermocouples needed for the measurement of the specimen temperatures and the control of the electrical power supply system (two thermocouples for each heating section) are inserted into the centre of the specimen stack at the required location. They leave the capsule through sleeves, and follow then the way of the heaters to the top end of the rig.

4. Design related thermal-hydraulic analyses

4.1 Computational tool

Extensive numerical analyses have been performed to study the thermal and hydraulic conditions in the test section with the main objective to investigate the feasibility of the envisaged design and possibilities for further improvements. The tool used for these analyses was the Computational Fluid Dynamics (CFD) code STAR-CD [7]. The system comprises the main analysis code STAR, and the pre- and post-processor PROSTAR. STAR-CD operates by solving the governing differential equations of the flow physics by numerical means on a computational finite volume mesh for different types of flow phenomena, e.g. steady and transient, laminar and turbulent, incompressible and compressible, and heat transfer by convection, conduction and radiation. Problem specification is possible by a large number of boundary conditions like pressure, temperature, mass flow or velocity at the channel inlet or outlet.

The choice of a suitable turbulence model is very important for the calculation of the near-wall layers and hence, the heat transfer and pressure drop. The main turbulence models offered in STAR-CD are:

- Standard k-ε High-Re-number-Model (HRM) (linear, quadratic, cubic), in which the high (turbulent) Reynolds number forms of the turbulent kinetic energy k and its dissipation rate ε equations are used in conjunction with an algebraic 'law of the wall' representations of flow, heat and mass transfer for the near wall region.
- Two-Layer-Model (TLM), which applies the standard form of k-ε equations everywhere except at viscosity-influenced near wall flow regions where a low-Re number representation of the turbulence equations is used.
- Low-Re-number-Model (LRM) (linear, quadratic, cubic), in which general transport equations for k and ε are solved everywhere, including the near wall region.

Test calculations on the suitability of the different models for the present application led to the following results:

The HRM requires special algebraic formulae - wall functions -, to represent the distributions of velocity, temperature, turbulence, etc. within the boundary layers. The

wall function conditions for near-wall cells in the HRM (central node P of the cell nearest to the wall is assumed to be positioned at a distance of 30 to $100 \cdot y^+$) lead to a grid resolution, which is not fine enough for the modelling of the helium flow in the narrow channel. If the node P is placed too close to the wall or within the viscous layer, the utility of the wall functions is lost. For example, in the calculation of the temperature distribution the wall function does not represent correctly the wall temperature.

In the TLM the basis for switching from the standard k-ε high-Re equations to the low Re representation of the turbulence equations is the f_μ coefficient of the turbulent viscosity equation. It increases monotonically from zero at the wall to ~0.95 when viscous effects become negligible. In the small channel flow with Reynolds number values of about 10^4 the f_μ coefficient sometimes cannot reach the asymptotic value in the near-wall region, and the TLM tries to apply the algebraic ε-prescription for the whole flow across the channel. If the near-wall layer has a fixed position in the model, the calculation leads to discontinuous distribution of the turbulent viscosity value in the switching area.

Only the LRM is suitable for the simulation of the flow in a narrow channel because the general transport equations for k and ε are also solved for the near-wall regions and the equation for the dissipation rate has the additional term for Low-Re-Number effects.

The HFTM design goal “maximum space and flexibility for the specimens” means on the other hand “minimum space for the heater, coolant channels and structural material”[8]. This creates a particular feature of the design: the flow regime can vary substantially for different sections of the HFTM. As for helium inlet and outlet sections of the HFTM, the Reynolds number of the flow is Re $\cong$ 40000 – 50000, and a standard high-Re-number model can be applied for thermal hydraulic simulation. At the same time, as was mentioned before, the cooling channels of the test section are narrow flat ducts and the Reynolds number is Re $\cong$ 8000 – 10000, i.e. the flow can become laminarized in the section with the rigs. Intense heating of the gas flow in the test section can result in its additional laminarization [9,10]. The LRM is more appropriate for this part of the module. But it requires very fine meshing of the flow area and consumes much more computing time. So, if this turbulence model is used for simulation of the HFTM as a whole, the number of mesh cells is very large

(several millions) and computation time is unacceptably high. In the case considered a reasonable approach is the following: Standard high-Re-number k-ε turbulence model is used for simulation of the HFTM as a whole (Sect. 4.2). At the same time, an additional task is carried out for an individual rig with detailed simulation of the design of the rig cooled by helium flowing in the narrow flat ducts using the low-Re-number turbulence model for the hydrodynamic calculations (Sect. 4.3). Both tasks are solved as an interconnected problem.

One of the modifications of the standard HRM used in the present calculations is the Chen k-ε model [15]. In the basic k-ε model the dissipation time scale, k/ε, is the only turbulence time scale used in closing the ε equation. In Chen's model the production time scale k/P, as well as the dissipation time scale, is used in closing the ε equation. This extra time scale is claimed to allow the energy transfer mechanism of turbulence to respond to the mean strain rate more effectively. This results in an extra constant in the ε equation.

The equations for conservation of mass, momentum and thermal energy for mean flow are well known. The equations for k and ε, used in this calculations, are the following.

For the turbulence energy k

$$\frac{1}{\sqrt{g}}\frac{\partial}{\partial t}\left(\sqrt{g}\ \rho\ k\right)+\frac{\partial}{\partial x_j}\left[\rho\, u_j\ k-\left(\frac{\mu+\mu_t}{\sigma_k}\right)\frac{\partial k}{\partial x_j}\right]= \\ \mu_t\left(P+P_B\right)-\rho\varepsilon-\frac{2}{3}\left(\mu_t\frac{\partial u_i}{\partial x_i}+\rho\ k\right)\frac{\partial u_i}{\partial x_i}+\mu_t P_{NL} \qquad (1)$$

Where

$$P\equiv 2s_{ij}\frac{\partial u_i}{\partial x_j}$$

$$P_B\equiv-\frac{g_i}{\sigma_{h,t}}\frac{1}{\rho}\frac{\partial\rho}{\partial x_i}$$

$$P_{NL}=-\frac{\rho}{\mu_t}\overline{u_i'u_j'}\frac{\partial u_i}{\partial x_j}-\left[P-\frac{2}{3}\left(\frac{\partial u_i}{\partial x_i}+\frac{\rho k}{\mu_t}\right)\frac{\partial u_i}{\partial x_i}\right],$$

$P_{NL}=0$ for linear models.

$$s_{ij} = \frac{1}{2}\left(\frac{\partial u_i}{\partial x_j} + \frac{\partial u_j}{\partial x_i} \right)$$

For the turbulence dissipation rate ε:

Chen HRM

$$\begin{aligned} &\frac{1}{\sqrt{g}} \frac{\partial}{\partial t}\left(\sqrt{g}\rho\,\varepsilon\right) + \frac{\partial}{\partial x_j}\left[\rho\, u_j \varepsilon - \left(\frac{\mu + \mu_t}{\sigma_\varepsilon} \right) \frac{\partial \varepsilon}{\partial x_j} \right] = \\ &C_{\varepsilon 1} \frac{\varepsilon}{k} \left\{ \mu_t P - \frac{2}{3}\left(\mu_t \frac{\partial u_i}{\partial x_i} + \rho\, k \right) \frac{\partial u_i}{\partial x_i} \right\} + C_{\varepsilon 3} \frac{\varepsilon}{k} \mu_t P_B \\ &- C_{\varepsilon 2} \rho \frac{\varepsilon^2}{k} + C_{\varepsilon 4} \rho\, \varepsilon \frac{\partial u_i}{\partial x_i} + C_{\varepsilon 5} \frac{\mu_t^2}{\rho} \frac{P^2}{k} \end{aligned} \qquad (2)$$

LRM

$$\begin{aligned} &\frac{1}{\sqrt{g}} \frac{\partial}{\partial t}\left(\sqrt{g}\rho\,\varepsilon\right) + \frac{\partial}{\partial x_j}\left[\rho\, u_j \varepsilon - \left(\frac{\mu + \mu_t}{\sigma_\varepsilon} \right) \frac{\partial \varepsilon}{\partial x_j} \right] = \\ &C_{\varepsilon 1} \frac{\varepsilon}{k} \left\{ \mu_t \left(P + P'\right) - \frac{2}{3}\left(\mu_t \frac{\partial u_i}{\partial x_i} + \rho\, k \right) \frac{\partial u_i}{\partial x_i} \right\} + C_{\varepsilon 3} \frac{\varepsilon}{k} \mu_t P_B \\ &- C_{\varepsilon 2}\left(1 - 0.3 e^{-R_t^2}\right) \rho \frac{\varepsilon^2}{k} + C_{\varepsilon 4} \rho\, \varepsilon \frac{\partial u_i}{\partial x_i} + C_{e1} \frac{\varepsilon}{k} \mu_t P_{NL} \end{aligned} \qquad (3)$$

where

$$P' = 1.33\left[1 - 0.3 e^{-R_t^2}\right]\left[P + 2 \frac{\mu}{\mu_t} \frac{k}{y^2} \right] e^{-0.00375\,\mathrm{Re}_y^2}$$

The turbulent viscosity μ_t is defined as

$\mu_t = f_\mu \dfrac{C_\mu\, \rho\, k^2}{\varepsilon}$ with f_m given by

$f_\mu = \left[1 - e^{-0.0198\,\mathrm{Re}_y}\right]\left(1 + \dfrac{5.29}{\mathrm{Re}_y} \right)$ for the LRM and f_μ = 1 for the Chen model

$$\mathrm{Re}_y = \frac{y\sqrt{k}}{\nu}$$

R_t is the turbulent Reynolds number given by $R_t = \frac{k^2}{\nu\,\varepsilon}$

Further parameters are

$\sqrt{g}$	determinant of metric tensor
g_i	gravity acceleration component along the i-th co-ordinate axis
x_i	Cartesian co-ordinate in stream-wise direction (i = 1,2,3)
y	normal distance from the wall
y^+	dimensionless wall distance $y^+ = y\left(\tau_w/\rho\right)^{\frac{1}{2}}\Big/\nu$
τ_w	wall shear stress
u_i	absolute fluid velocity component in direction x_i
s_{ij}	rate of strain tensor
ρ	density
μ	molecular viscosity
ν	kinematic viscosity

The constants are:

Model	C_μ	σ_k	σ_ε	σ_h	$C_{\varepsilon1}$	$C_{\varepsilon2}$	$C_{\varepsilon3}$	$C_{\varepsilon4}$	$C_{\varepsilon5}$
LRM	0.09	1.0	1.22	0.9	1.44	1.92	0.0 or 1.44	-0.33	-
Chen	0.09	0.75	1.15	0.9	1.15	1.9	0.0 or 1.4	-0.33	0.25

The calculations for the rig were carried out with the linear LRM. This model cannot calculate anisotropic effects in the turbulent flow. The non-linear normal-Reynolds-stress effects in the turbulent channel flow can lead to the occurrence of secondary flows in the corner regions of the rectangular ducts. Although the secondary flows are quite small in magnitude (ca. 1% of the axial velocity) they can influence the heat transfer in the cooling channel. The length of the vortices in corner regions normally is not larger than the channel width. Consequently in our case with a channel aspect ratio (height/length) of 0.025 the secondary flows play hardly a role in the heat transfer, i.e. the use of the linear LRM is justified.

In the calculations of gas flow with heating, there are limit conditions ("intense heating") with strong influence on turbulence and heat transfer behavior, which can

be described adequately by standard k-ε equations only up to a heating rate q^+ of about 0.003 [10]. The non-dimensional heating rate is defined as:

$$q^+ = q''_w / G \bullet C_{p,in} \bullet T_{in},$$

with:

q''_w	wall heat flux (W/m^2)
G	mean mass flux, M/A_{cs} ($kg/s \bullet m^2$)
M	mass flow rate (kg/s)
A_{cs}	cross-section area (m^2)
$C_{p,in}$	specific heat ($J/kg \bullet K$)
T_{in}	flow temperature (K)

In the Cases 3a and b (see Sect. 4.3.3) with maximal nuclear and electrical power, the maximum heating rate q^+ on the channel wall is 0,001. This means that the k-ε model can be employed for the calculation of turbulence and heat transfer without change of turbulence variables.

4.2 Integral analysis of the test section

4.2.1 Modelling

The flow laminarization reduces the mixing of the fluid in the cooling channels. Moreover, the HFTM design provides for subdivision of the irradiation zone into four separate compartments and flow mixing is impossible between them. So, if the flow distribution is non-uniform at the entry of the irradiation zone, then it is practically impossible to redistribute the cooling flow between the rigs, and between the compartments. In this respect, one of the main tasks of the thermal-hydraulic calculation is the choice of the HFTM layout at which the cooling system provides the conditions for effective cooling of the rigs. At the same time, low pressure is desirable to avoid excessive mechanical loads to the structures. Hence, the pressure loss should not be significant in the system, so that the absolute pressure is higher than 0.1 MPa everywhere in the HFTM to prevent impurity inflow to the helium loop.

The design of the HFTM test section including the rigs is described in Sect. 3. The modelling of the module is performed in accordance with this design. The model under consideration consists of the test section and the helium supply system. The irradiation zone of the module is simulated as four parallel boxes, each containing three rigs with specimens - Fig. 5,6. The isometric view of the rig is shown in Fig.7a. Its simulation is adopted taking into account the following circumstances. Naturally, it contains the irradiation zone housing the desirable number of specimens. On the other hand, the nuclear calculations show that using a reflector around the test section increases the dpa-rates in the irradiation specimens. It was found that an optimum reflector thickness is 100 mm [11]. An electrical heating system as well as the temperature control system should also be integrated in the rig design. So, the rig is simulated to consist of a central section with the specimens (section S in Fig.8), the intermediate (I) and the reflector (R) sections.

The irradiation zone, in its turn, consists of the external rig wall and internal capsule with the specimens, surrounded by electrical heaters. The gas gap (filled with helium) is foreseen between the rig wall and the capsule to provide the required temperature level for each rig. In the present model a simplified simulation of the gas gaps and electrical heaters is adopted: they are considered as layers of defined thickness with individual properties – Fig.9. The rigs are positioned with equal gaps between them. The gap width in z-direction is equal to 1 mm in sections S and I, and is equal to 2 mm in section R. The gas gaps of 0.5 mm in x-direction are also provided between the rigs and the walls dividing the irradiated section in four compartments – Fig.6a. There are special elements between the rigs designed to direct the gas flow to the cooling channels. These elements are also simulated - Fig. 6b,c. The lower reflector section is not divided in four boxes as it is done for central and intermediate ones, but it is designed as a single part. This design enables to redistribute the gas flow between the compartments with the rigs. So, the reflector section is simultaneously used as element for smoothing the velocity and pressure fields at the entry to the irradiation zone. These sections are simulated as solids with the properties of the T91-type steel [12]. It is supposed in these calculations that the section I is partially filled with helium and partially with heater and steel - Fig.7b. The specimen volume is also simulated as a solid whose properties are estimated taking into account that 20% of the volume is filled with liquid metal (properties assumed to be those of sodium) and 80% is filled with stainless steel. The properties of the regions

composed of different materials, are calculated as a combination of the properties for these materials, e.g., for a property P:

$$P = \sum_{i} x_i \bullet P_i \ ,$$

where x_i is the volume fraction of the i'th material and P_i is the property P of the i'th material. The wall material of the helium supply system and the test section is 316L-type stainless steel. The material properties used in these calculations are compiled in Table 1.

Table 1. Material properties.

Material	Property		
	Density, kg/m3	Thermal conductivity, W/(m*K)	Specific heat, J/(kg*K)
irradiation specimens (stainless steel and sodium)	6460	29.2	579
gas volume of section I, Fig.7b	0.16	0.18	5193
reflector	7650	28.8	550
electrical heater	3500	5	1000.2
gas gap, Fig. 9	0.22	0.18	5193
wall material (stainless steel)	7950	$\lambda = \lambda$ (T)	534

The cooling helium thermal conductivity and the stainless steel thermal conductivity are approximated as follows:

$$\lambda_{He} = 0.56 + 0.00031 * T$$

$$\lambda_{SS} = 10.5 + 0.015 * T$$

where T is the absolute temperature, K.

The heat source distribution due to nuclear heating in the test section and in the reflector is obtained from nuclear calculations using the MCNP code [11]. An interface program was elaborated to transfer the heat source distribution, obtained in

the nuclear calculations, to the calculation domain used in thermal-hydraulic analysis. The dimensions of the calculation domain used by the MCNP code are 250×150×75 mm for the x, y, z co-ordinate axes, respectively. For the rest of the test section volume and reflector, the heat source distribution is extrapolated assuming a law of $1/r^2$, where r is the distance along the corresponding co-ordinate axis. The obtained heat source distribution in the model due to nuclear heating is shown in Fig.10.
The helium supply system layout is chosen on the basis of preliminary calculations (see Sect. 4.2.3) and is shown in Fig.11. The difference between the variants considered is the following. The gas supply system shown in Fig.11a consists of a single tube of rectangular cross section with dimensions of 49×90 mm, a bend section and again a straight tube and a diffuser which are 100 mm and 200 mm long, respectively. The layout presented in Fig.11b has two identical gas supply tubes of rectangular cross section of 49×45 mm positioned symmetrically on both sides of the test section. The thickness of the lateral reflector is equal to 100 mm.

4.2.2 Helium flow rate

The heat deposition in the HFTM due to nuclear heating is equal to 16.6 kW. About 35% of this power are deposited in the lateral reflector. In the present study it was assumed that this heat is removed by a separate cooling system. On the other hand, at least 25% of the total heat deposition in the specimens should additionally be provided by electrical heaters. To estimate the helium coolant mass flow rate in the model simulated we restrict the temperature increment of the helium flow along the rigs to the value of ~ 30 K, to reduce the axial temperature gradient in the specimens. On the basis of this condition the coolant mass flow rate is assumed to be equal to 0.083 kg/s at the pressure of 0.3 MPa. The choice of the helium pressure is discussed later, Sect. 4.2.7. The helium velocity changes considerably in the model simulated. The flow velocity in the test section is high enough, so that the Mach number can exceed the value of 0.2 – 0.3. Under these conditions the flow compressibility should be taken into consideration. Therefore, the helium density variation as a function of the temperature and pressure is accepted and is described by the perfect gas equation of state.

4.2.3 Preliminary calculations

The first calculations were carried out using a simplified simulation of the test section as a porous medium. A lot of variants were considered which differ from each other by different length of the input section, its design and the layout of the gas supply system, Fig. 12. Three different regions indicated in Fig. 12 as R1 – R3 denote the following: Region R2 simulates the irradiation section itself as an orthotropic porous medium with permeability in the vertical direction only. Regions R1 and R3 simulate the bottom and top sections of the reflector as an isotropic porous medium. The simulation of the test section as a porous medium is indeed approximate, but such approach is reasonable at the initial stage of the investigation. It enables one to consider different variants of the HFTM layout with minimal computing time consumption and to choose the more appropriate ones for subsequent analysis. The velocity distribution in the model and pressure loss are considered as criteria for the comparison of different variants.

The baffles in the gas supply tubes are also investigated as a method to smooth the velocity distribution at the inlet to the test section. The baffles redistribute the gas flow in the input section of the model making the velocity field more smooth; at the same time they do not practically influence the pressure loss in the model. The baffle location and their influence on the velocity field are shown in Fig.13. The results are obtained for adiabatic flow. The use of the baffles can be considered as a way to reduce the length of the input section.

As was mentioned, the preliminary calculations enabled us to choose the HFTM layouts for a subsequent more detailed simulation, Fig.11. The first calculations for these layouts were carried out without heat deposition in the test section, i.e. for adiabatic conditions. Two different variants of the inlet-outlet of the test section are investigated, see Fig.14. The test section shown in Fig.14a is 40 mm longer than the one shown in Fig.14b. Nevertheless, the presence of stagnation zones at the inlet and significant recirculation regions at the outlet of the test section of the model of Fig.14b results in greater (~8%) pressure loss in it. Therefore, the geometry of the inlet-outlet parts of the test section shown in Fig. 14a is chosen for subsequent analysis.

4.2.4 Thermal-hydraulic characteristics of the module with nuclear heating

The next step of the analysis is the calculation of thermal-hydraulic characteristics of the model simulated with heat source distribution due to nuclear heating (Fig. 10).

The results of calculation show that the velocity, pressure and temperature distributions are practically identical in the test section for the layouts presented in Fig.11. Some differences are observed in the inlet sections of these models. The total pressure loss for the model with a single-tube gas supply system is ~ 2% greater than for the model with a double-tube one.

Each of these layouts has its advantages and disadvantages. So, the model with the single-tube layout has only one tube for helium supply. Hence, only one monitoring system is needed to control the gas flow rate. Furthermore, one side of the HFTM is free for other purposes with it. On the other hand, this layout has a longer inlet section and a non-symmetrical velocity distribution in this section with a small recirculation zone. However, the lower reflector sections of the rigs smooth effectively the velocity field at the inlet to the irradiation section. The double-tube layout has a shorter inlet section and creates a symmetrical velocity distribution in it. At the same time, the monitoring system is probably needed for each helium supply tube. Additionally, pipelines occupy both sides of the HFTM, which restricts the degree of freedom for other purposes with the HFTM.

The final choice of the HFTM layout will, probably, depend on other design features of the test module and on geometrical restrictions.

As the thermal-hydraulic characteristics of the test section are identical for both HFTM layouts, the calculated results obtained for the variant with a double-tube helium supply system are discussed below. It should be noted that the calculations are carried out for two different dimensions of the test section in x-direction: L = 173 mm and L = 205 mm, see Fig. 6a; the related dimensions of the rig are L1 = 41 mm and 49 mm, respectively. If L = 173 mm then the test section is positioned in the volume without significant gradient of the neutron flux [11]. On the other hand, the HFTM design goal is the maximum space and flexibility available for the specimens. Consequently, it is reasonable to enlarge the test section dimension in x-direction up to 205 mm. Some results of these calculations are discussed below.

Two different designs of spacing elements between the rigs are considered: T-shape and rectangular-shape (Fig. 6b,c). The dimension of the T-shape elements (3mm) is

chosen taking into account that a part of the rig cross section has lower nuclear heating and should be cooled less intensively to reduce the temperature gradient in the rig cross section area. The other variant is a rectangular cross section element of 1×0.5 mm; these dimensions follow directly from the cooling channel geometry chosen. The velocity distribution and pressure fields for these two variants are presented in Fig.15 (L1 = 41 mm). One can see large regions with vortexes at the outlet of the test section in case of using the T-shape elements between the rigs, Fig. 15d. These regions are much smaller for the case of rectangular elements. This results in higher (~34%) pressure loss in the test section for the case of T-shape elements, Fig. 15a,b.

At the same time it is interesting to analyse the temperature distribution in the irradiation volume for these two cases. Fig. 16 shows the temperature profile along the line o-o (see Fig.9) passing the geometric centre of the rig (rig 12 in Fig.6a is chosen for analysis as the most heavily loaded one). The calculation shows that the non-uniformity of the temperature distribution is maximum in this cross section. The temperature profile for the case of L1 = 49 mm is also presented for comparison (line 3 in Fig. 16). One can see that the difference between maximal and minimal temperature is different for these two cases, but this difference is insignificant, it is ~2°C lower for the case of T-shape elements. The temperature level is also ~3°C lower for the case of T-shape elements because the coolant velocity and heat transfer intensity is higher for this variant at the same mass flow rate.

Taking into account the pressure loss in the test section as well as the temperature distribution in the rigs, the variant with rectangular elements between the rig is chosen as more preferable and is used for subsequent calculations. Moreover, the results discussed below are obtained for the rig dimension L1 = 49 mm (L = 205 mm).

As was mentioned, the main task of this section is the thermal-hydraulic analysis of the HFTM, i.e. choice of the geometry at which the velocity and pressure distribution in the model are optimum for effective cooling of the rigs with the specimens. At the same time, an attempt is undertaken to take into account the thermal loads in the model due to nuclear and electrical heating. Some results of thermal calculations were also discussed. Not all details of rigs are simulated in the model considered; so, the temperatures may be overestimated because of these circumstances. In this

sense the thermal characteristics discussed in this section can be considered rather qualitative than quantitative.

Fig. 17 shows the heat flux distribution, the temperature profile along the line a-a (Fig. 9) and the temperature field in the x,y-plane passing the geometrical centre of the rig for the most heavily loaded one (rig 12 in Fig. 6a). One can see a considerable non-uniformity of these characteristics. This fact can result in a significant temperature gradient in the irradiation section. It is also evident that the desirable temperature level of 650°C is not achievable with nuclear heating only. So, with a helium gap of 0.5 mm in the rig electrical heating is needed to achieve the required temperature in the rigs and to reduce the temperature gradient.

4.2.5 Influence of electrical heating

The location of the electrical heaters and their lengths is shown in Fig.7b (item No. 9). The geometrical data as well as the electrical heater power were obtained from the special analysis of an individual rig with detailed simulation of its design (see Sect. 4.3). Three different conditions of electrical heating are simulated:

- nuclear heating together with bottom and top heaters to minimise the temperature gradients in the irradiation volume,
- nuclear heating together with all the heaters to minimise the temperature gradient in the irradiation volume and to achieve the required temperature level,
- electrical heating only using all the heaters.

The volumetric heat generation rate of electrical heaters for all these variants are summarised in Table 2 (see Sect.4.3). These values are applied to the heaters in all rigs.

Some results of the calculation are shown in Figs. 18 and 19. These results are presented for the most heavily loaded rig. The temperature field and temperature profile along the centreline (line a-a in Fig. 8) of the rig presented in Fig. 18 demonstrate the influence of the top and bottom heaters. One can see that the temperature of the irradiation volume becomes smoother in comparison with the condition of the nuclear heating only. The temperature level is increased, but it does not reach the required value of 650°C even for the hottest rig. The helium flow removes more heat from the model, and the He temperature rises. This results in a

rise of velocity and pressure loss: the pressure loss is 3.6% higher than for the case of the nuclear heating only.

Table 2. Volumetric heat generation rate of electrical heaters, W/m^3

Condition	Heater		
	bottom	middle	top
Nuclear heating with top and bottom heaters	$7.4*10^7$	-	$7.1*10^7$
Nuclear heating with all heaters	$1.58*10^8$	$9.0*10^7$	$1.49*10^8$
Electrical heating only	$2.06*10^8$	$1.99*10^8$	$1.94*10^8$

An attempt to increase the temperature level in the rig by increasing the power of the top and bottom heaters results in distortion of the temperature field and an increase of the temperature gradient. So, to reach the required temperature level of the specimens the heat generation of all three electrical heaters is applied to the rigs. Fig. 19a shows that the temperature level is high enough and the temperature field remains smooth in the rig. The pressure loss for this case is 8.7% higher than under the condition of the nuclear heating. The temperature distribution with electrical heating only is also presented in Fig. 19a. One can see that the required temperature of the rig is maintained. Finally, the heat flux distribution along the Y-axis is shown in Fig. 19b for all the cases with electrical heating. The heat flux is not constant in the irradiation section but its profile results in a sufficiently smooth temperature distribution in the region of interest with low temperature gradients.

4.2.6 Cooling of the reflector

The axial reflector of the HFTM is cooled directly with the main coolant flow. As for the lateral reflector, initial calculations were carried out without cooling. An example of the temperature distribution for these conditions is presented in Fig.20a. One sees that the temperature of the reflector is substantially higher than the temperature of the sections with the specimens. Cooling the lateral reflector can be done either with a separate cooling system or with a system integrated in the main one. In the model simulated the separate cooling system is considered. Cooling gas is helium at a pressure of 0.3 MPa at the entry. Firstly, it was foreseen that each lateral reflector has two rectangular cooling channels, each of 1 mm width and positioned at the distance of 20 and 50 mm from the rigs. The temperature distribution in the lateral

reflector for this case is shown in Fig. 20b. One sees the region of maximum temperature at the periphery of the lateral reflector. Then the distances of the cooling channels from the rigs were changed to 30 and 70 mm, Fig. 20c. Finally, three cooling channels were considered positioned 20, 50 and 80 mm from the rigs, Fig. 20d. The mass flow rate is chosen to be 0.00285 kg/s for each cooling channel. One can see that the maximum temperature of the reflector can be decreased substantially and the temperature distribution will be sufficiently smooth especially in case of using three cooling channels. The case of the lateral reflector cooling system integrated into the main one as foreseen in the design (see Fig. 2) should be also considered in the future as an alternative variant.

4.2.7 Choice of the gas pressure

In choosing the reference pressure of the helium flow one should take into account that the absolute pressure must be higher than 0.1 MPa throughout the model. In this case there is no impurities inflow to the helium loop from outside. The calculations have been performed for two values of the reference pressure of the helium flow: 0.3 MPa and 0.25 MPa. The results of the calculations show that with nuclear heating only the maximum pressure loss in the modelled section of the HFTM is equal to 0.063 MPa for the reference pressure of 0.3 MPa, and is equal to 0.078 MPa at the reference pressure of 0.25 MPa. Besides, the estimation shows that the pressure loss exceeds 0.1 MPa at a reference pressure of 0.2 MPa. Therefore, taking into account some uncertainties of the calculations and a certain margin against the lower limit of the pressure in the helium loop, it is reasonable to choose a reference pressure in the cooling system of at least 0.25 MPa. The reference pressure of 0.3 MPa has been used in these calculations.

4.3 Analysis of the rig

4.3.1 Modelling

The three-dimensional model used in the analyses (see Figs. 21 and 22) represents basically the design of the rig shown in Fig. 4, but with the following simplifications:

- The interior of the capsule is modelled as a homogeneous mixture of steel specimens (80 %) and NaK (20 %) with a thermal conductivity of 25 W/mK and a density of 6.42 g/cm^3.
- The electrical heaters are represented as a homogeneous plane layer of 1 mm thickness with properties corresponding to a mixture of steel and alumina (thermal conductivity 5 W/mK, density 3.5 g/cm^3).
- The thermal insulation between the rig wall and the capsule is modelled as plane gap of 0.5 mm thickness. The thermal conductivity of the gap is chosen according to the conductivity of a helium layer of the envisaged thickness.
- The spacer ribs at the large side walls of the rig are not yet included in the model.
- Symmetry is assumed with respect to the x,y and y,z-plane. Consequently, only half of the cooling channel at the large side of the rig is part of the model. At the small side, the symmetry plane splits the stiffening plates of the container into two halves with only one half and the full small cooling channel being included in the model. Figs. 21 and 22 show one quarter of the model according to these symmetry conditions.

The principal dimensions of the model are as follows:

- Length of the specimen stack: 81 mm.
- Thickness of the specimen stack: 9.3 mm, thickness of the rig 14.9 mm.
- Width of the specimen stack: 40 mm.
- Length of the electrically heated section: 120 mm
- Length of the rig: 138 mm.
- Length of the model: 154 mm; i.e. short sections of the upper and lower reflector are included in the model.
- Width of the cooling channels: 1 mm at the large side wall and 0.5 mm at the small side wall of the rig; 2 mm in the reflector regions.

4.3.2 Initial and boundary conditions

With respect to heating and cooling, the following conditions have been applied:

- Nuclear power density distribution in y-direction according to the nuclear calculations see Fig. 1 [5]; the power variation in x- and z-direction has been

ignored. The power generation in other materials than the test specimens has been determined by multiplying the calculated values with the corresponding density ratio; i.e. for massive steel a factor of 1.25.

- He conditions at the model inlet: temperature 50 ^{0}C, pressure 0.3 MPa, mass flow rate 9.5 g/s per rig.
- Natural convection and radiation inside the insulation gaps has been ignored.

4.3.3 Results

In total a number of 9 cases has been analysed. The applied mesh is shown in Fig. 22. The main parameters and results are compiled in Table 3. The parameters changed against the previous case have been marked by bold printing.

Table 3: STAR-CD Thermal-hydraulic Calculations: Parameters and Main Results

Case	1a	1b	2	3a	3b	4a	4b	5a	5b
Parameters									
Eff. He gap size (mm)	0.5	0.5	0.5	0.5	0.5	**0.8**	0.8	**0.25**	**0.25**
Lower cap	thin	**thick**	thick	thick	thick	thick	thick	thick	thick
Heating	nucl.	nucl.	**nucl./el**.	nucl./el.	**el.**	el.	**nucl./el.**	nucl./el.	**el.**
El. power in section									
upper (W/cm^3)	-	-	71	**149**	194	147	108	65	111
middle (W/cm^3)	-	-	-	**90**	199	148	39	-	118
lower (W/cm^3)	-	-	74	**158**	206	154	110	70	124
Results									
Fig. No.	23	24	25 to 30	31	32	33	34	35	36
Max. spec. temp.(^{0}C)	403	404	465	650	655	650	650	337	339
Max. temp. diff. in specimens (K)	121	121	30	31	35	13	22	33	33
Max. Helium velocity (m/s)	478	479	504	550	547	514	518	501	499
Stat. press. drop (MPa)									
-modelled section	0.086	0.086	0.089	0.095	0.095	0.091	0.092	.089	0.089
-rig only	0.053	0.053	0.056	0.06	0.06	0.057	0.058	0.055	0.055

Case 1a and 1b

In Case 1a an insulation gap equivalent to a of 0.5 mm thick helium layer and nuclear heating only were assumed. The lower cap was assumed to have a thickness of 2 mm as originally planned. It should be recalled that the dimensions of the specimen stack are: 40 mm in x-direction, 81 mm in y-direction, and 9.3 mm in z-direction. The overall temperature distribution (top of Fig. 23) is predominantly determined by the nuclear power distribution. The temperature varies between about 400 ^{0}C in the mid plane and 282 ^{0}C at the top and bottom plane. This difference of 118 K is much larger than the specified temperature variation, which shows that compensation by electrical heating is mandatory. The temperature variation in the horizontal (x,z-) planes amounts to 9 K at the top and 20 K at the bottom. The lower value at the top – which is in the order of the temperature variance specified for the specimens – is a consequence of the good thermal conductivity of the NaK pool at the top of the rig. To achieve at the lower end of the rig similar heat conduction conditions as at the upper end, the thickness of the lower steel cap was increased from 2 to 20 mm as shown in Fig. 22. The result of the calculation with the modified model (Case 1b) is shown in Fig 24. The temperature variation at the bottom plane is now about 10 K as at the top plane. As this design modification can easily be realised, it was adopted for all subsequent calculations.

Case 2

Subsequently, several trial calculations were carried out to determine the segmentation of the electrical heaters and the level of the electrical power. The optimum temperature distribution (Case 2) is obtained when the heater is divided into three sections of the following lengths: upper section 36 mm, middle section 50 mm, lower section 34 mm; see Fig. 22. The electrical power density is 71 W/cm^3 in the upper section, and 74 W/cm^3 in the lower section. Electrical heating in the middle section is not necessary. The overall temperature distribution in the rig is shown in Fig. 25. Two distinct temperature ranges can be recognised: the rig with temperatures between about 50 and 100 ^{0}C, and the capsule including the specimens with temperatures between 318 and 468 ^{0}C. It is interesting to point out that the maximum temperature is now 65 K higher than in Case 1b although only the two end sections are additionally heated. The temperature distribution of the specimens is presented in Fig. 26. The temperature in the central plane (y=0) ranges from 452 to 465 ^{0}C, i.e. the

difference amounts to 13 K which is in agreement with the specification. Temperatures below 450 ^{0}C appear only at the upper and lower end of the specimen column. Limitation of the temperature difference to 15 K would reduce the usable length of the specimen column to 66 mm (see bottom of Fig. 26). This is still about 30 % larger than the height of the beam footprint, i.e. the gain against the previous test volume is significant.

Figs. 27 to 30 show some details related to the thermal hydraulics of Case 2. Due to the pressure drop and the resulting expansion, the helium temperature decreases initially in the inlet section of the cooling channel: the average value in the cross section shown on top of Fig. 27 amounts to 43 ^{0}C which is 7 K below the inlet temperature. In the further course of the channel, thermal heating dominates against cooling by expansion. The average temperature in the channel outlet section (bottom of Fig. 27) amounts to 84 ^{0}C, i.e. the average temperature rise in the channel is 34 K. The local temperature rise depends strongly on the channel location and varies between 15 K and 48 K. Additionally to the coolant temperatures, Fig. 27 illustrates the dimensions of the cooling channels: 0.5 mm at the lower end of the rig (top of the figure), and 1 mm at the model outlet (bottom of the figure). It should be noted that due to the applied symmetry conditions the width of the larger leg is only half of the real dimension of 1 and 2 mm, respectively.

The near-wall helium temperature shown in Fig. 28 reflects additionally the distribution of the heat flux and the heat transfer coefficient. The maximum of 136 ^{0}C appears at the large side of the rig in the upper third of the channel. The helium velocity in the cooling channels is shown on top of Fig. 29. The distribution in the large channel is characterised by a more or less steady increase from the inlet to the outlet which is a consequence of the temperature increase and pressure decrease. The minimum value in the 1 mm wide main section is about 300 m/s, the maximum about 500 m/s. In the small channel of 0.5 mm width the velocity is about one order of magnitude less. Cross section changes cause significant vortex flows with negative velocities up to 81 m/s. The bottom part in Fig. 29 shows the pressure distribution in the cooling channels. It is characterised by a relatively steady gradient in the vertical (y-) direction. The static pressure drop in the modelled section of the rig amounts to 0.089 MPa. Fig 30 shows the heat transfer coefficient, the heat flux and the wall/coolant temperature distribution in the middle of the broad cooling channel. The heat transfer coefficient (top of Fig. 30) is characterised by a slight, almost linear

decrease in the direction of the flow in the central section of almost 120 mm length (y = - 60 to + 60 mm), and significant variations in the inlet and outlet section. The average value in the central section amounts to about 2250 W/m^{2}K. The heat flux distribution (middle of Fig. 30) is completely different from the heat source distribution: the stepwise changes of the sources at the beginning and the end of the electrically heated sections (-60; -26; +24 and +60 mm) are completely smoothed out by heat conduction inside the rig. The flat maximum in the centre of about 15*10^4 W/m^2 is determined by the nuclear power generation. The wall and helium temperature in the lower part of Fig. 30 reflect the variation of the heat flux and heat transfer coefficient, and additionally the effects of pressure changes.

Case 3a

In the next step of the analysis it was investigated whether the maximum irradiation temperature of 650 ^{0}C can be reached with the same geometry as in Case 2 by increasing the power of the electrical heaters. It is evident, that in this case heating of the middle section is necessary, too. The best temperature distribution was obtained with an electrical power of 158, 90 and 149 W/cm^3 in the lower, middle and upper section, respectively. The calculated temperature distribution in the specimens is shown on top of Fig. 31. The maximum of 650 ^{0}C is reached along the central y-axis (x = z = 0), but a significant fraction of the test volume is below 630 ^{0}C. The maximum temperature difference amounts to about 31 K. Furthermore, rather large temperature differences (97 K) appear in the rig wall (see Fig. 31, bottom). This may cause high thermal stresses.

Case 3b

In Case 3b the power level and power distribution were determined in order to obtain by electrical heating only the same temperature as in Case 3a with nuclear/electric heating. An electrical power density of 209,199 and 194 W/cm^3 was obtained in the lower, middle and upper section, respectively. The calculated temperature in the specimens is shown on top of Fig. 32. The maximum temperature amounts to 655 ^{0}C, the temperature difference in the specimens to 36 K. Both values are similar to those obtained in Case 3a. The temperature difference in the rig wall (105 K, see bottom of Fig. 32) is little larger than in the case before.

Case 4a

To reduce the large temperature difference in the specimens – in particular in Case 3b – the helium gap between the rig wall and the capsule was increased from 0.5 to 0.8 mm. The related increase in thermal insulation should reduce the electrical power, and likewise the differences of the heat flux from the capsule to the rig wall. This expectation is confirmed by the results of the analysis which are shown in Fig. 33. To reach a temperature of 650 ^{0}C with electrical heating only a power level between 147 and 154 W/cm^3 is necessary. The temperature difference in the specimens has dropped to 13 K, and in the rig wall to 60 K.

Case 4b

Case 4b corresponds to Case 4a but with nuclear and electrical heating. The temperature level of 650 ^{0}C and the optimum temperature distribution in the specimens are obtained with electrical power densities of 110, 39, and 108 W/cm^3, respectively, in the top, middle and bottom section (see Fig. 34). The temperature difference in the specimens amounts to 22 K, which is less than the difference at 465 ^{0}C with the smaller helium gap (Case 2). It may likewise be possible to improve the conditions in Case 2 by increasing the helium gap size and reducing the electrical power.

Case 5a

Case 5a is related to the lower range of irradiation temperatures. Low temperatures can be reached by reducing the thermal resistance between the rig wall and the capsule as far as possible, e. g. by conserving all ribs between the heaters at the capsule surface, and by applying the concept with the lower pressure inside the capsule. It was estimated that in this case a thermal resistance can be achieved equivalent to a helium layer of 0.25 mm thickness. The result of the STAR-CD analysis is shown in Fig. 35, on top the temperature distribution in the specimens, and on bottom in the rig wall. The electrical power in this case is 65 and 70 W/cm^3 in the top and bottom section, respectively. The specimen temperature is between 305 and 337 ^{0}C; this means that the average specimen temperature is about 70 K higher than the specified minimum temperature. The temperature difference in the specimens can be reduced by a further adjustment of the electrical power including

the middle heating section, but this would simultaneously rise the average temperature.

Case 5b

Case 5b is complementary to Case 5a – i.e. the isolating gap between the rig and the capsule corresponds to a helium layer with an effective thickness of 0.25 mm – but with electrical heating only. The electrical power has been determined such that the same temperature level is reached as in Case 5a at minimum temperature differences. From Table 3 it can be seen that power densities between 111 and 124 W/cm^3 are necessary to reach these conditions. The resulting temperature distribution in the specimens and the rig wall is shown in Fig. 36. The temperature difference in the specimens amounts to 33 K which is identical to Case 5a. The temperature distribution looks like the other cases with electrical heating only (3b, 4a): the field is almost two-dimensional with the significant variations in the x,z-plane and small differences in the y-direction. The maximum helium velocity and the static pressure drop are practically the same as in Case 5a.

5. Layout of electrical heaters

The electrical heater requirements are determined by the maximum electrical power, i.e. the case with the maximum temperature and electrical heating only. Assuming that a larger helium gap will be approved for the upper temperature range, Case 3b can be ignored, and Case 4a is prevailing with power densities between 147 and 154 W/cm^3 (see Table 4). From the power density the specific heater power can easily be calculated using the superficial heater density of 6.25 cm/cm^2 corresponding to the heater distance of 1.6 mm. The latter value likewise determines – together with the length of the heating sections (see Fig. 22) – the number of heater windings and – together with the circumference of the capsule - the heater length. With the specific heater resistance of 12.5 Ω/m the heater power, voltage and current can then easily be determined.

Critical parameters of the envisaged type of heater are the specific power and the voltage with maximum values of 2.37 W/cm and 191.5 V. respectively, in the middle section. According to the recommendations of the heater manufacturer [12], at a

specific power above 1.5 W/cm optimum thermal contact conditions between the heater and the base material is necessary. This confirms the decision to braze the heaters into grooves. The heater voltage is almost by a factor of 2 higher than the maximum voltage of 100 V recommended for heaters of 1 mm diameter. This problem can be solved by using a special power supply system consisting of two continuous current units (voltage U each) arranged in series [13]. This allows to operate the heater between +U and –U, i.e. with 2xU, whereas the voltage against ground which is considered as critical is only 1xU. With this arrangement even a small power margin of 9 % would be given without exceeding the maximum recommended voltage difference to ground.

Table 4: Data of Electrical Heaters (Case 4a)

Section	top	middle	bottom
Power density (W/cm^3)	147	148	154
Spec. power (W/cm)	2.35	2.37	2.46
Section length (cm)	3.6	5.0	3.4
No. of windings	22.5	31.25	21.25
Heater length (cm)	253.4	351.9	239.3
Resistance (Ω)	31.7	44.0	29.9
Heating power (W)	596	833.4	589.6
Voltage (V)	137.4	191.5	132.8
Current (A)	4.34	4.35	4.44

6. Summary and conclusions

The thermal-hydraulic analyses carried out in the frame of the present work confirmed the potential of the CFD code STAR-CD for the thermal hydraulic analysis of complex systems like the HFTM. However, careful selection of an appropriate turbulence model is necessary. The small size of the cooling channels inside the irradiation zone requires the use of the Low Reynolds number Model of STAR-CD with the consequence of fine meshing and high computing times. The application of the same turbulence model to the whole test section would lead to a very large number of mesh cells and unacceptably high computing time. These circumstances led to the

separation of the analysis in two parts: the integral analysis of the test section with a rather coarse meshing using the standard high-Reynolds-number k-ε turbulence model, and a detailed analysis of a single rig using the low Reynolds model. The obtained results, in particular with respect to heat transfer, velocity distribution and pressure drop, are reasonable. Nevertheless, experimental confirmation is desirable. Suitable experiments are under preparation [5].

The detailed analysis of the rig has confirmed the feasibility and suitability of the optimised design of the HFTM test section with rigs shaped like chocolate plates. In particular it has been shown that the envisaged irradiation temperatures can be reached with acceptable temperature differences inside the specimen stack. The latter can be achieved only by additional electrical heating of the axial ends of the capsules. Division of the heater in three sections with separate power supply and control is necessary. Maintaining of the temperatures during beam-off periods likewise requires electrical heating. The remaining temperature differences in the specimens depend on the extent of thermal insulation between the rig wall and the capsules. The better the thermal insulation, the lower is the temperature difference. Consequently, the temperature differences in the capsules at high temperatures - which require more thermal insulation - are less than those in capsules with low temperatures.

The adjustment of the specified temperature requires careful design of the thermal insulation between the capsules with the specimens and the helium cooled walls of the rig. The most suitable solution for the upper temperature range is the separation by a helium gap of up to 0.8 mm width. For the low temperature range direct contact between the capsule and the rig wall is suggested, eventually with spacers machined out of the webs between the heater grooves at the surface of the capsules. Defined contact conditions and stable geometry can be assured by defined pressure differences between the single components. To reach the lowest temperature (250 ^{0}C) it may be necessary to fill the gap between the rig wall and the capsule with either a liquid metal, e.g. NaK as inside the capsule, or with a solid metal like a braze. The feasibility of such a concept should be investigated. To confirm the assumption made on the thermal conductivity of the contact faces and layers between the two shells of the rig, dedicated experiments are suggested.

The available space and the required power density prohibits the installation of redundant electrical heaters. Consequently, failure of one electrical heater means

loss of constancy of the temperature of the specimens during irradiation and in particular during beam-off periods. The envisaged operational data of the heaters are within the specified limits. Nevertheless, a qualification program should be carried out to assure sufficient reliability.

The integral thermal-hydraulic analysis of the test section has shown that the chosen test section and rig design and layout effectively smooth the velocity and pressure distribution in the irradiation section. This creates favourable conditions for the cooling of the module as a whole. Due to the parallelism of the different activities, the design and the thermal hydraulic analyses are not yet fully harmonised. The remaining minor discrepancies – which are not expected to affect the results of the present study in general – have to be eliminated in the next step of work.

The present work must be complemented by the thermal mechanic analysis of the module. Most critical component in this respect seems to be the rig wall. Furthermore, it will be necessary to investigate the response of the HFTM to power transients, and to determine the requirements on the electrical heating control system. This can be done only when information has become available on possible accelerator transients and on the helium cooling system layout.

References

[1] M. Martone (Ed.): IFMIF International Fusion Materials Irradiation Facility, Conceptual Design Activity, Final Report, IFMIF CDA Team, ENEA Frascati, Report ENEA-RT/ERG/FUS/96-11, Dec. 1996.

[2] MÖSLANG, A.; [HRSG.]:
IFMIF - International Fusion Materials Irradiation Facility. Conceptual design evaluation report. A supplement to the CDA by the IFMIF TEAM.
Wissenschaftliche Berichte, FZKA-6199 (Januar 99).

[3] HEINZEL, V.; DOLENSKY, B.; FISCHER, U.; GORDEEV, S.; MÖLLENDORF, U.VON; SCHLEISIEK, K.; SIMAKOV, S.P.; STRATMANNS, E.:
Design optimization of the IFMIF high flux test module. 10th Internat. Conf. on Fusion Reactor Materials (ICFRM-10), Baden-Baden, October 14-19, 2001.

[4] A. Möslang et al.: Suitability and Feasibility of the International Fusion Materials Irradiation Facility (IFMIF) for Fusion Materials Studies. Nucl. Fusion Vol. 40 No. 3Y (2000) p. 619 – 627.

[5] HEINZEL, V.; FISCHER, U.; DOLENSKY, B.; GORDEEV, S.; SCHLEISIEK, K.; SIMAKOV, S.P.; SLOBODTCHOUK, V.; STRATMANNS, E.:
Lay-out activities for the IFMIF high flux test module.
Proc.of the 6th Internat.Symp.on Fusion Nuclear Technology (ISFNT-6), San Diego, Calif., April 7-12, 2002. Fusion Engineering and Design, 63-64(2002) S.47-52.

[6] St. Simakov: Personal communication.

[7] STAR-CD Version 3.15 User Guide, Computational Dynamics Limited (2001).

[8] IFMIF-Key-Engineering Phase – Technical Meeting on Target & Test Facility Systems, September 19-20, 2000, ENEA-Brasimone, Italy. Book of presentations edited by B. Ricardi, ENEA CR Frascati, October 2000.

[9] A. Mohsen Shehata, Donald M. McEligot: Mean structure in viscous layer of strongly-heated internal flows. Measurements. International Journal of Heat and Mass Transfer 41 (1998) 4297-4313.

[10] Dariusz P. Mikelewicz, A. Mohsen Shehata, J. Derek Jakson, Donald M. McEligot. Temperature, velocity and mean turbulence structure in strongly heated internal flows. Comparison of numerical predictions with data. International Journal of Heat and Mass Transfer 45 (2002) 4333-4352.

[11] SIMAKOV, S.P.; FISCHER, U.; HEINZEL, V.; MÖLLENDORFF, U. VON:
International fusion material irradiation facility (IFMIF): neutron source term simulation and neutronics analyses of the high flux test module.
Wissenschaftliche Berichte, FZKA-6743 (Juli 2002).

[12] J.H. Fokkens. HCPB Submodule Design. Material Parameters. Report ECN Nuclear Research 71477/NUC/JF/mb/016286, September1998.

[13] THERMOCOAX SAS, 61430 Athis de l'Orne, France.

[14] G. Schmitz: Personal communication.

[15] Chen, Y.S., Kim, S.W.. Computation of turbulent flows using an extended k-e turbulence closure model. NASA CR-179204 (1987)

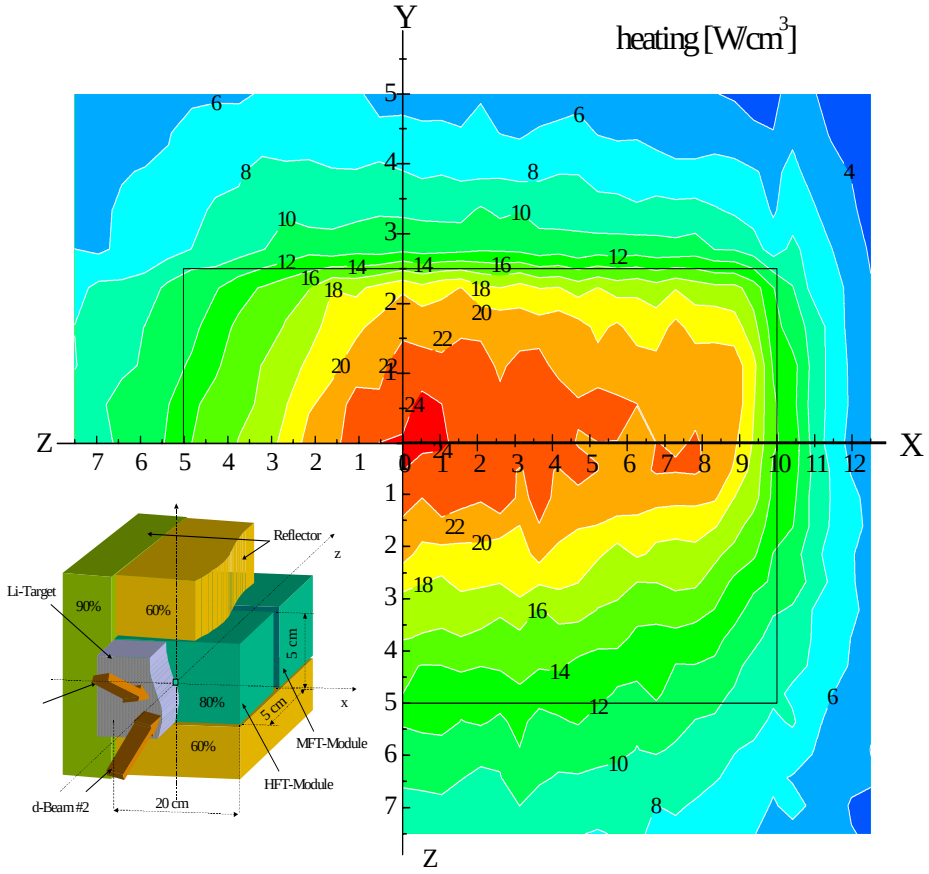

Fig. 1. Heat production in and around the HFTM with EUROFER reflector of 10 cm thickness (bottom left). Black lines show geometrical boundaries of the reference test module (20×5×5 cm^3)

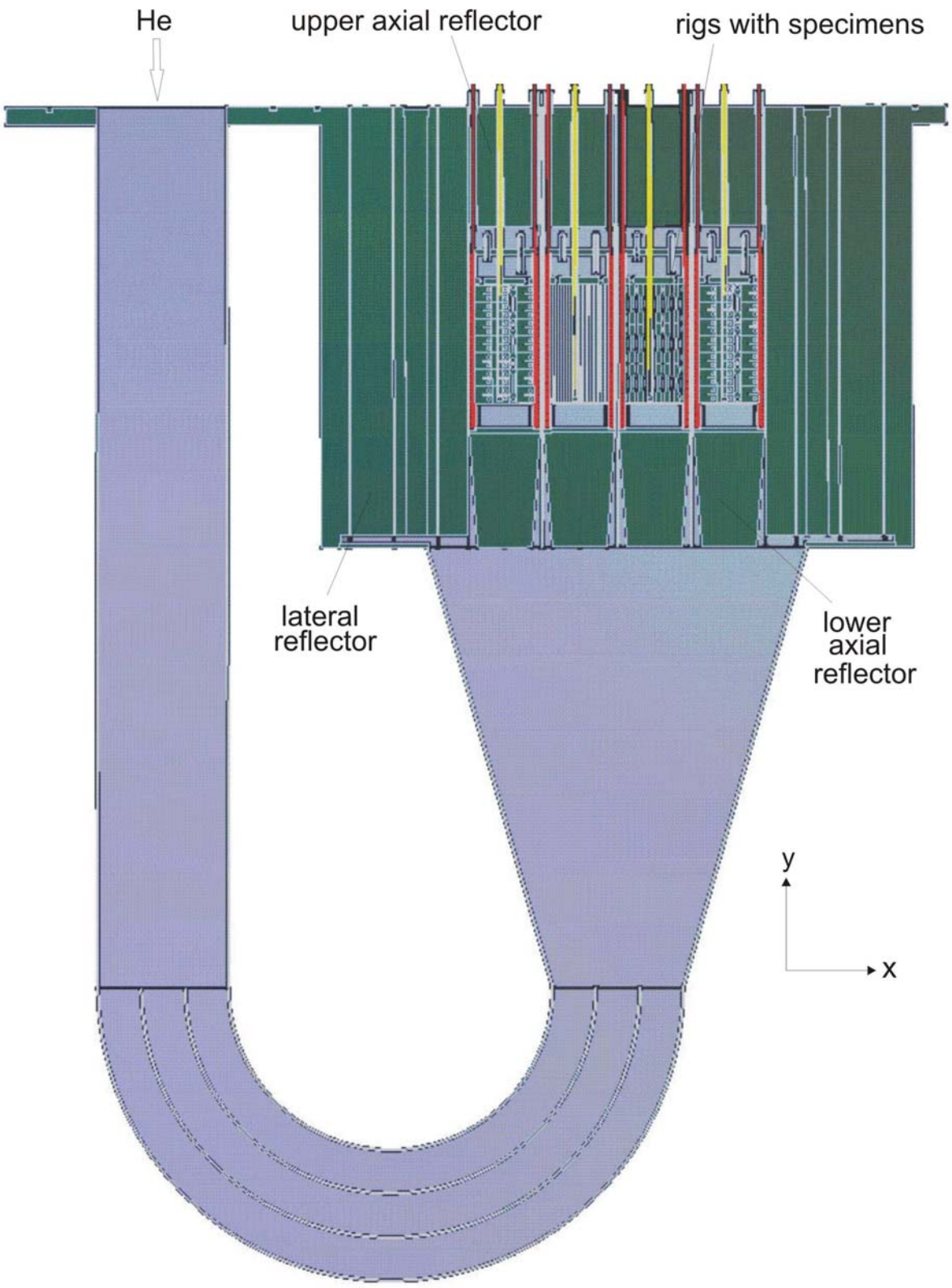

Fig. 2. IFMIF Helium cooled High Flux Test Module (HFTM)

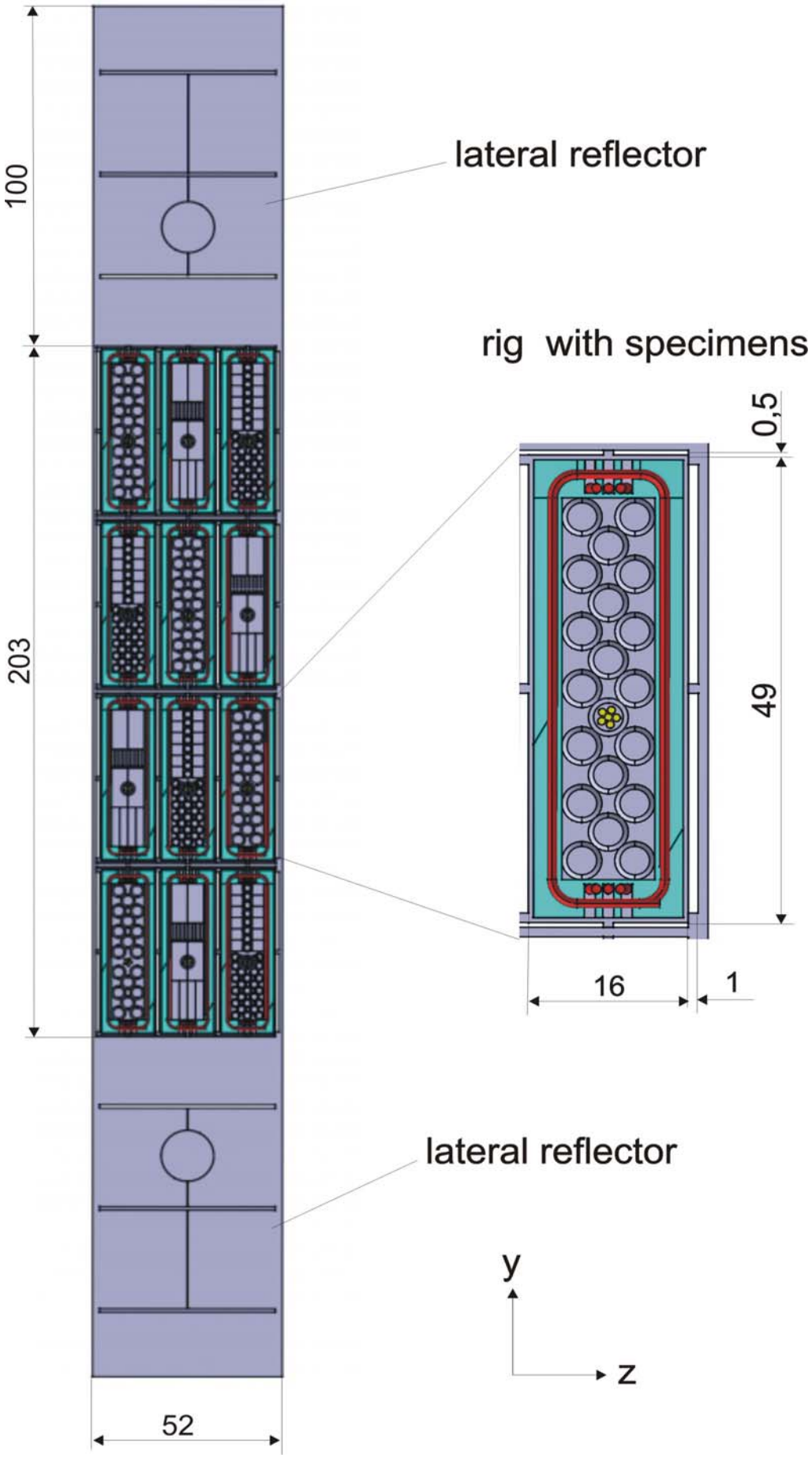

Fig. 3. High Flux Test Module cross section

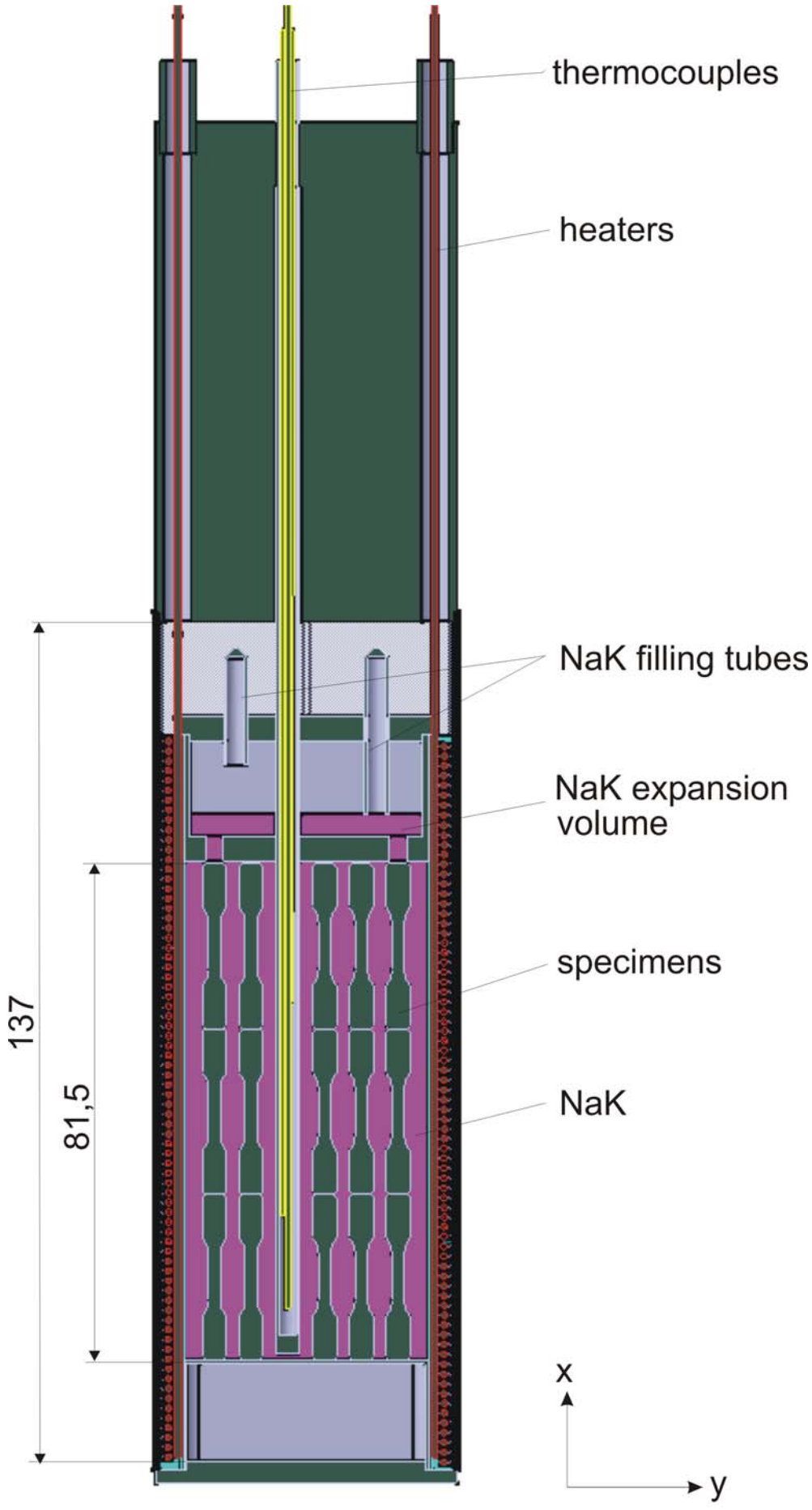

Fig. 4. Test rig with specimens

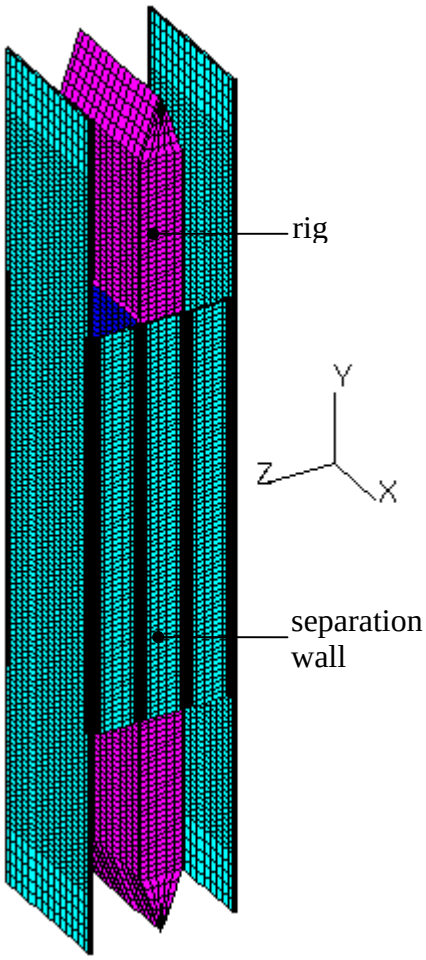

Fig.5. Isometric view of the test section (part of the section containing one box with one rig).

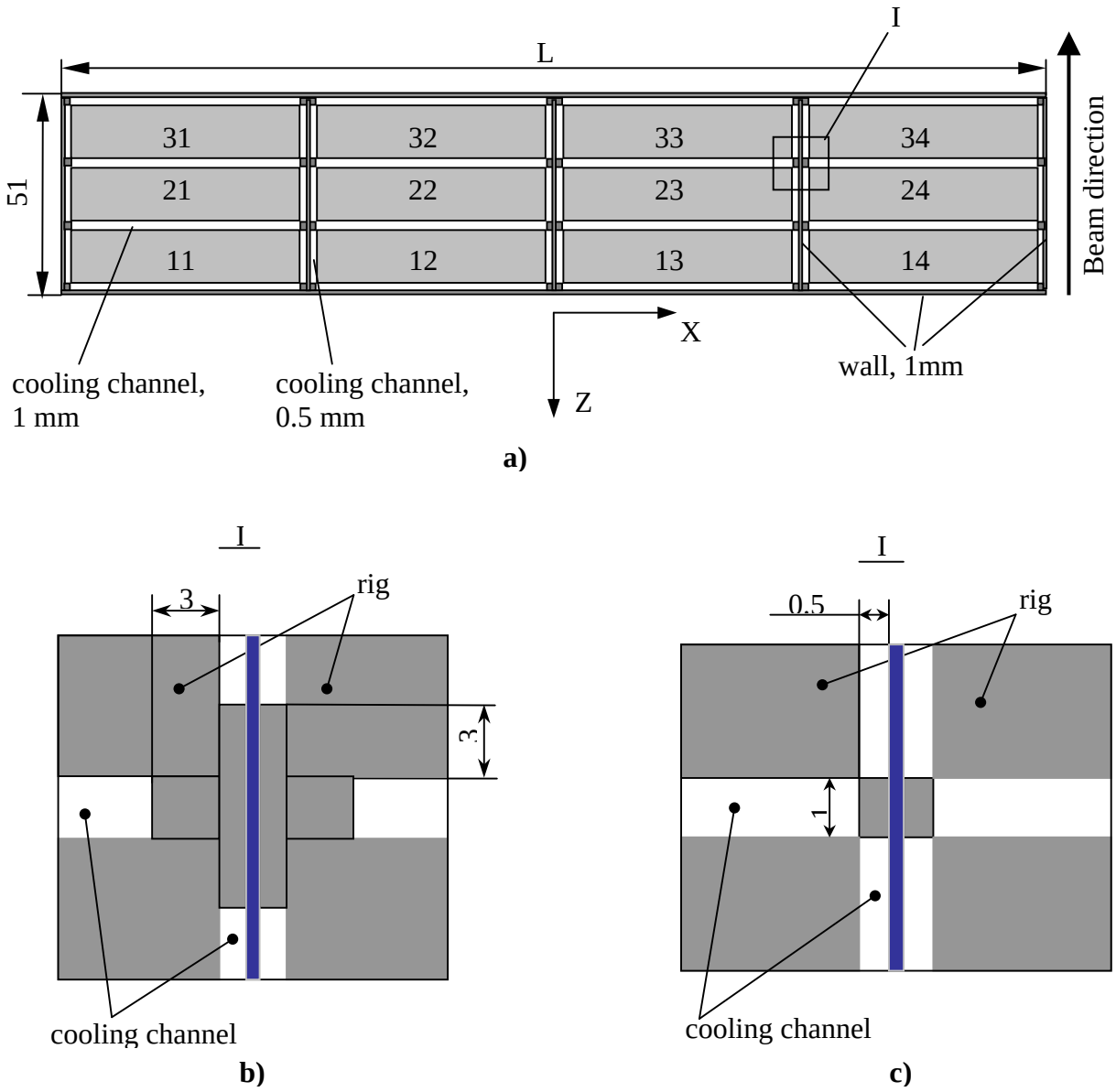

Fig.6. Schematic representation of the irradiated section simulated: section in x,z-plane (**a**) and the elements between the rigs to direct the gas flow to the cooling channels (**b**, **c**), (L = 205 or 173 mm).

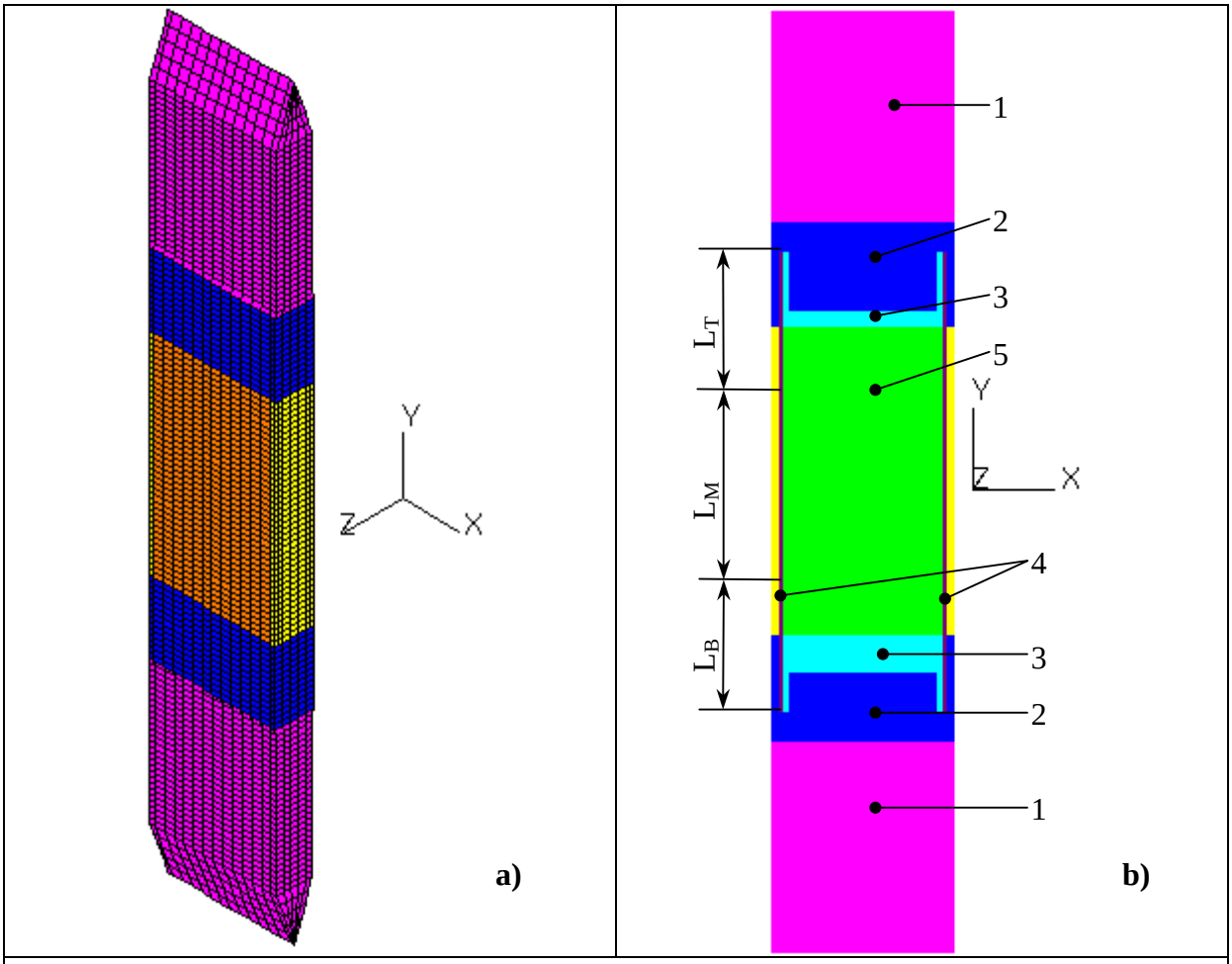

Fig.7. Isometric view of the rig (**a**) and elements of its design simulated (**b**): 1- reflector, 2- gas volume, 3- steel plate, 4- electrical heaters, 5- volume with samples, L_B = 34 mm – bottom heater, L_M = 50 mm – middle heater, L_T = 36 mm – top heater.

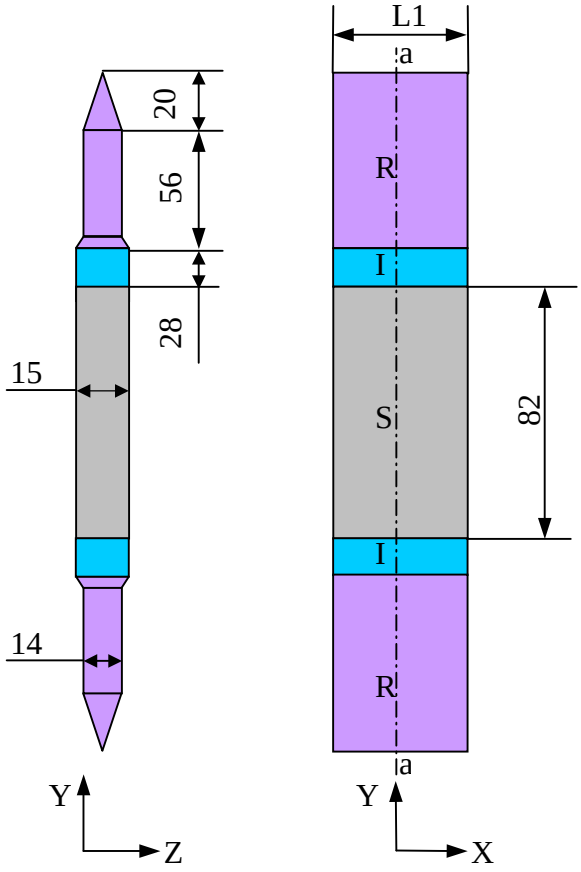

Fig.8. Main geometrical dimensions (mm) of the rig; S – section with samples, I – intermediate sections, R – reflector sections, (L1 = 49 or 41 mm).

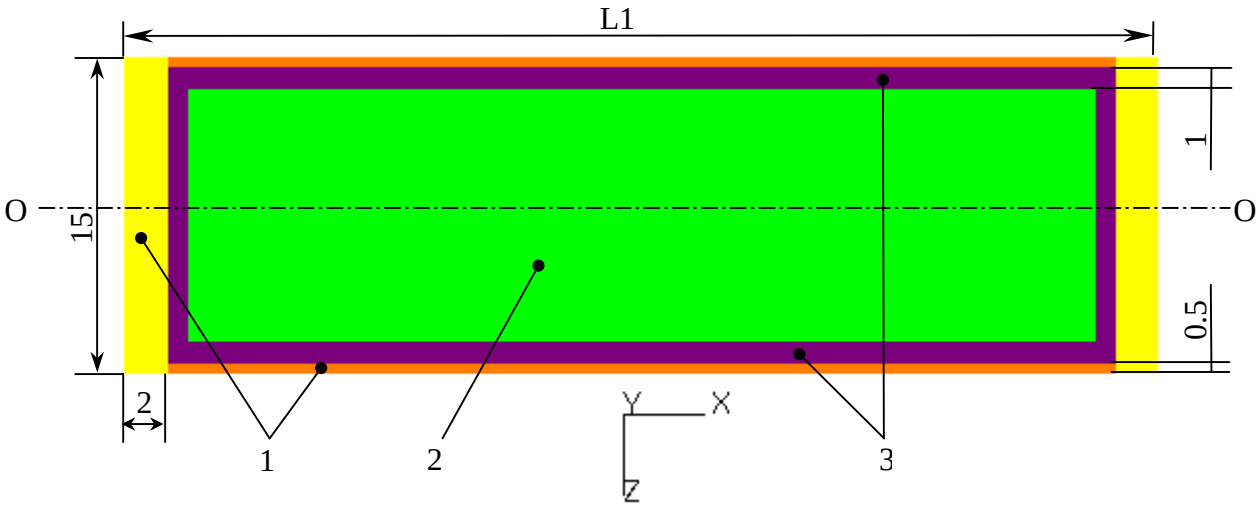

Fig.9. Simulation of the section with samples (x,z-plane): 1 – gas gap, 2 – volume with samples, 3 - electrical heater, (L1 = 49 or 41 mm).

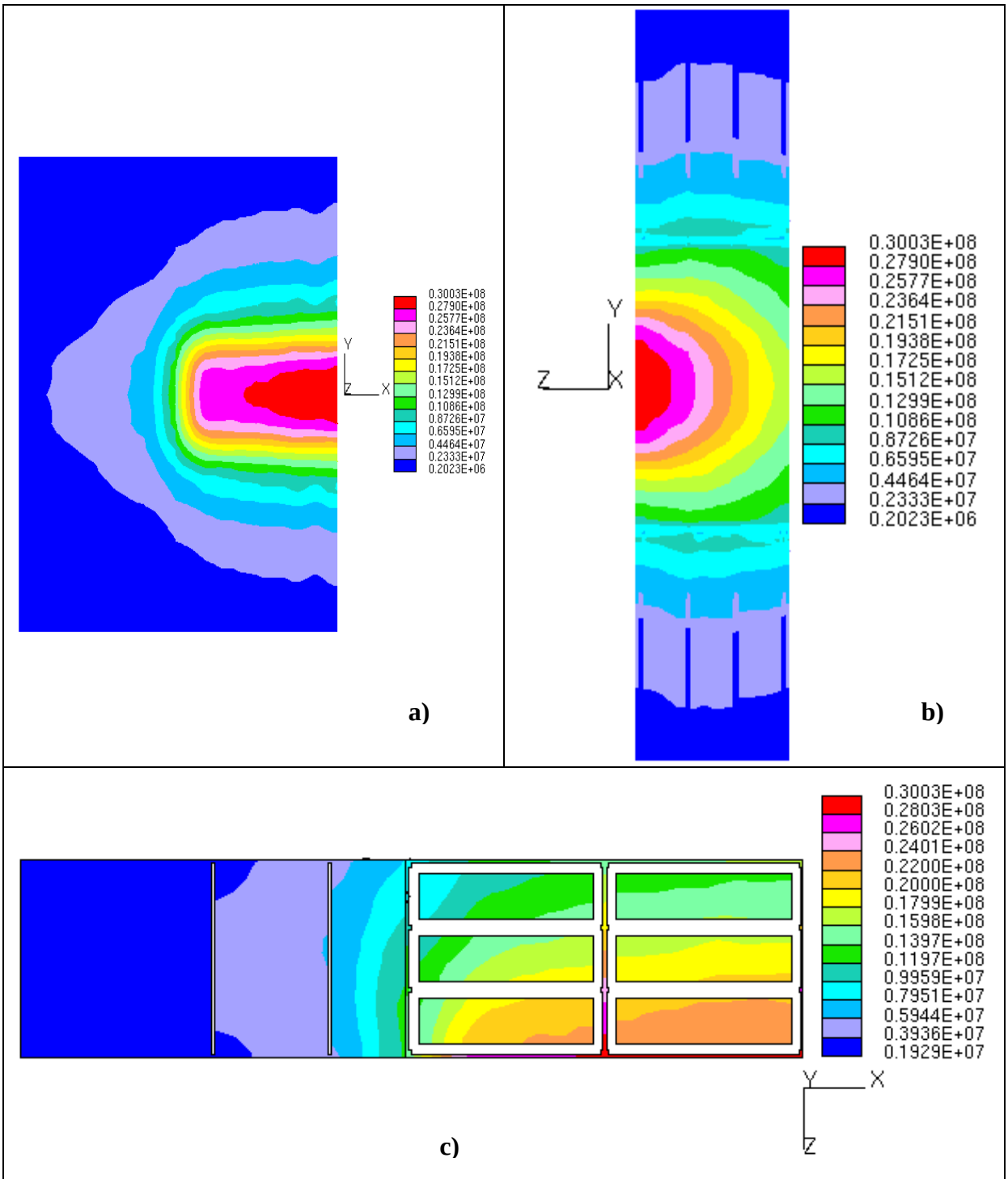

Fig.10. Volumetric heat source distribution, W/m^3; **a** – x,y- plane, z=0, **b** –y,z – plane, x=0, **c** – z,x – plane, y=0. Co-ordinate system origin is located on the front wall of the HFTM irradiated section in its geometrical centre.

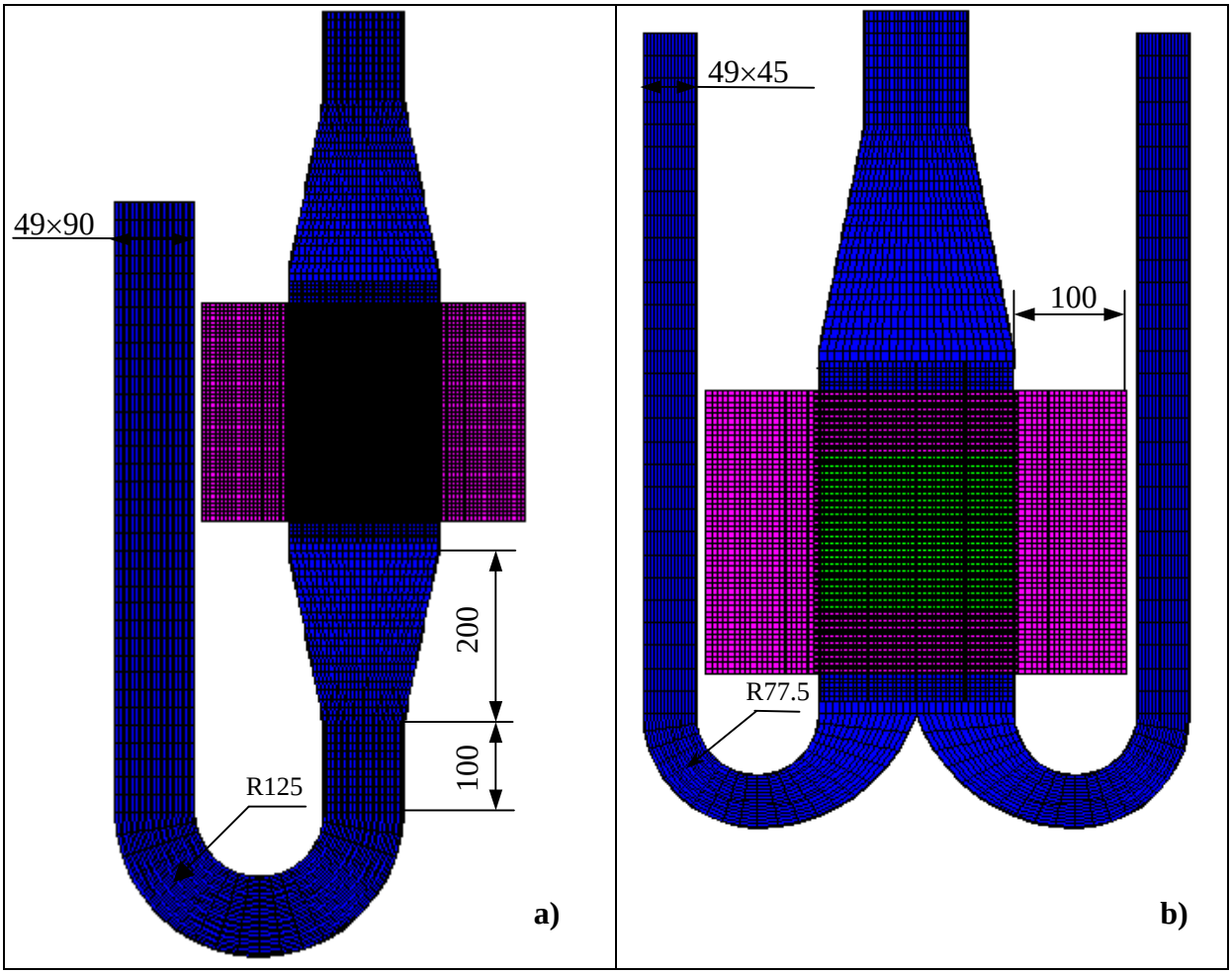

Fig.11. Layout of the HFTM used for detailed simulation, **a** – single-tube gas supply system, **b** - double-tube gas supply system.

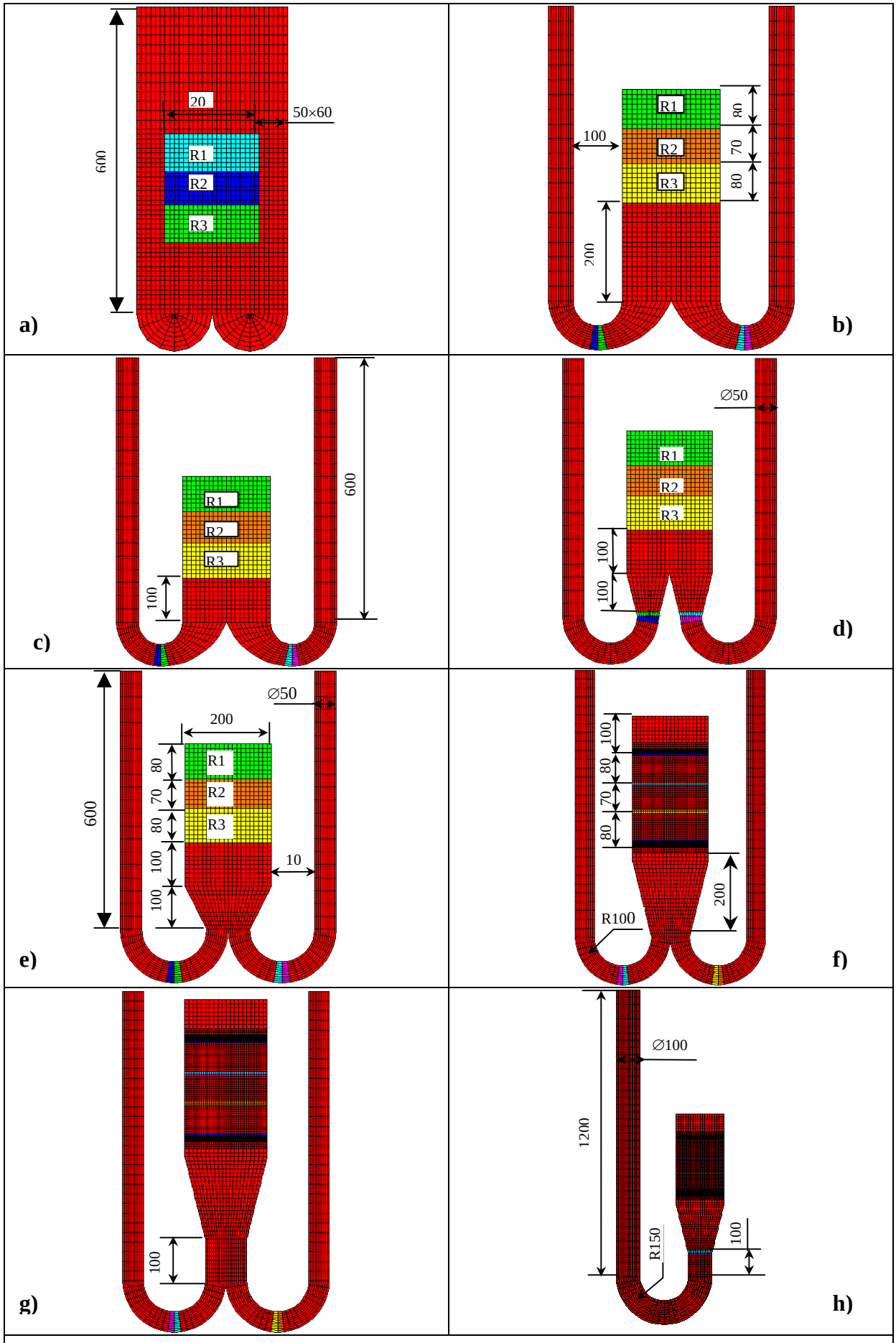

Fig.12. Main layouts of the HFTM used in preliminary calculations

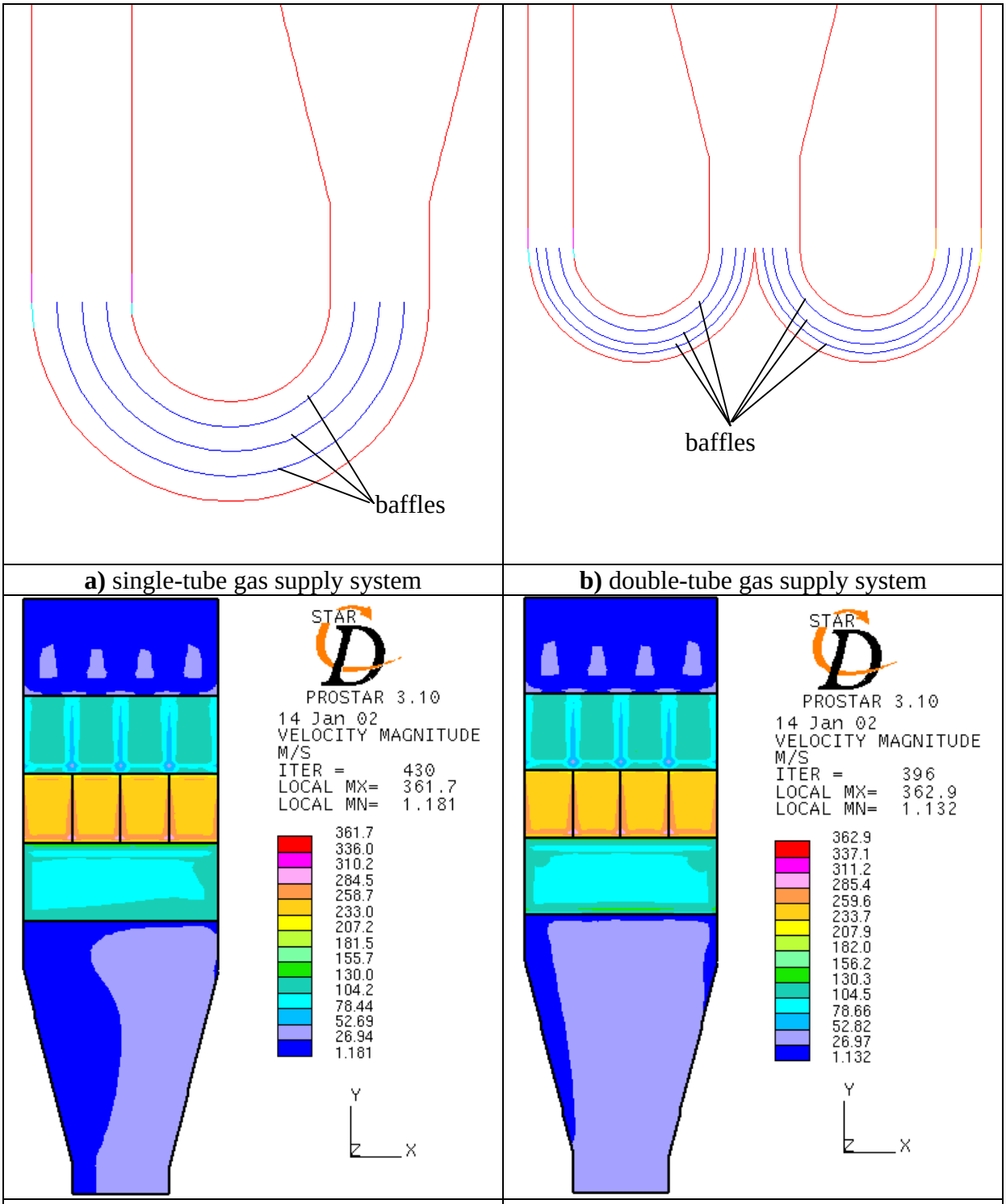

a) single-tube gas supply system

b) double-tube gas supply system

c) variant **12h** without baffles

d) variant **12h** with baffles

Fig.13. Baffle location in the gas supply tubes and their influence on the velocity field in the test section and diffuser.

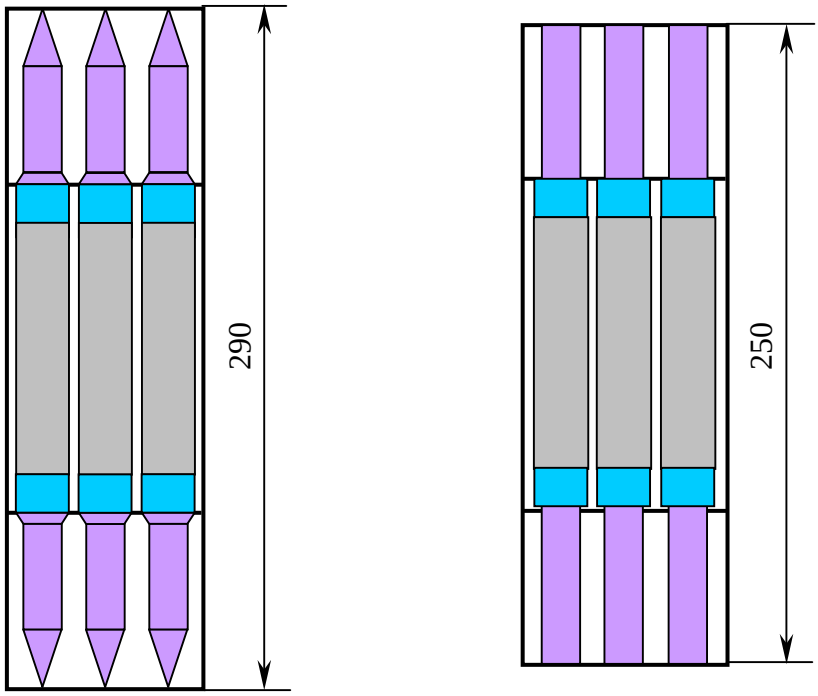

Fig.14. Schematic representation of two different variants of the inlet-outlet parts of the test section: **a** - „cone-wise“, **b** – „step-wise“.

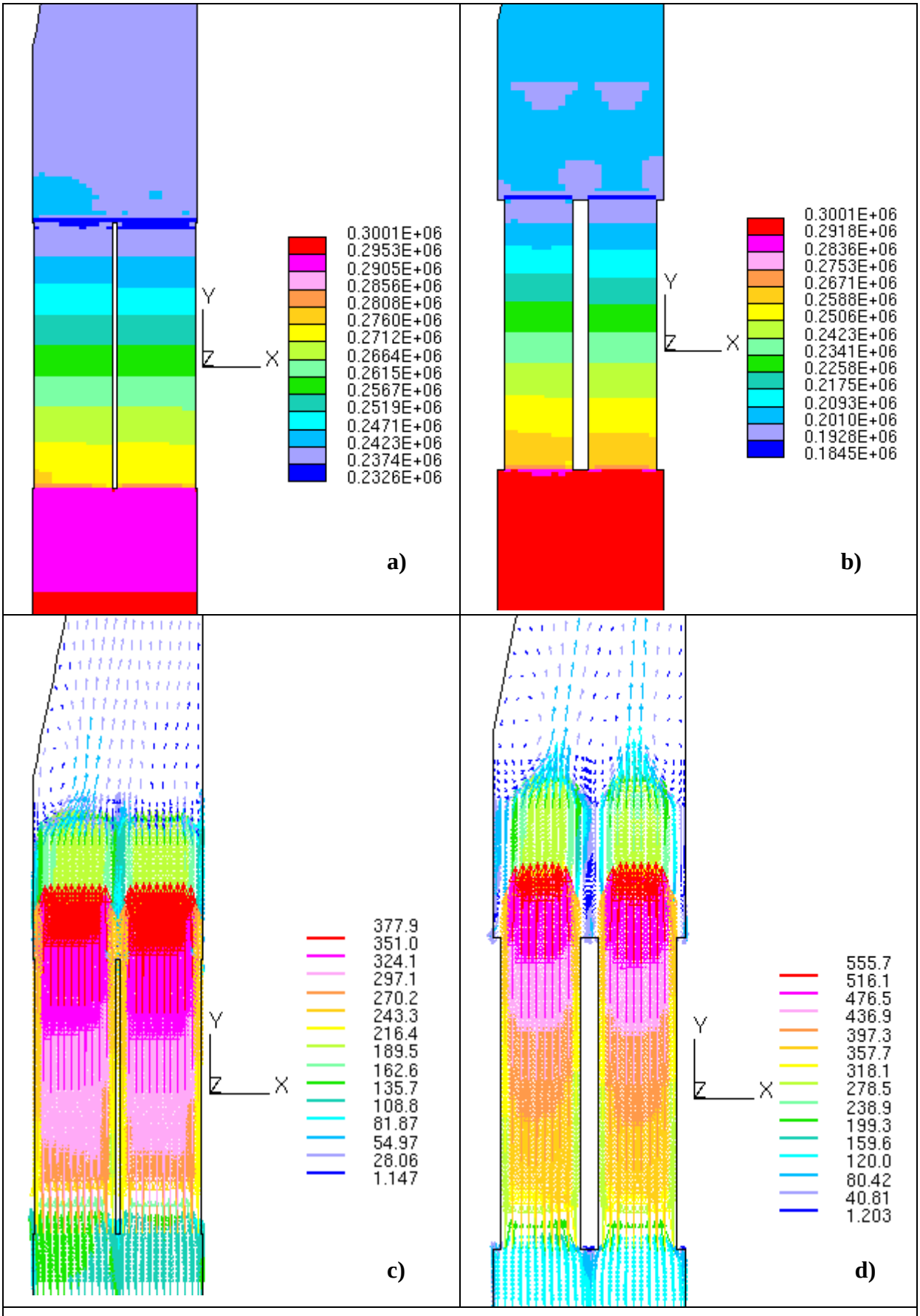

Fig.15. Pressure field and velocity distribution in the test section for rectangular-shape (**a, c**) and T-shape (**b, d**) elements installed between the rigs (see Fig.6b,c).

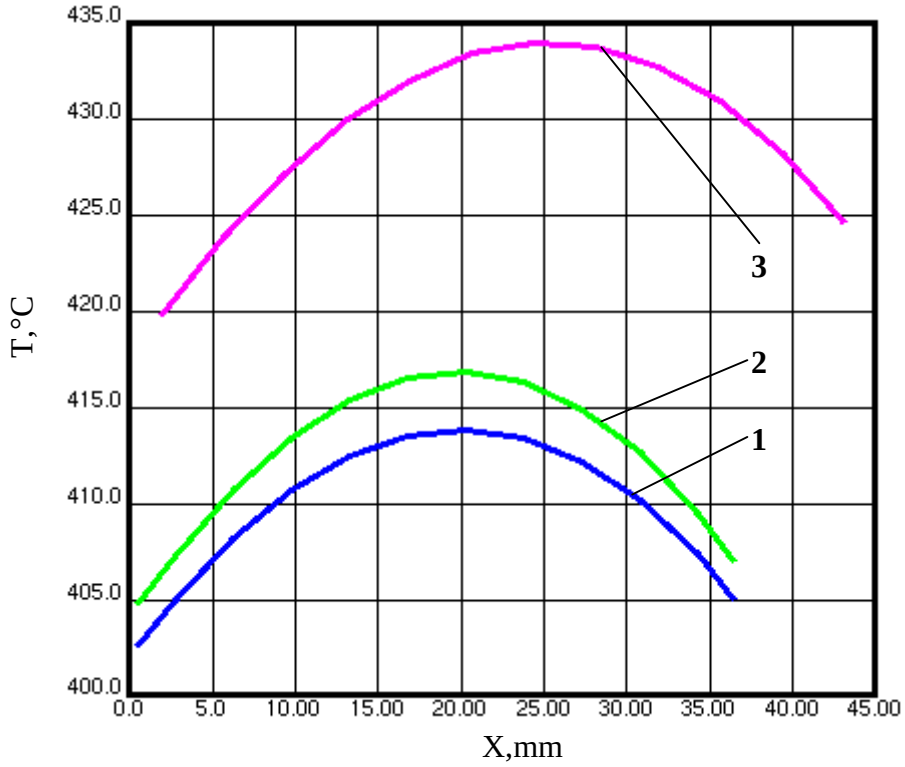

Fig.16. Temperature profile in the rig cross section: line o-o in the z,x-plane passing the rig geometrical centre (see Fig.9).
1 – T-shape elements between the rigs, L1 = 41mm;
2 – rectangular-shape elements between the rigs, L1 = 41mm;
3 - rectangular-shape elements between the rigs, L1 = 49mm

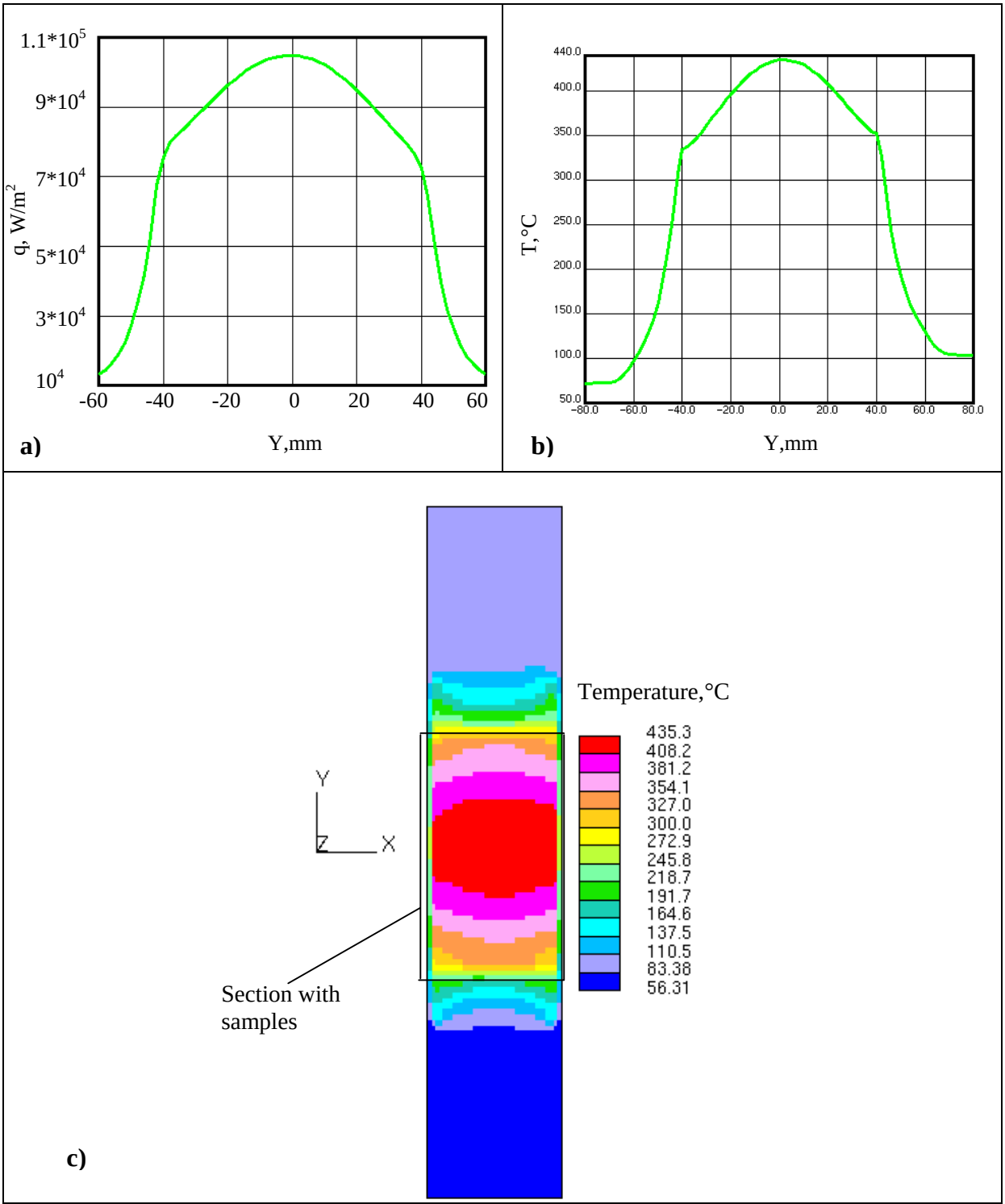

Fig.17. Heat flux distribution along the rig (**a**), temperature profile along the line a-a (**b**) and temperature field in the rig in x,y-plane (**c**) under the nuclear heating only (section with specimens is in the range from –41 to 41 mm). Data are presented for rig 12 in Fig.6a; line a-a - see in Fig.8.

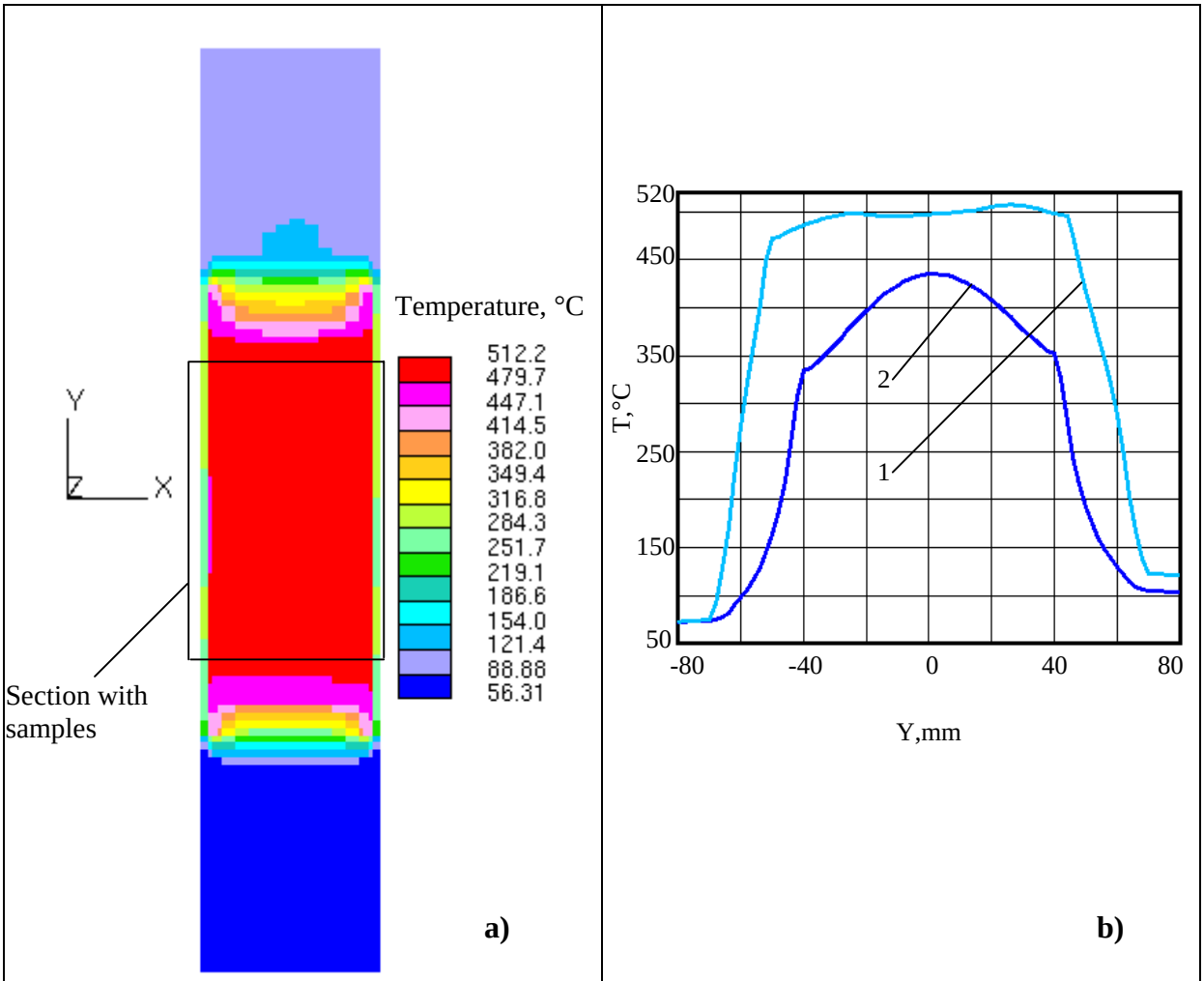

Fig.18. Influence of the bottom and top electrical heaters on the temperature field
(a) in the section with samples and on the temperature profile along the line a-a
(b) in the most heavily loaded rig (section with specimens is in the range from –41 to 41 mm). 1 – temperature profile with electrical heaters, 2 – temperature profile with the nuclear heating only; line a-a – see Fig.8.

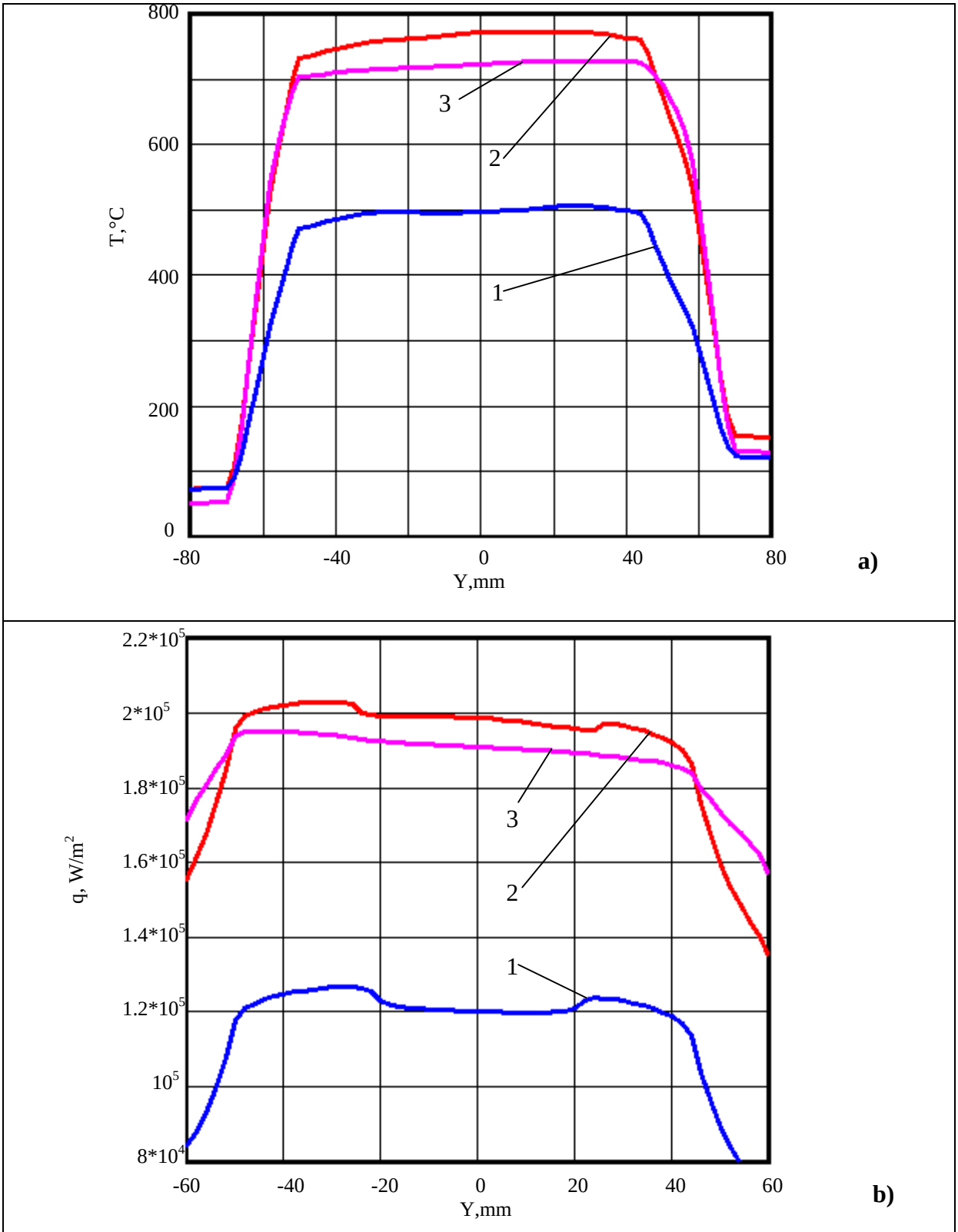

Fig.19. Temperature profile (**a**) along the line a-a (see Fig.8) and heat flux distribution (**b)** along the most heavily loaded rig under different conditions of the use of electrical heaters. 1 – top and bottom electrical heaters together with nuclear heating, 2 – all electrical heaters together with nuclear heating, 3 – electrical heaters only.

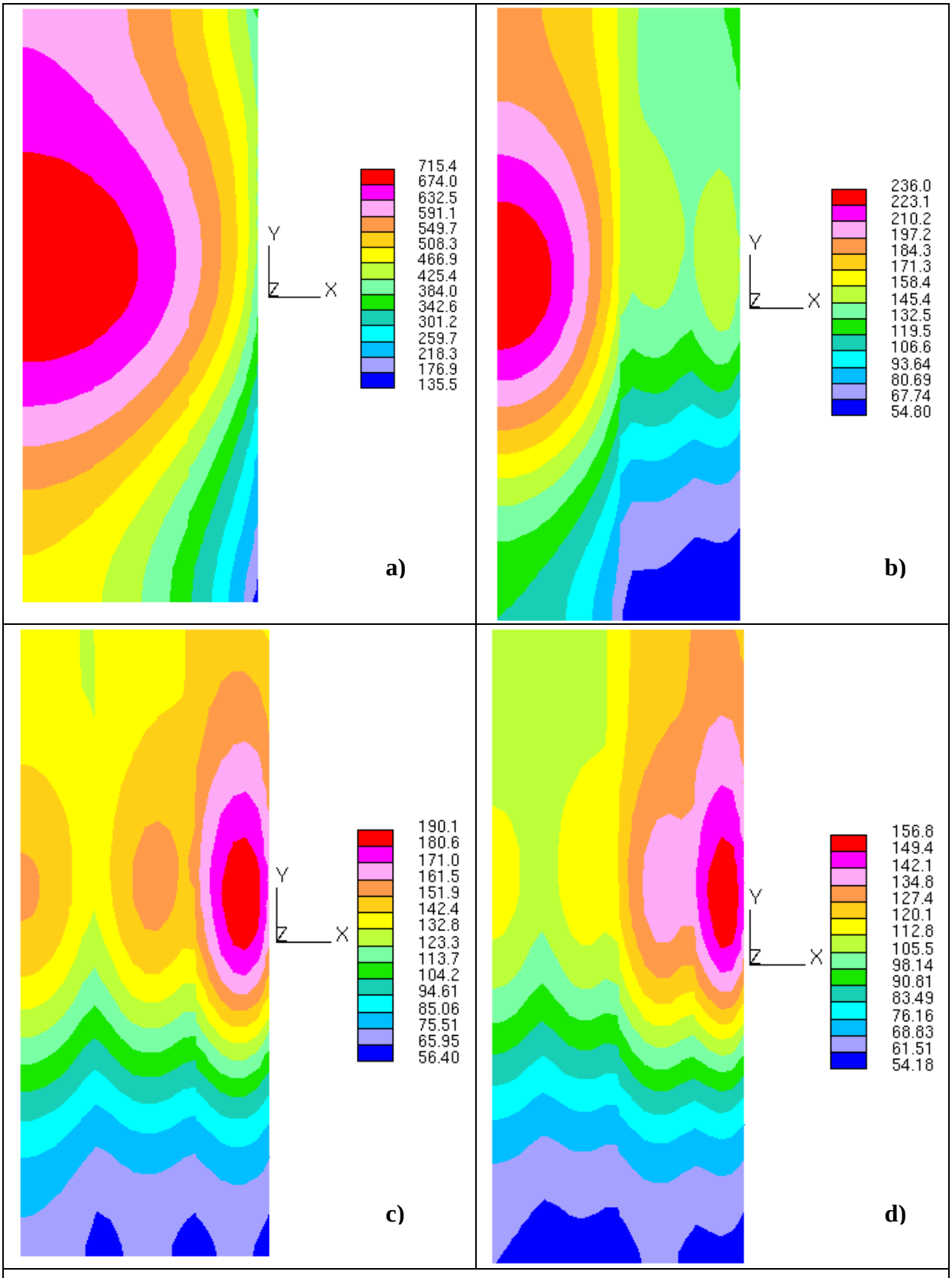

Fig.20. Temperature field in the lateral reflector under nuclear heating: **a** - without special cooling the reflector, **b** – cooling the reflector with two channels positioned 20 and 50 mm from the rigs, **c** - cooling the reflector with two channels positioned 30 and 70 mm from the rigs, **d** - cooling the reflector with three channels positioned 20, 50 and 80mm from the rigs.

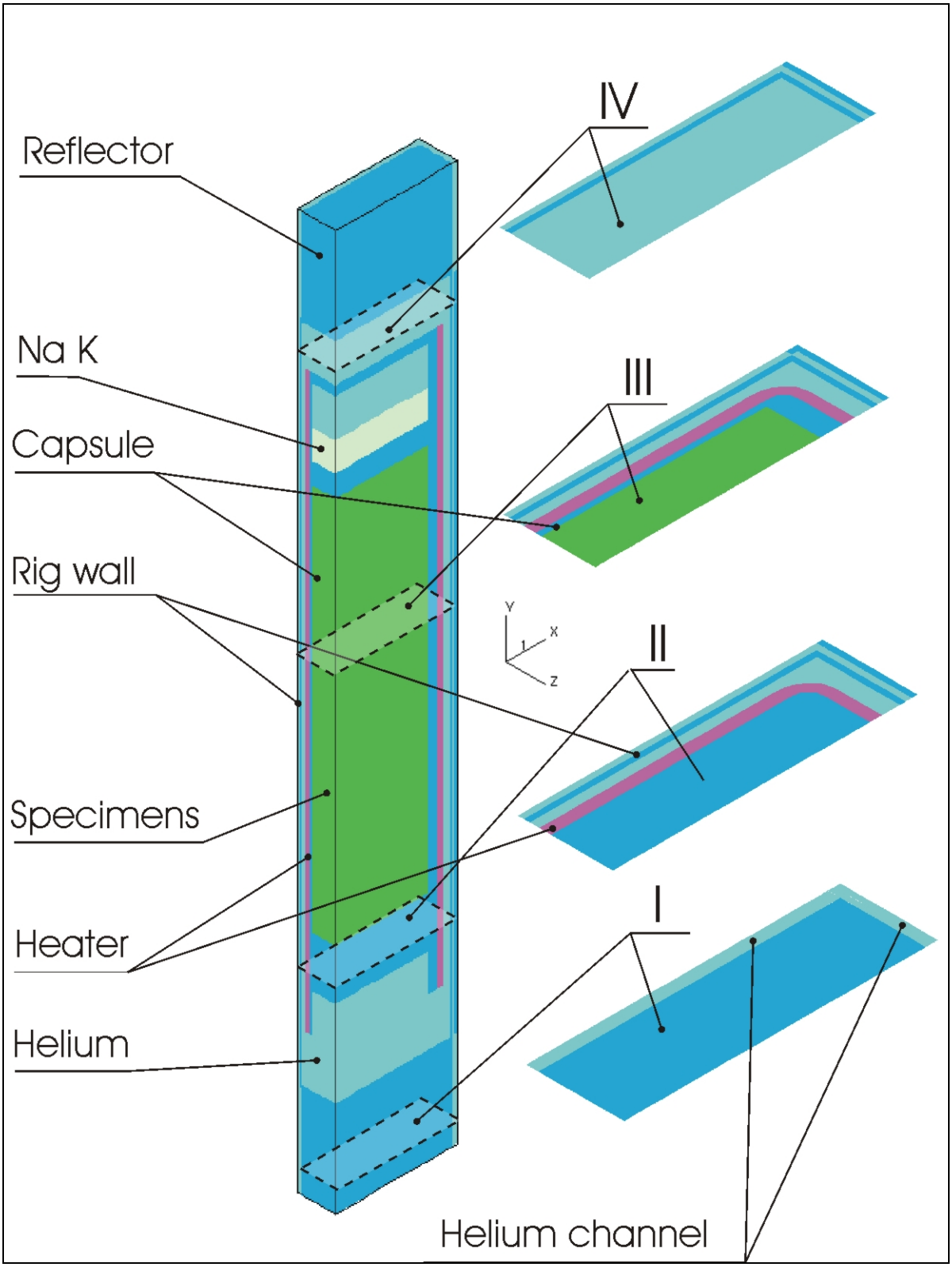

Fig. 21. Reference model of the rig for the thermal-hydraulic calculations.

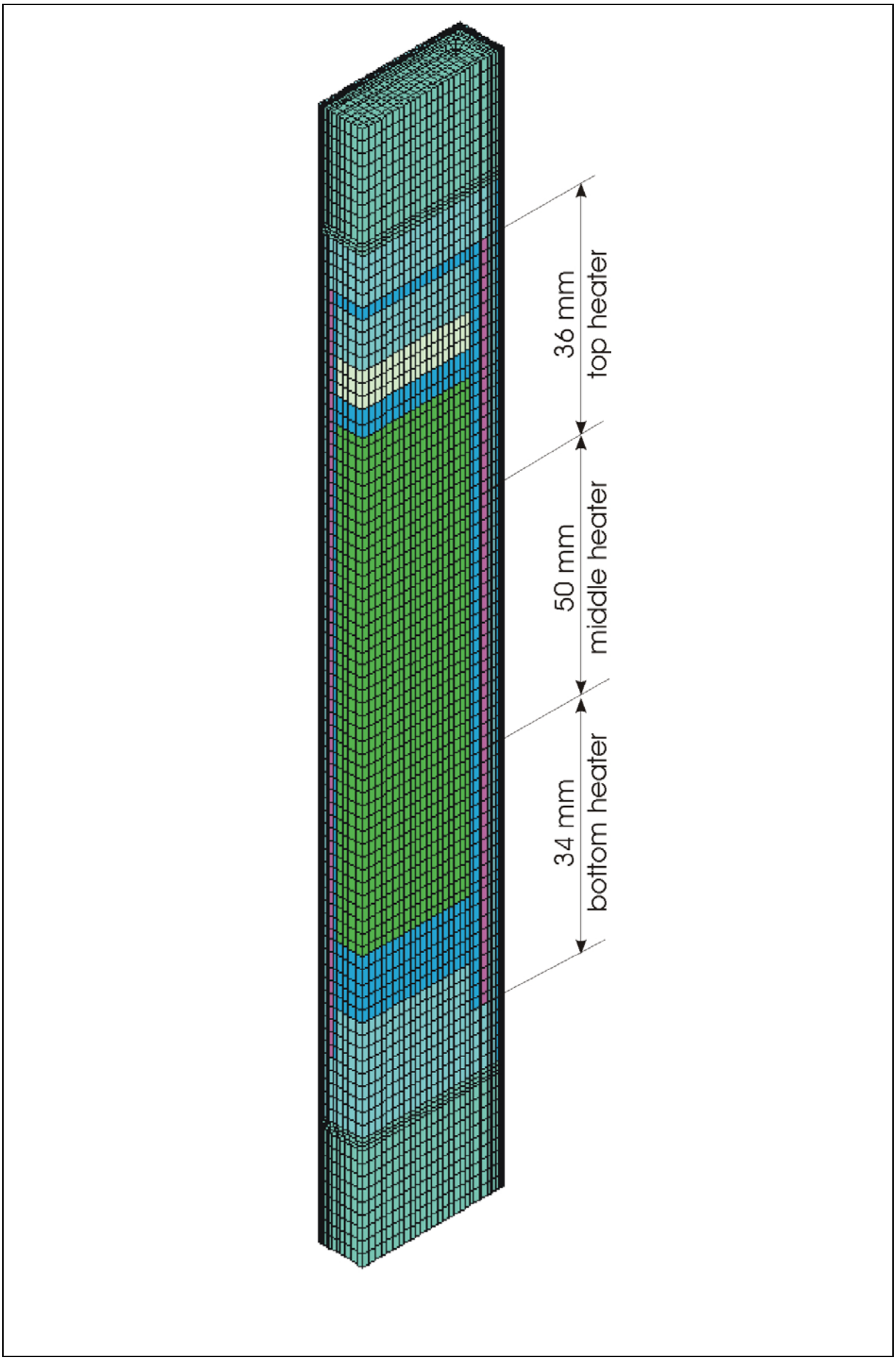

Fig. 22. Computational mesh of the rig (electrical heaters in red color)

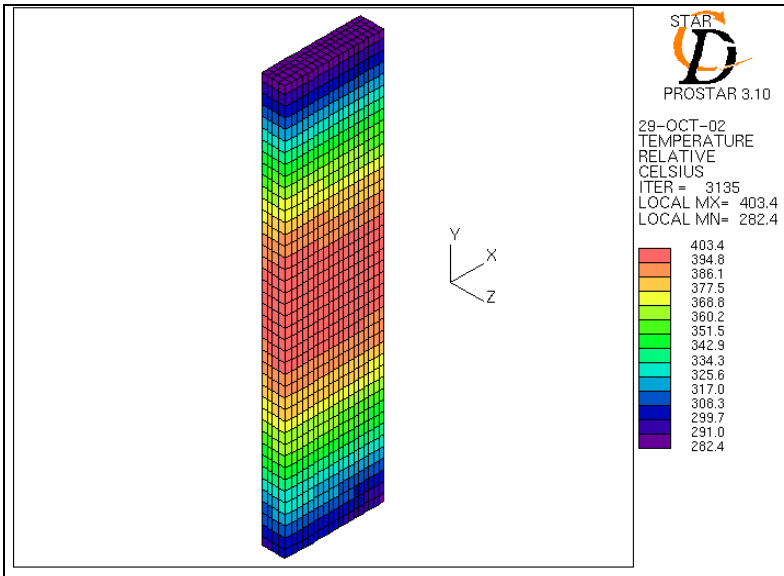

Temperature distribution in the testing zone

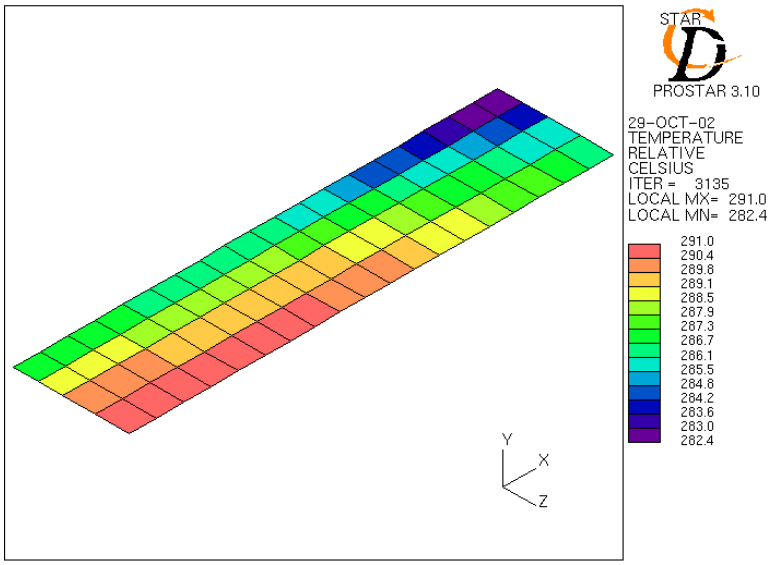

Top cross-section

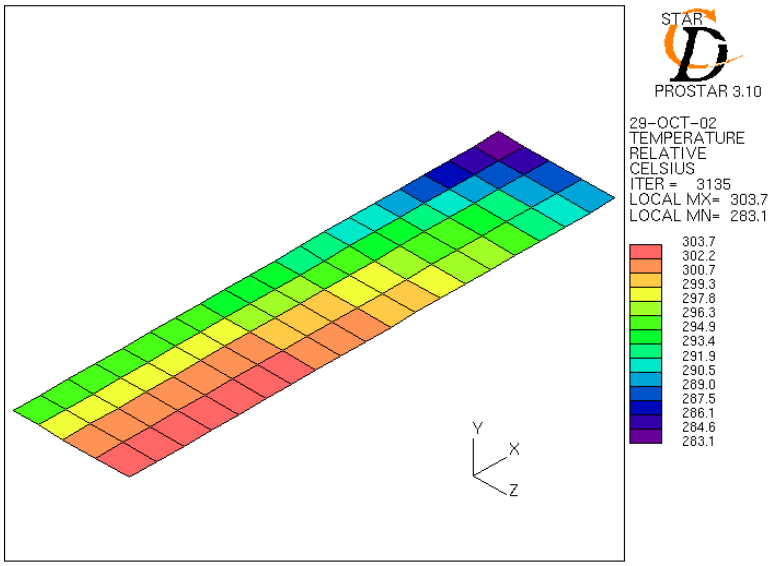

Bottom cross-section

Fig.23. Temperature distribution in the specimens with nuclear heating, variant with the thin lower cap, He gap=0.5 mm (Case 1a).

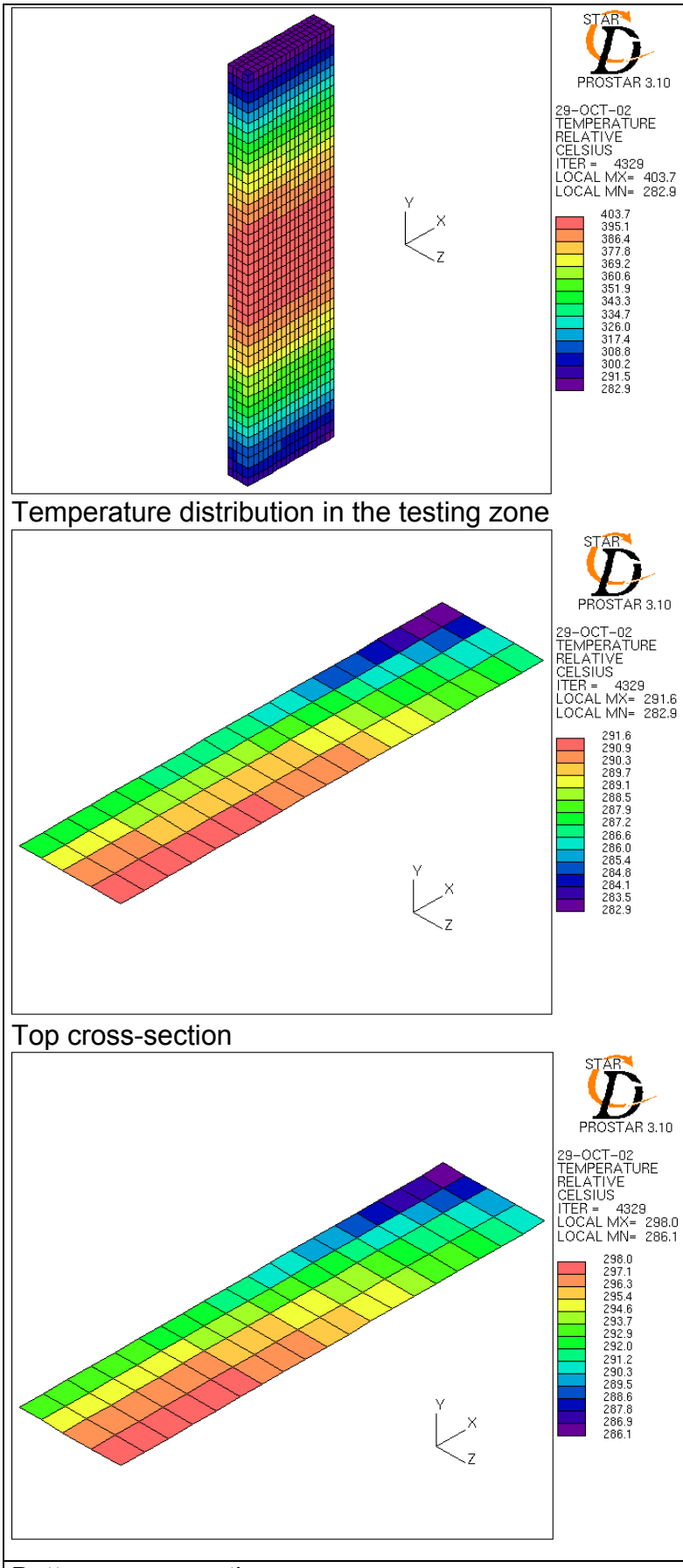

Fig.24. Temperature distribution in the specimens with nuclear heating, variant with the thick lower cap, He gap=0.5 mm (Case 1b).

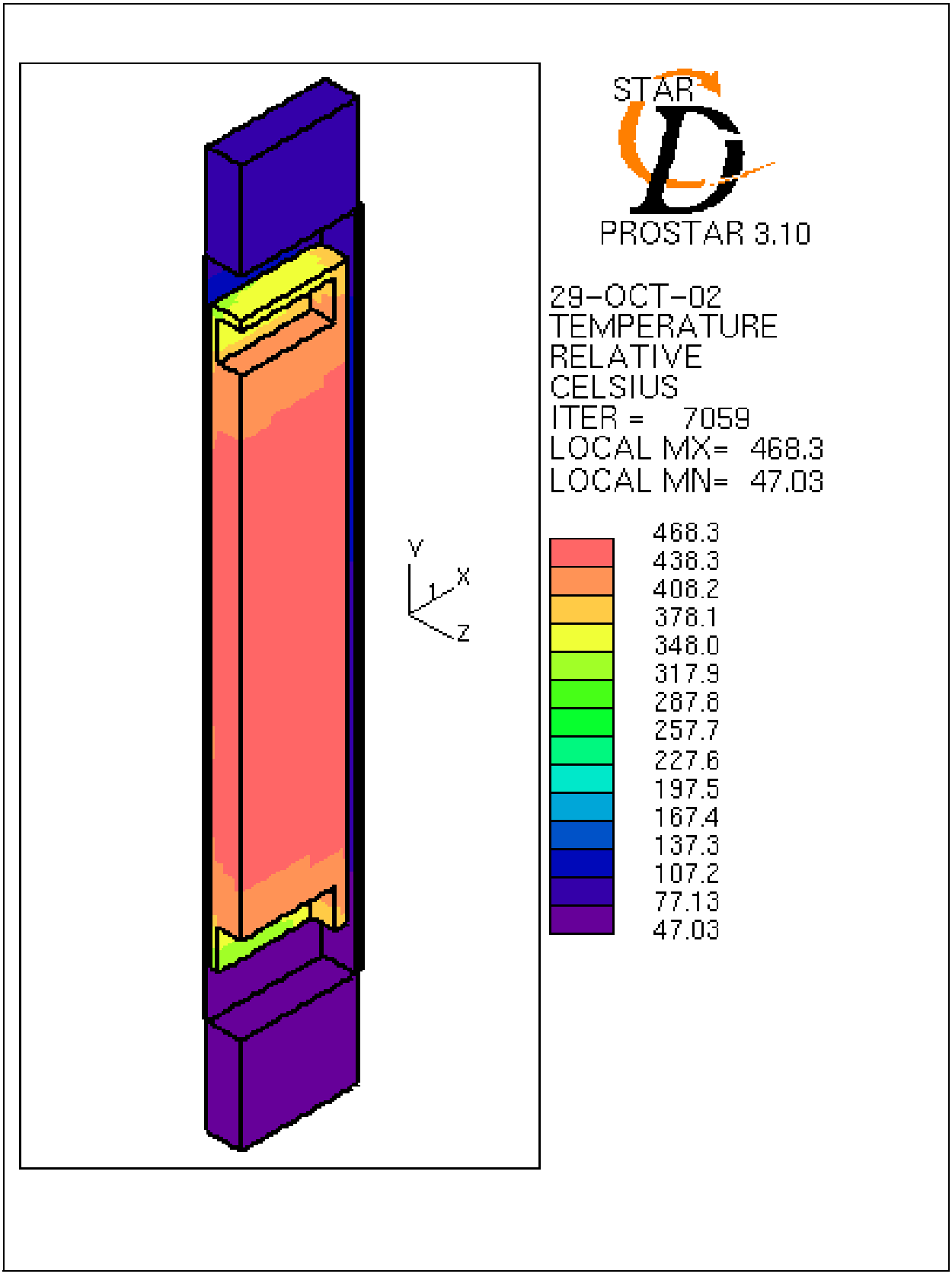

Fig.25. Temperature distribution in the rig structure with nuclear and electrical heating, heater power (top/ middle/ bottom)=71/ 0/ 74 W/cm^3, He gap=0.5 mm (Case 2).

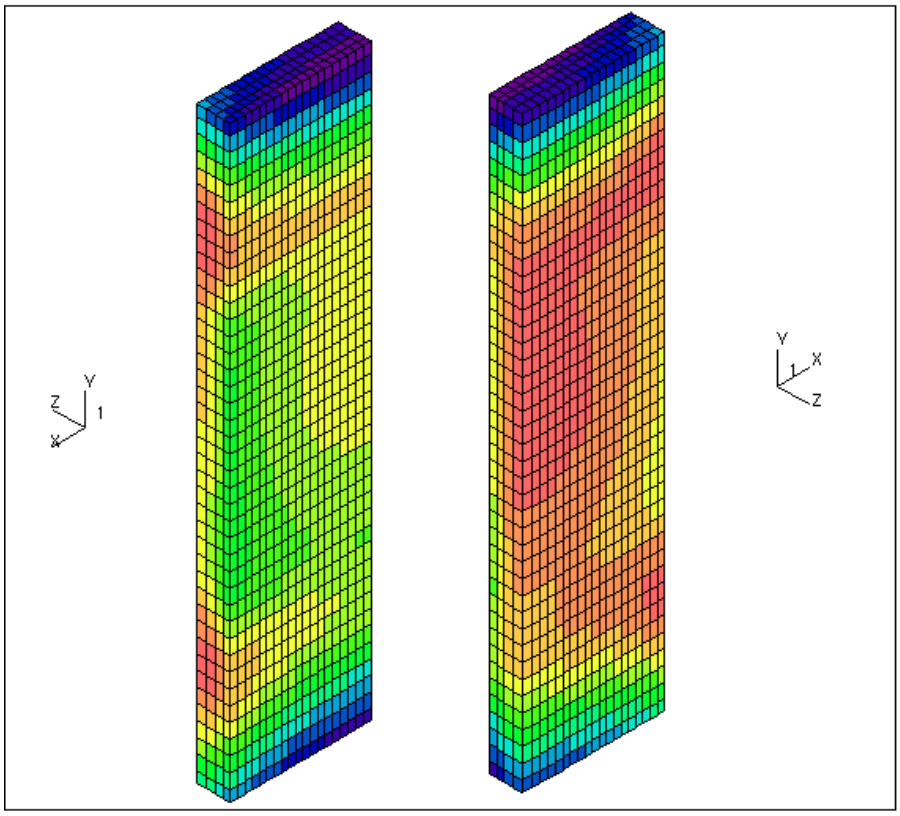

Temperature distribution in specimens

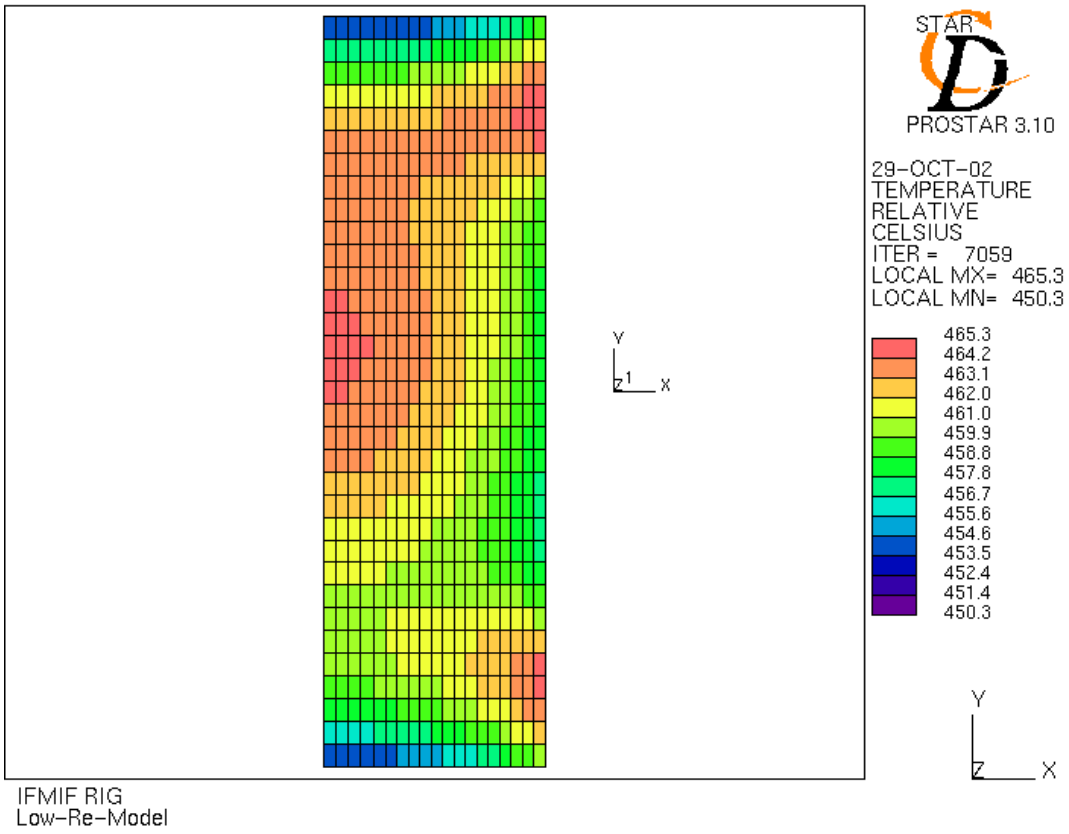

Zone with the temperature difference ≤ 15 K (length: 66 mm)

Fig. 26. Temperature distribution in the specimens with nuclear and el. heating, He gap=0.5 mm, heater power=71/ 0/ 74 W/cm^3 (Case 2).

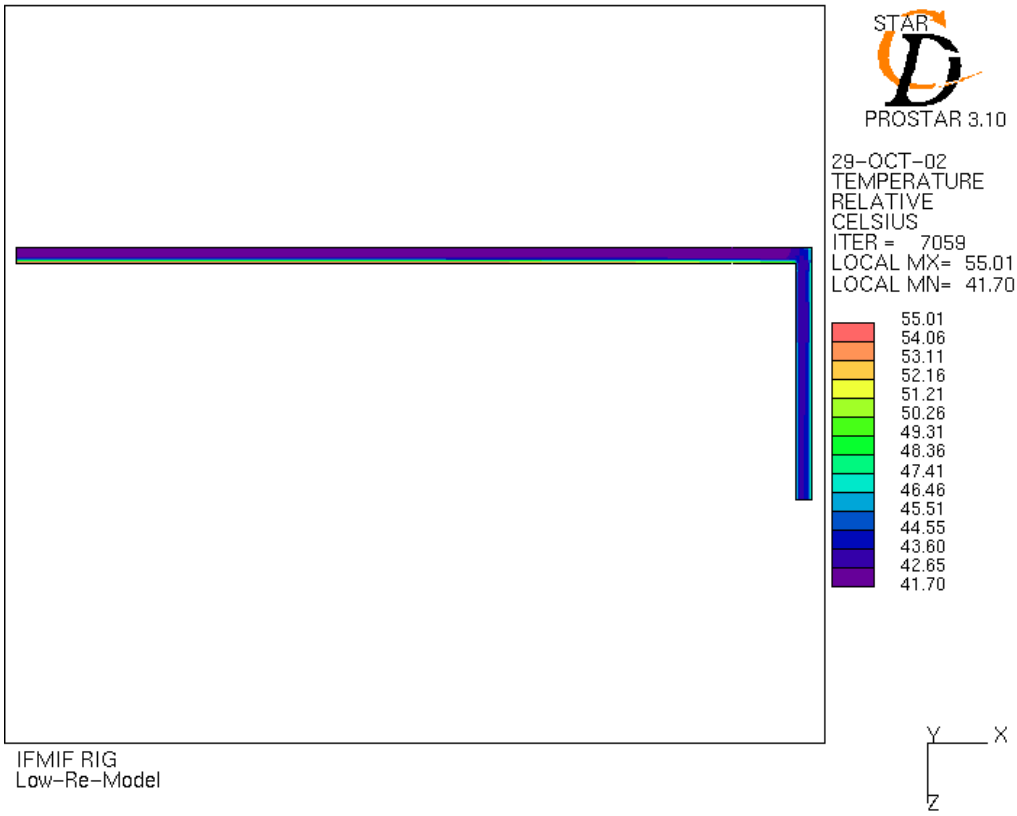

Lower end of the rig (y=-68 mm)

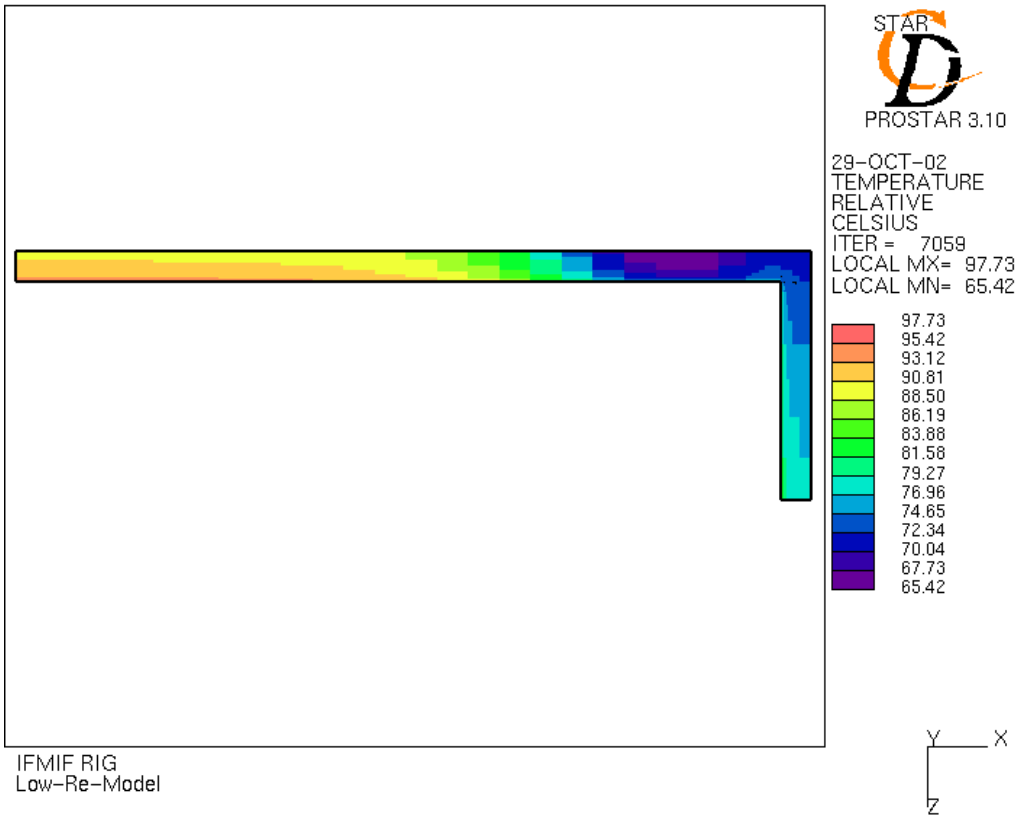

Cooling channel outlet (y=76 mm)

Fig. 27. Helium temperature distribution with nuclear and electrical heating, He gap=0.5 mm, heater power=71/ 0/ 74 W/cm^3 (Case 2).

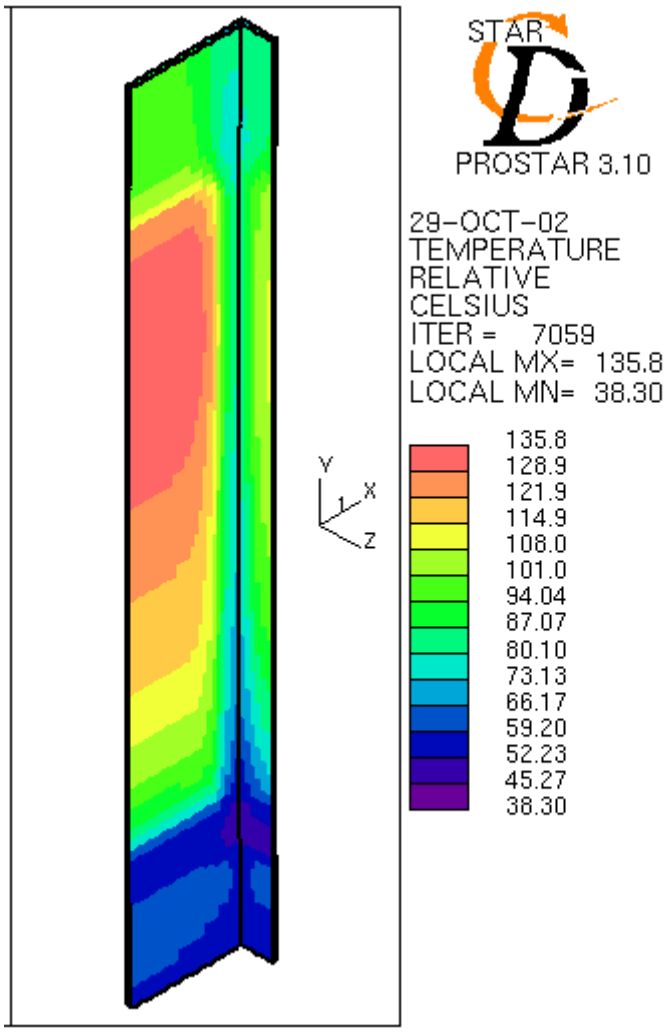

Helium temperature on the rig wall

Fig. 28. Near wall helium temperature distribution with nuclear and electrical heating, He gap=0.5 mm, heater power=71/ 0/ 74 W/cm^3 (Case 2).

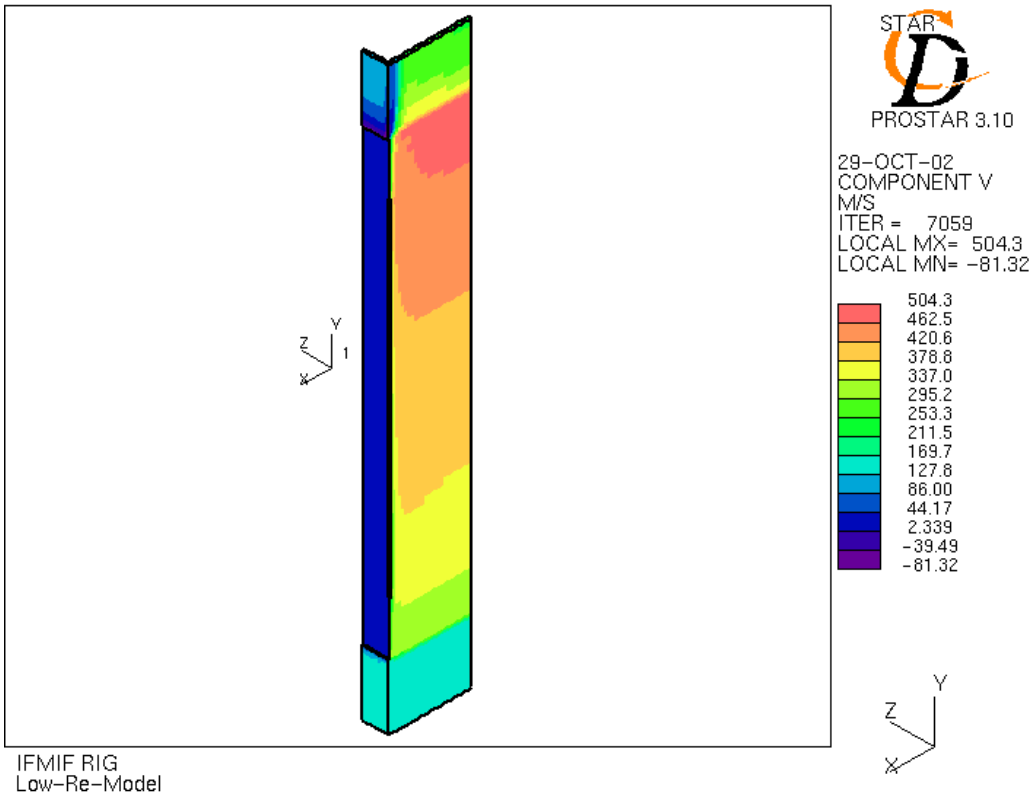

Helium velocity

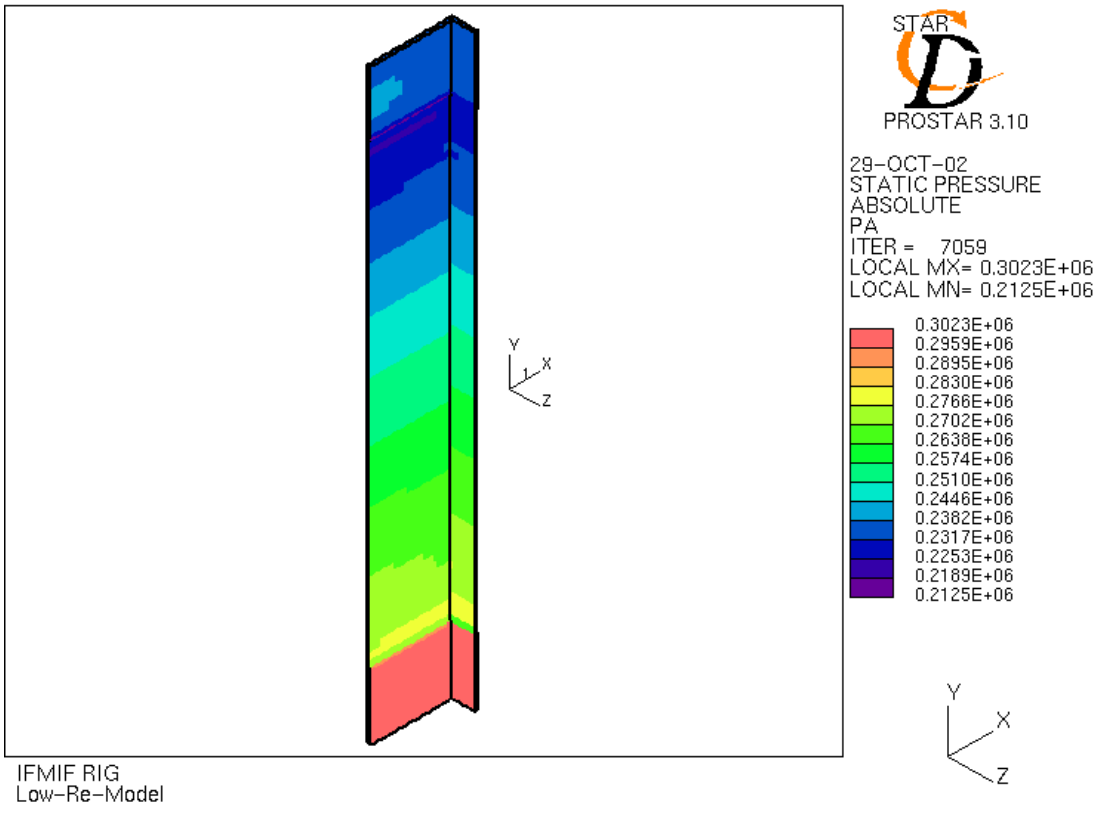

Static pressure

Fig. 29. Helium velocity and static pressure distribution with nuclear and electrical heating, He gap=0.5 mm, heater power=71/ 0/ 74 W/cm^3 (Case 2).

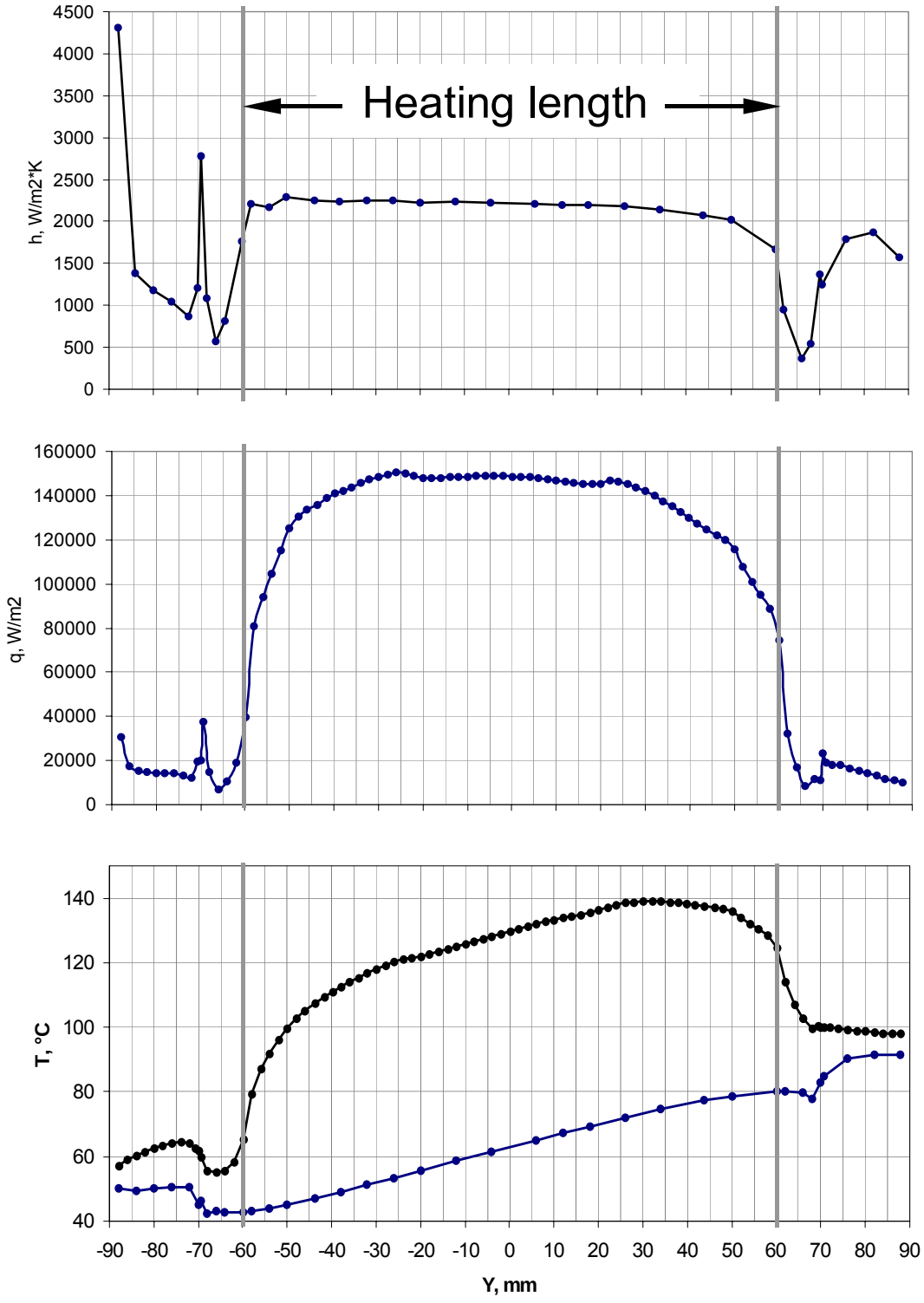

Fig.30. Heat transfer coefficient, heat flux and wall/coolant temperature distribution in the middle of the cooling channel at the large rig side, heating zone between –60 and + 60 mm (Case 2)

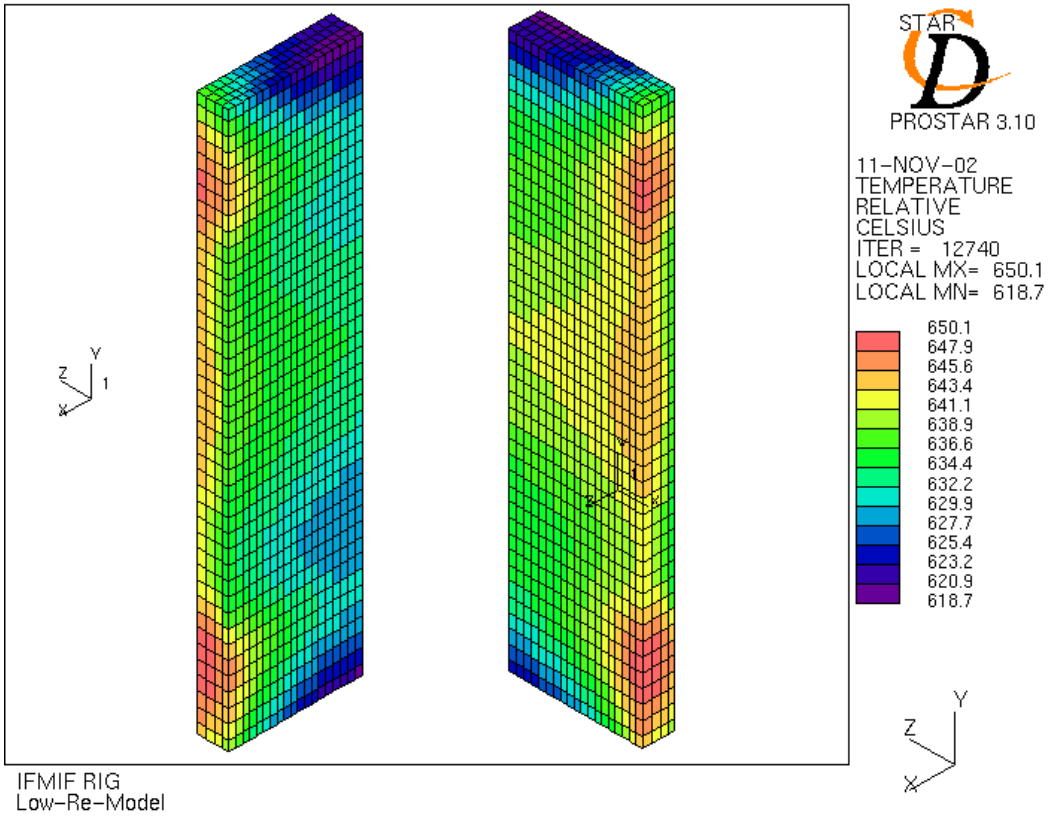

Temperature distribution in specimens

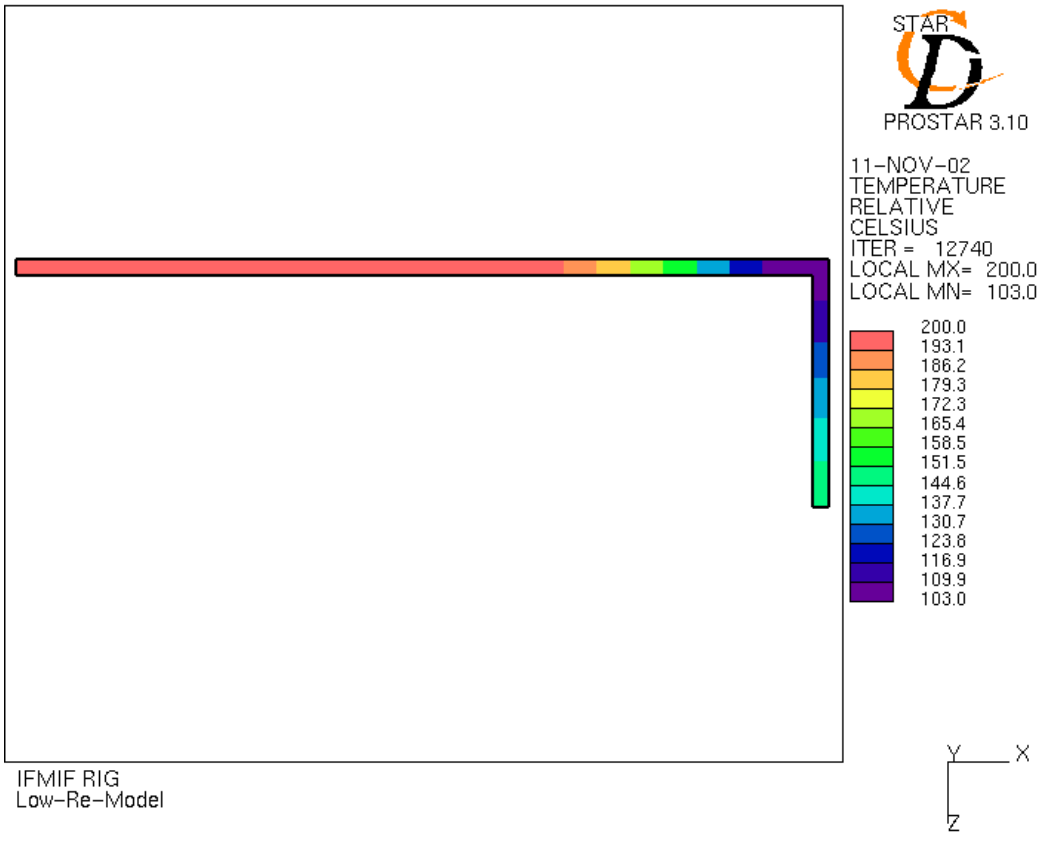

Maximal temperature difference in the rig wall (y=0).

Fig. 31. Temperature distribution with nuclear and electrical heating, He gap=0.5 mm, heater power=149/ 90/ 158 W/cm^3 (Case 3a)

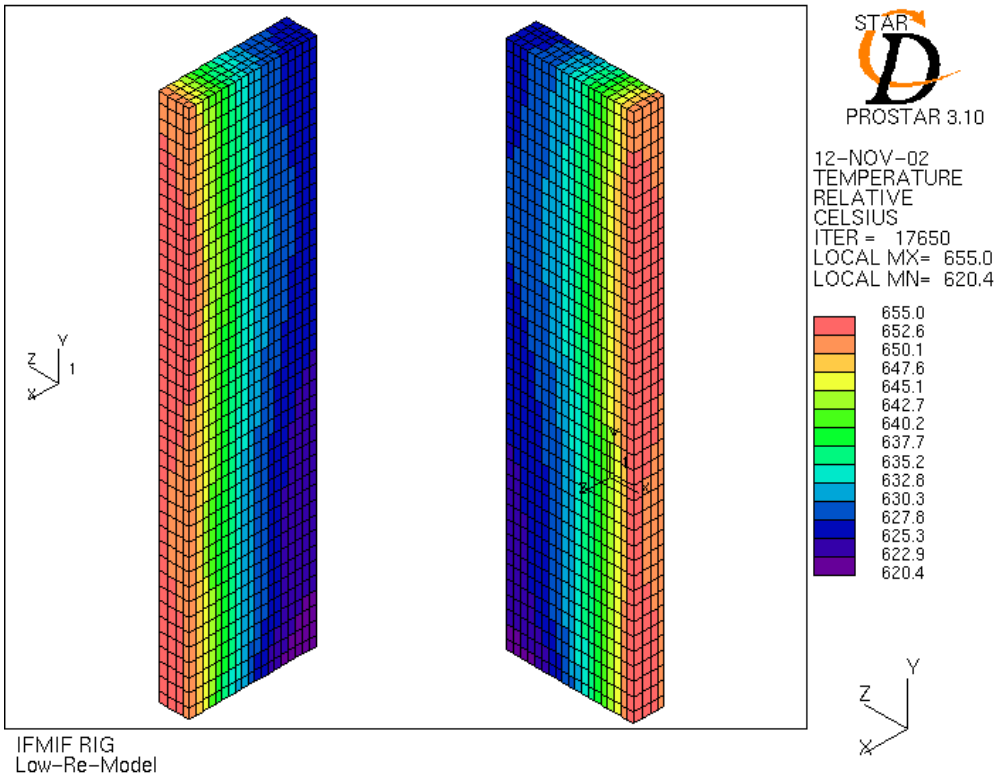

Temperature distribution in specimens

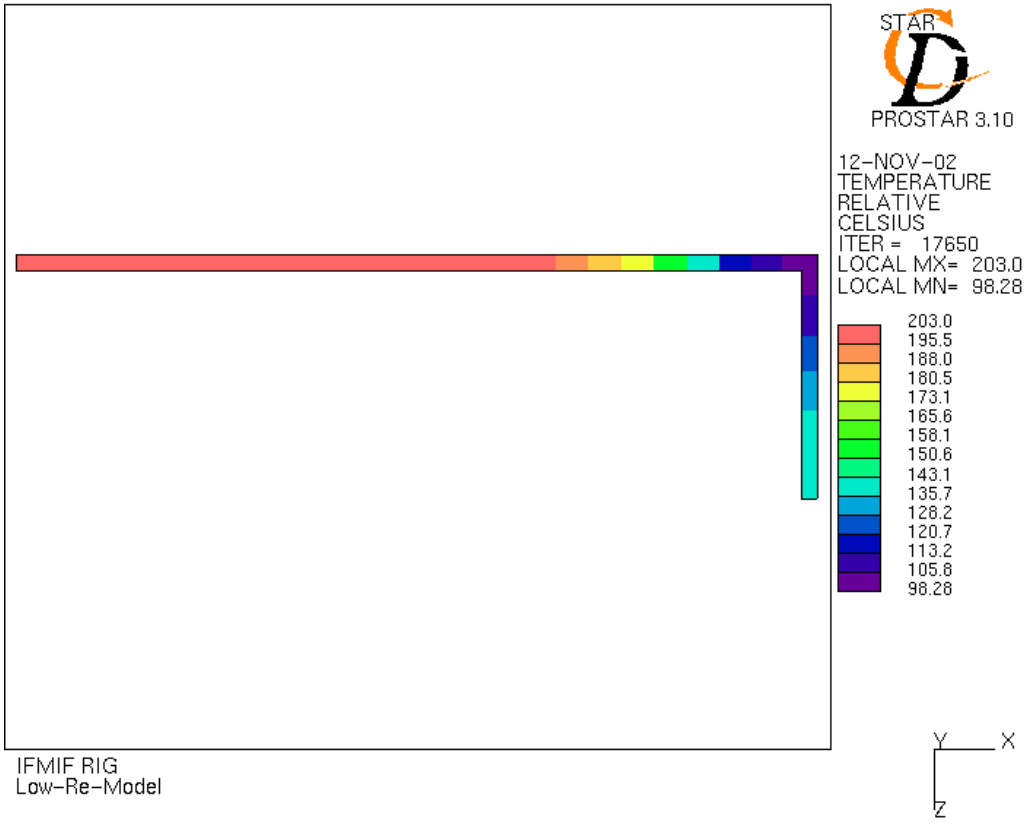

Maximal temperature difference in the outer capsule wall (y=0).

Fig. 32. Temperature distribution with electrical heating only, heating power=194/ 199/ 206 W/cm^3, He gap=0.5 mm (Case 3b)

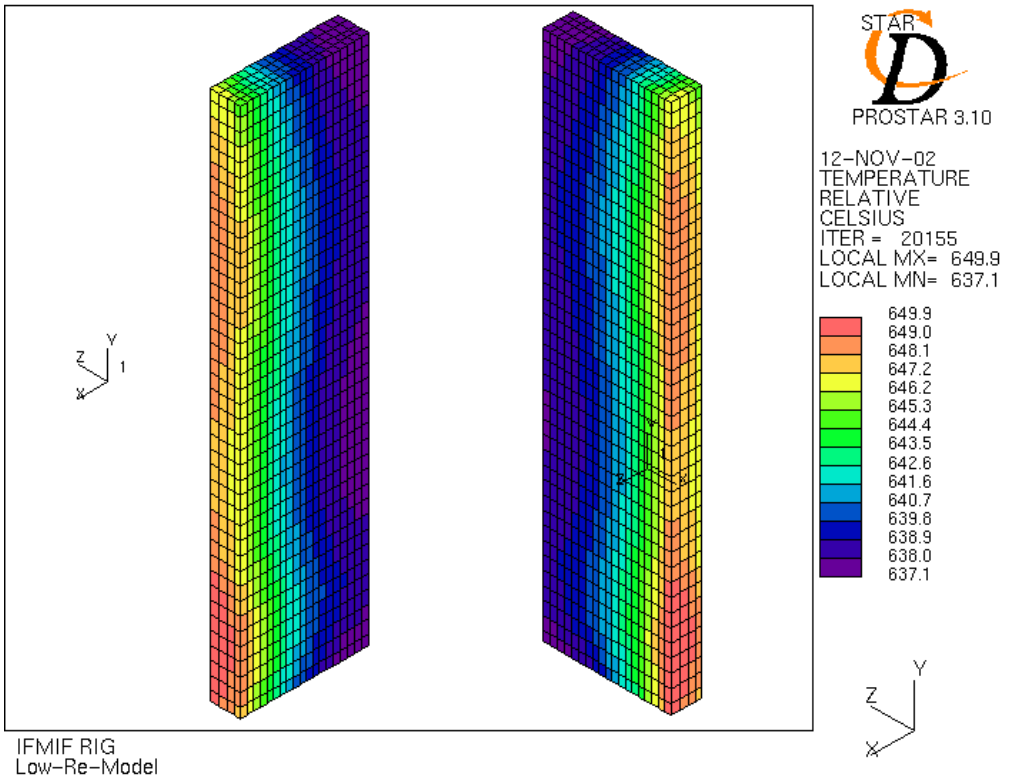

Temperature distribution in specimens

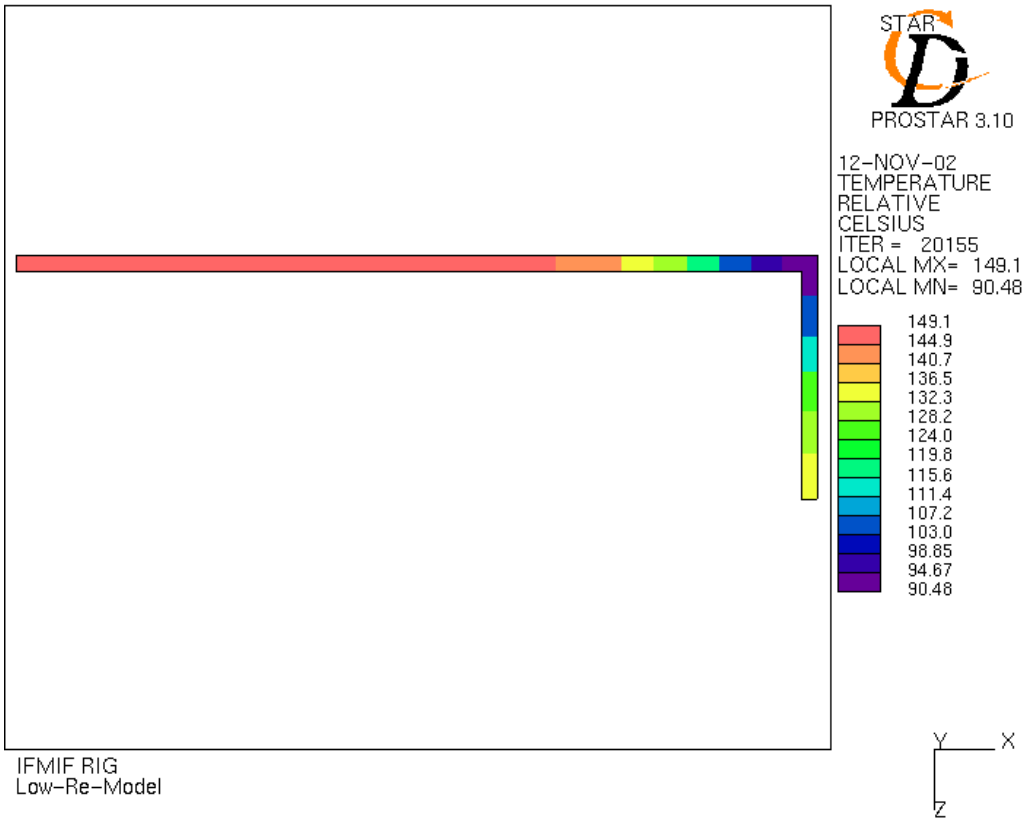

Temperature distribution in the rig wall (y=0).

Fig. 33. Temperature distribution in the specimens and in the rig wall with electrical heating only, heating power=147/ 148/ 154 W/cm^3, He gap between rig and capsule wall 0.8 mm (Case 4a)

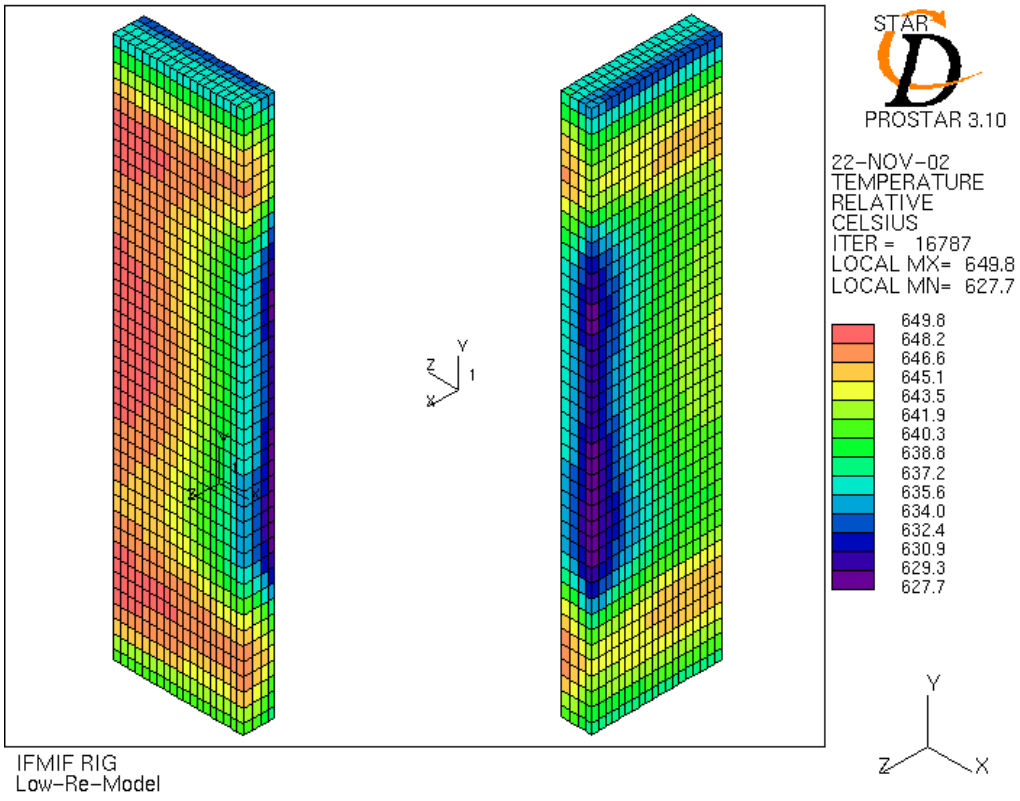

Temperature distribution in specimens

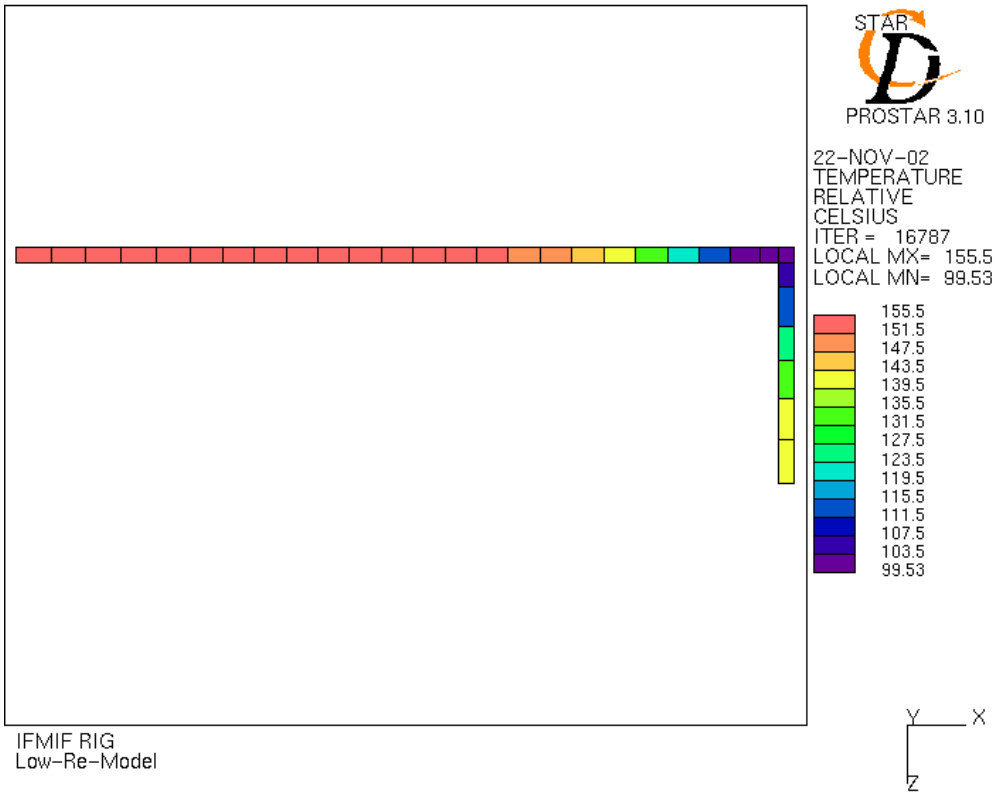

temperature distribution in the rig wall (y=0).

Fig. 34. Temperature distribution in the specimens and the rig wall with nuclear and electrical heating, heater power=108/ 39/ 110 W/cm3, He gap=0.8 mm (Case 4b)

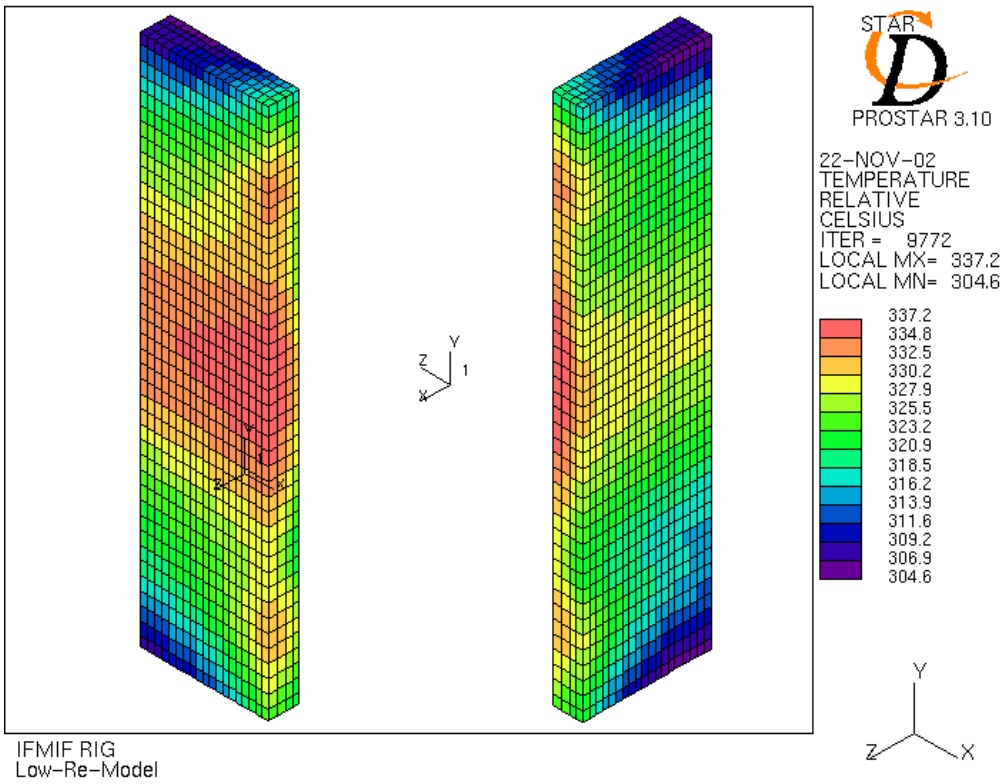

Temperature distribution in specimens

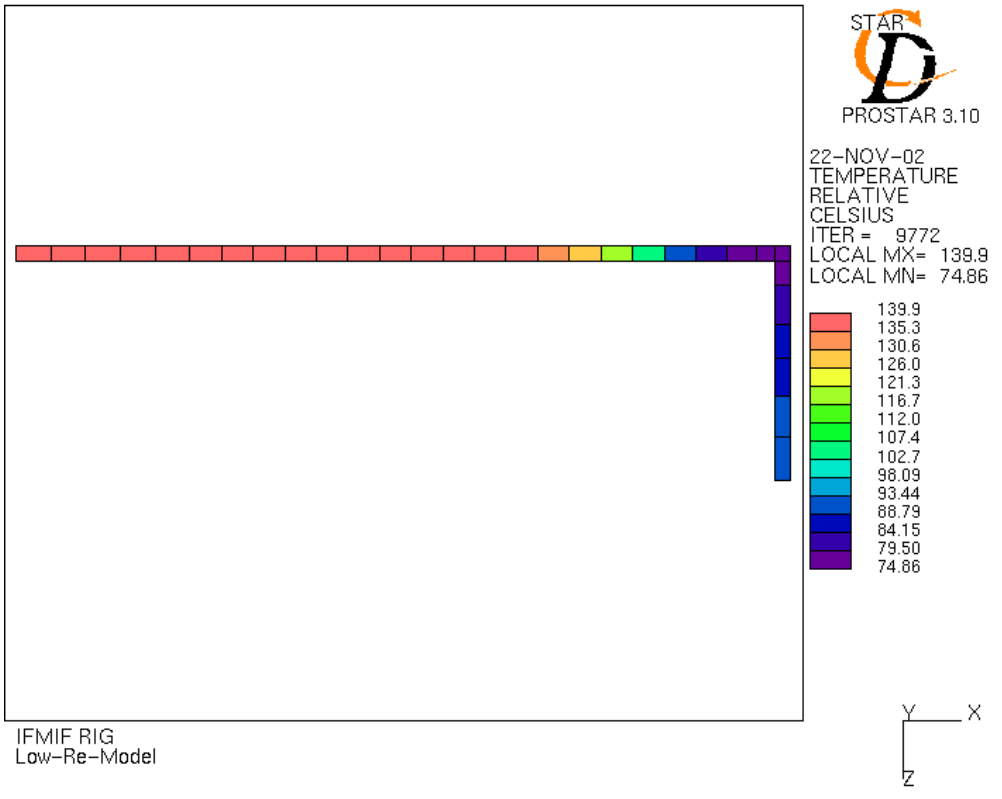

Temperature distribution in the rig wall (y=0).

Fig.35. Temperature distribution in the specimens and in the rig wall with nuclear and electrical heating, heater power=65/0/70 W/cm^3, He gap= 0.25 mm (Case 5a)

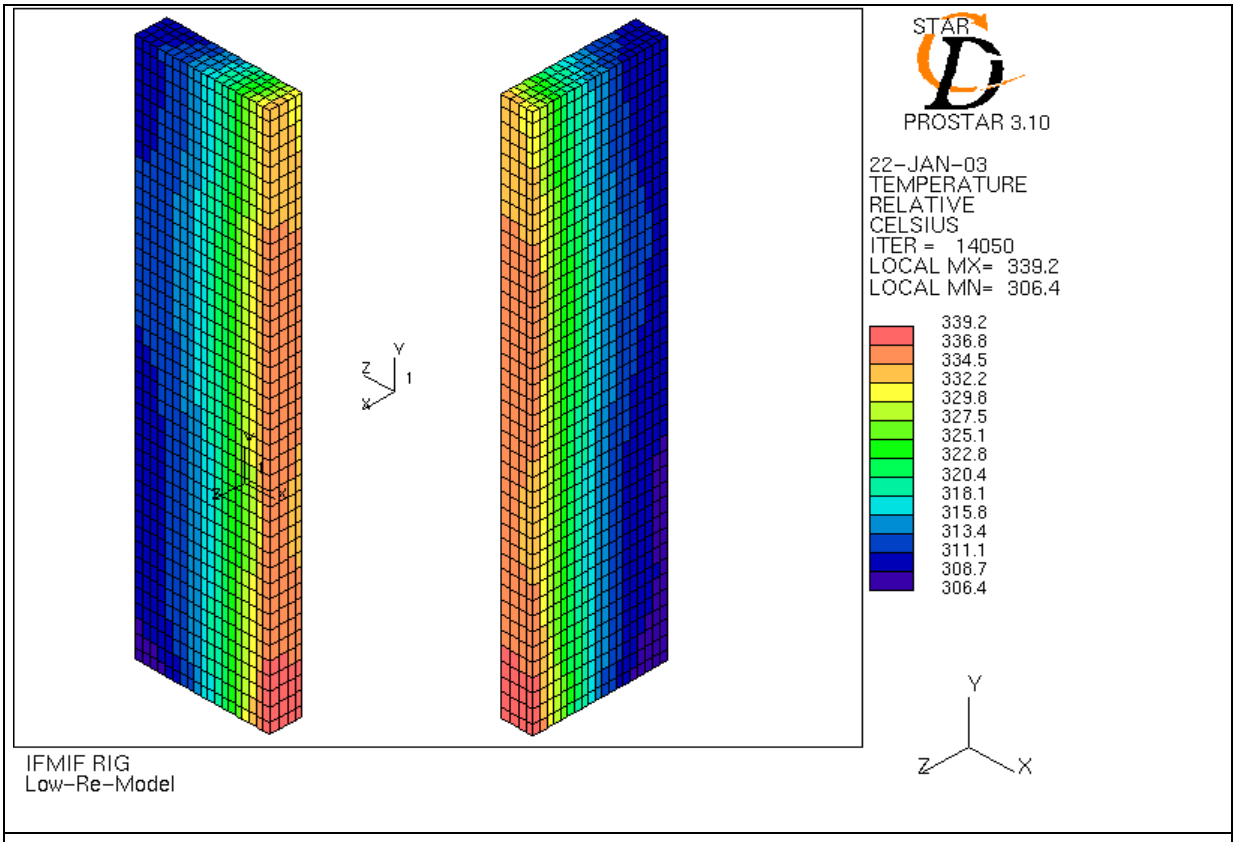

Temperature distribution in specimens

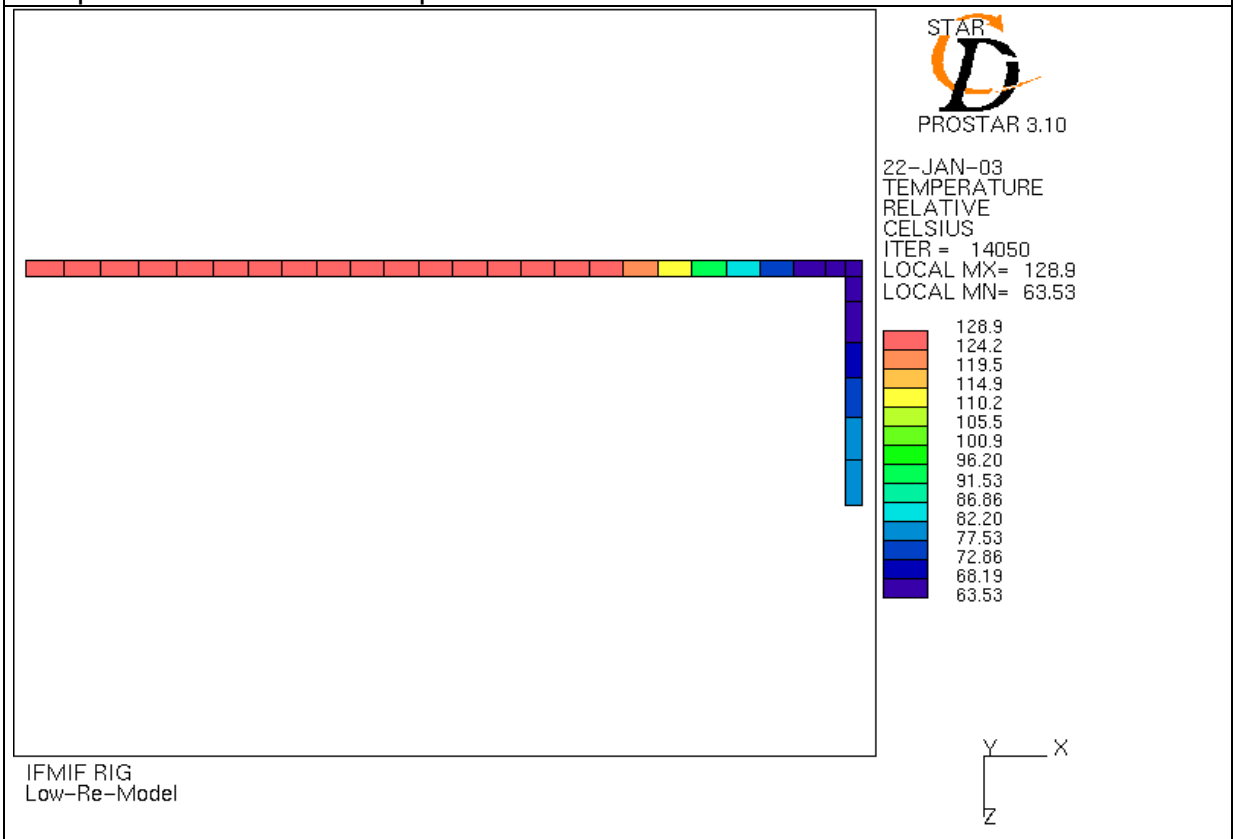

Temperature distribution in the rig wall (y=0)

Fig. 36 . Temperature distribution with electrical heating only, heating power = 111/118/124 W/cm^3,He gap=0.25 mm (Case 5b)

Annex 1: Development steps toward the optimised design

1. Rig design with squared cross section

The design analysis started from the reference design with rigs of an almost squared cross sections [2]. The reasons for the transition to a chocolate plate like cross section are given before the new design is presented.

The temperature distribution within the specimen volume of a squared rig was calculated with the code PERMAS for the highest power density at the beam entrance position. Only with a temperature control or heat removal from all 4 rig sides the temperature variation can be kept below 10°C. This entails a cooling gap on the four sides of the rigs and for temperature control at beam shut-down situation electric heaters on all four surfaces of the capsule.

Additional heaters are necessary in order to balance the power density variation (see Fig. 1) and to prevent a vertical temperature gradient. To achieve such a power distribution with electric jacket wire heaters as usually applied would require too much space. Therefore, flat plate heaters were suggested which consume less space and which can be placed inside the capsule. A possible design is shown in Fig. A1. Two heaters are embedded in a ceramic carrier. They can be arranged so that they balance the nuclear heating as well as create an apt power distribution without a nuclear contribution. A promising development on the basis of AlN-ceramic with heater tracks from TaC is investigated together with an ceramic manufacturer.

2. Heat transfer from specimen to specimen to capsule wall

Specimen inserted into the capsule will fill up the space according to their shape. The voids between the specimens will alter the nuclear power release on the one hand. This may be mitigated by filler pieces. On the other hand the power must be transported across the boundary from specimen to specimen and finally to the capsule wall. However the heat transfer can hardly be defined or guarantied in practice if the gap between two pieces is filled by a gas. This is demonstrated in Fig. A2 where the gap width was changed from 0.02 (top) to 0.01 mm (middle). The lower figure shows the temperature distribution for a gap filled with sodium. The temperature variation reaches 15 °C compared to 36 °C in the upper case.

Supplemented by further analyses, the results led to the decision, that the capsules have to be filled with sodium. Nuclear calculations showed, that the small amount of sodium in the capsules had no impact on the neutron flux and the power release [6]. The use of the eutectic alloy Na/K in order to alleviate the handling is still under discussion. Capsules filled with a liquid metal preclude the open boxes with flat heater plates as shown in Fig. A1. Therewith, electric heaters from the jacket wire type placed at the outer surface of the capsule have to be used. Nevertheless, the material development for the flat ceramic heaters is continued for capsules in positions with lower power density.

3. Chocolate plate rig design

Smaller width of the specimen volume, the need for wire heaters and the need for reduced space for the wire heaters led to the decision to analyse rigs with a chocolate plate like cross section. The wish to keep individual rigs independent at different temperatures levels caused the subdivision of the container into four compartments filled with 3 rigs each. The major contour dimensions of the specimen is shown in Fig. A3 (top right). Different arrangement of the specimen within the capsules were studied (Fig. A3 left). It was found, that the better the space was used up for a maximum of specimen the less is the flexibility in changing a specimen type or the possibility to preserve a certain position for an individual specimen.

Mainly two rig types were analysed in detail and some variants of each. Fig. A3 (middle right) shows the variant with wire heaters wound vertically around the capsule. The axial inner length of the capsule respectively the specimen stack is 81 mm. The length in horizontal or x-direction is 46.4 mm and the width comes to 10.74 mm. The capsule is closed by weld seams at both ends. The seam is located at an extension of the capsule wall and consequently removed from the high flux area (an expansion volume for the sodium still has to be added in this design.) Additional axial heaters may be installed into the hat like caps of the capsules. Spacer pins with low heat conduction secure the position in the rigs. On one side of the rig leaning pads keep the distance to the container wall or the next rig. Therewith the helium channel is formed with one manufacturing tolerance only.

The electric wire heaters are embedded in grooves on the capsule. Caps with a comp like outer surface are fixed by the end closure hats. They prolong the heater

positioning grooves, so that the heater wires can be wound like a coil around the capsule ends.

4. 2D thermal analysis of the chocolate rig with variable gap between capsule and rig walls

As noted before the electric heaters on the capsules have to control the temperatures of the specimen at different temperature levels during beam operation as well as during short beam-off periods. They have to supplement the nuclear power and to cope with the nuclear power shape in axial direction. During beam-off periods the non-uniform power contribution does not occur.

In order to come along with one heater coil, we analysed a design where the gap between capsule and heater was varied in axial direction. It increases stepwise from the specimen stack mid plane till the upper and lower stack ends, therewith, providing a stepwise increase of the thermal barrier between capsule and rig. The 2-D simulation with PERMAS assumes a constant helium temperature and a constant heat transfer coefficient on the outside of the rig.

For comparison Fig. A4a presents a reference design with a constant axial gap width. With the nuclear heating only the relative temperature difference in the specimen stack amounts to 127°C. If the gap width is enlarged in 3 steps the temperature difference is reduced to 14°C. However at the beam-off situation a temperature difference of 64°C occurs whereas the constant gap width has a relative temperature variation of 7°C only (Fig. A4b). Fig. A4c demonstrates that a heater system with incrementally differentiated heater power in axial direction is indispensable.

6. Conclusion

As a conclusion it was decided to take the chocolate plate rig with horizontally wound heaters as basis for the further design optimisations and analyses of the HFTM test section.

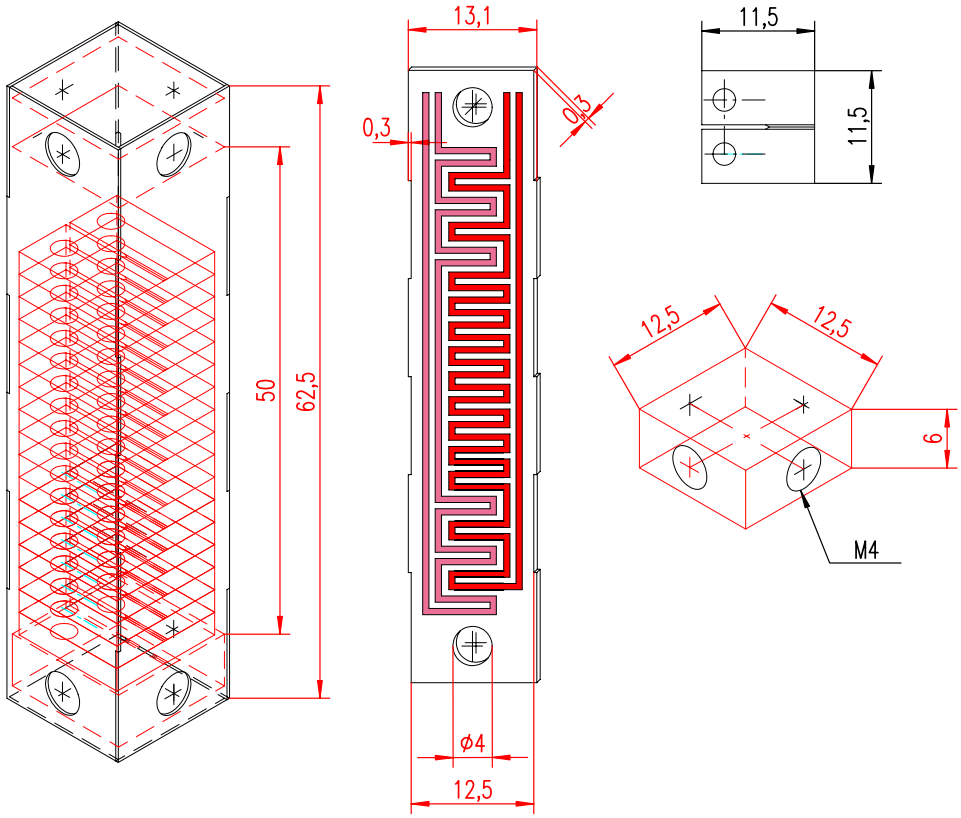

Fig. A1: Open capsule with flat heater plates

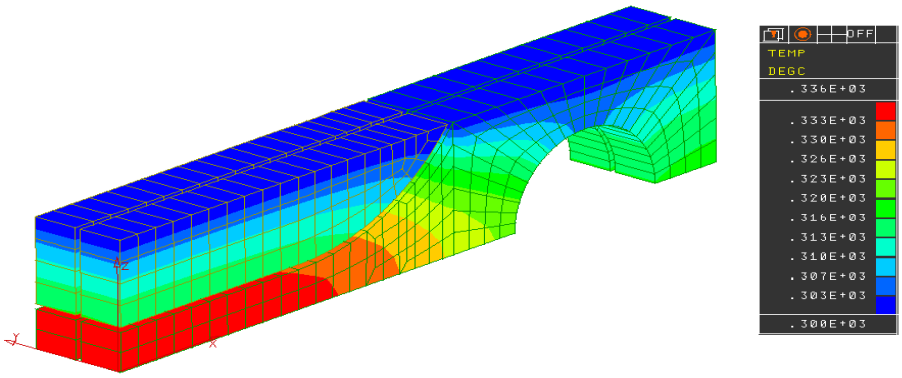

He gap of 0.02 mm between the specimen and a steel filler peace

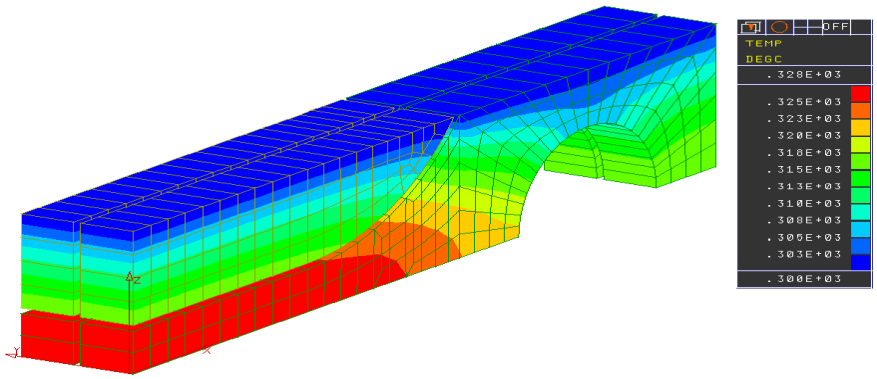

He gap of 0.01 mm between the specimen and a steel filler peace

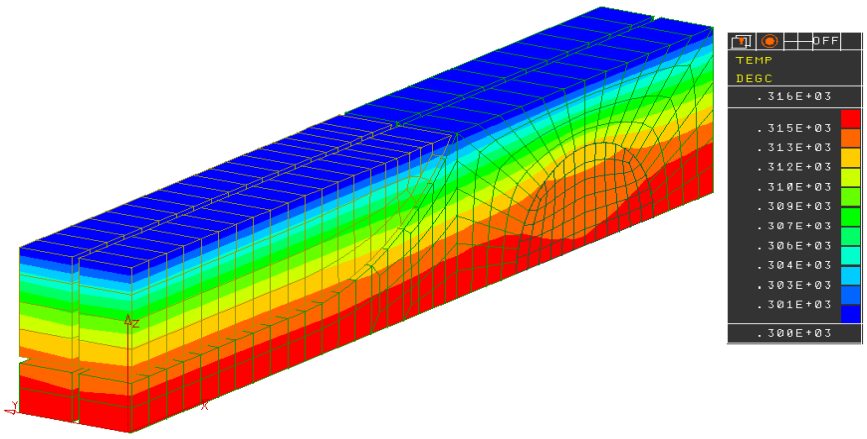

Gap between the specimen and the steel filler piece filled with Na

The nuclear power is 28W/cm^3, the cooling temperature 30°C.

Fig. A2: Temperature distribution in a specimen for tensile tests together with a steel filler peace, calculated with the code PERMAS for a volume heating of 28W/cm^3; the gap between the filler peace and the specimen is filled with helium at a width of 0.02mm (top), 0.01mm (middle) and filled with sodium (below)

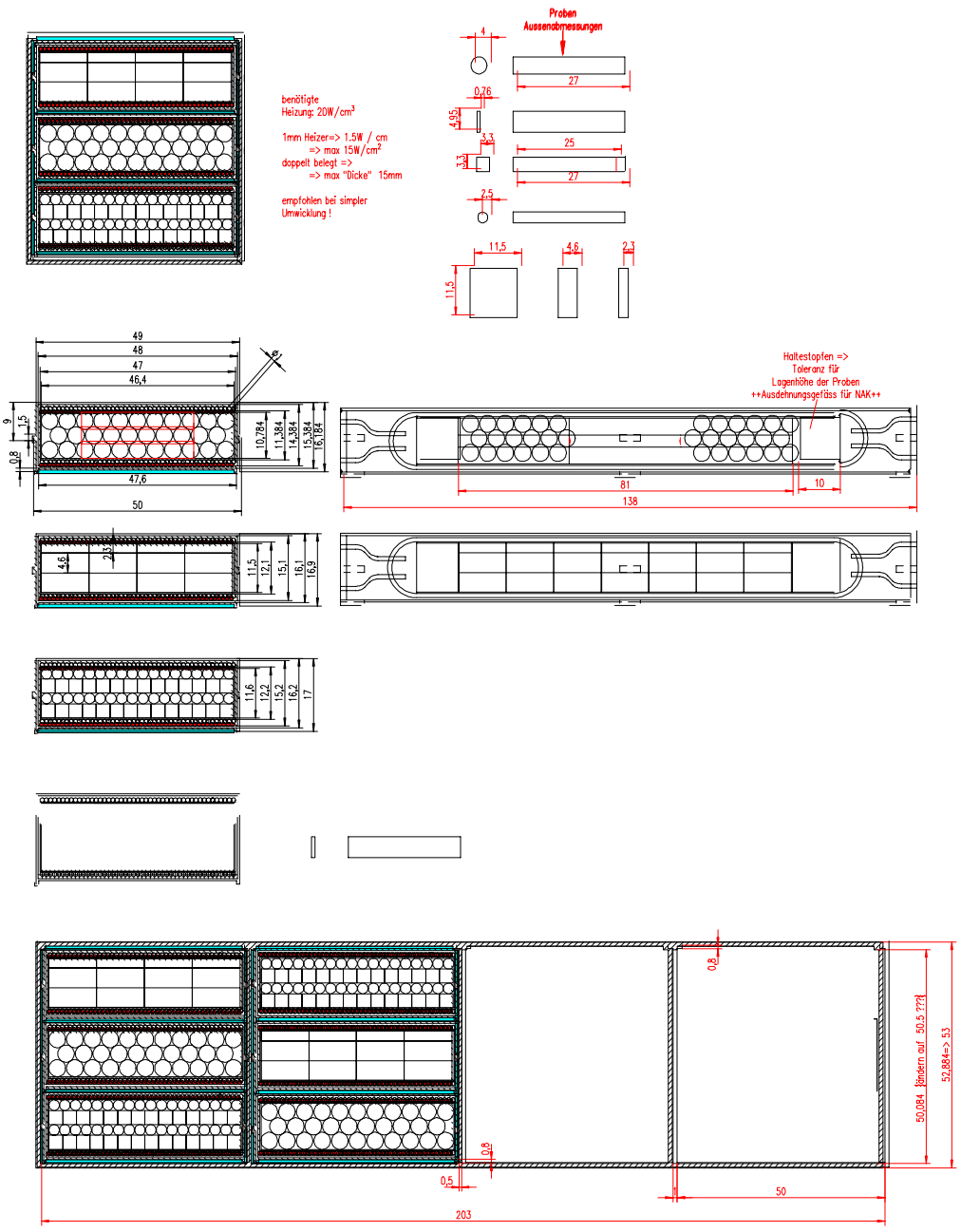

Fig. A3: Rigs with chocolate plate like cross section installed in the container which is subdivided into 4 compartments; the specimen types are depicted right on top; studies with specimen arrangements are shown on the left side; the container with compartments and rigs is presented on bottom

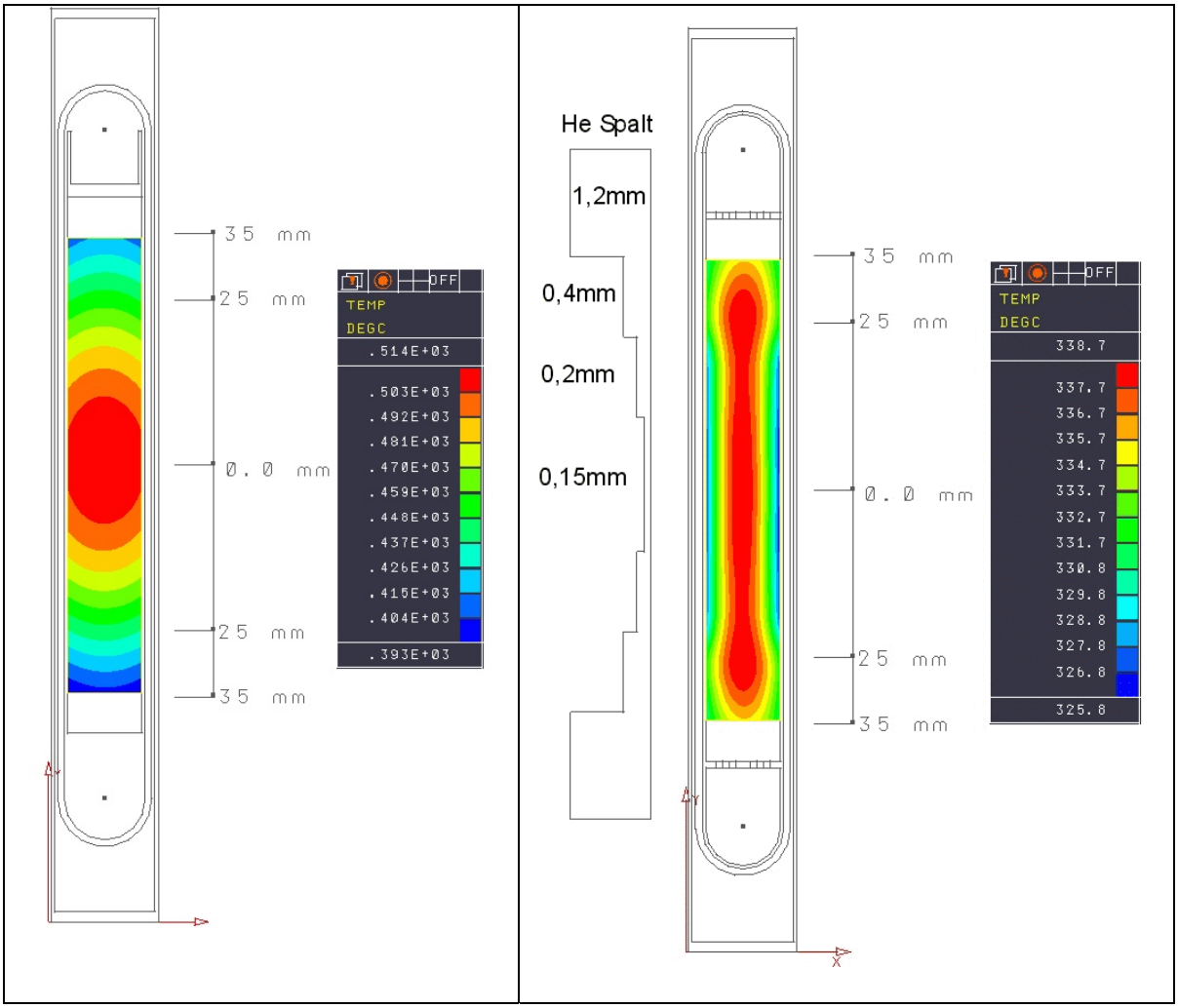

Fig. A4a: Specimen capsule with constant (left hand side), and variable (right hand side) He gas gap between specimens and inner capsule wall. Only nuclear heating is taken into account.

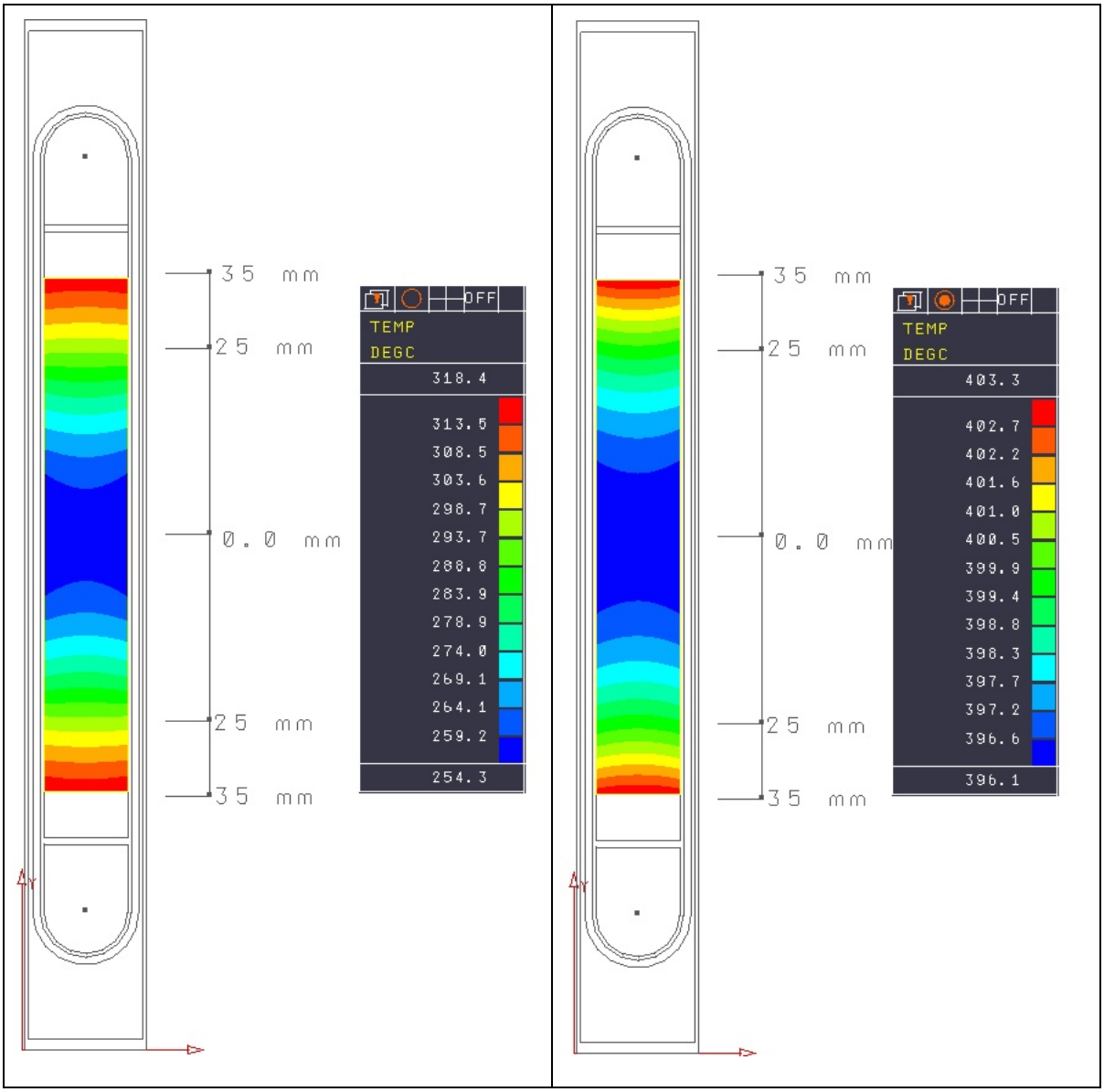

Fig. A4b: Only electrical heating with ohmic wires (150 W/m) is taken into account. Left side: variable He gap from the middle (0.15 mm, 0.2 mm, 0.4 mm, 1.2 mm). Right side: constant He gas gap of 0.5 mm.

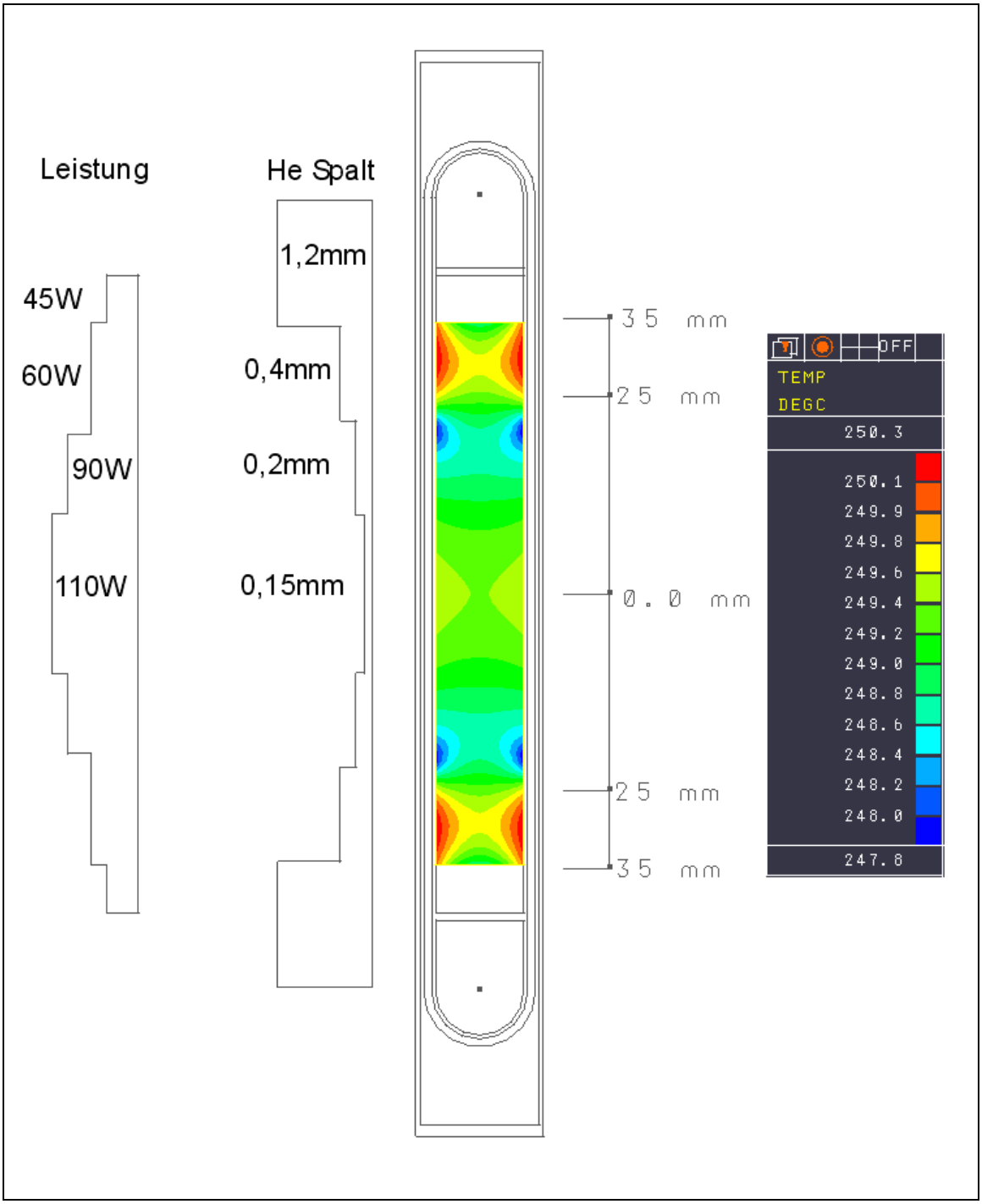

Fig. A4c: Capsule/rig-design with variable He gap width between capsule and rig walls and variable power distribution of electric heater